Robin Hofmann, B.Sc.

Investigation of diamino-anthraquinones for possible applications in organic solar cells

MASTERARBEIT

Zur Erlangung des akademischen Grades

Diplom-Ingenieur

Masterstudium Technische Chemie

eingereicht an der

Technischen Universität Graz

Betreuer

Assoc. Prof. DI Dr. Gregor Trimmel

Institut für Chemische Technologie von Materialien

Graz, November 2015

EIDESSTATTLICHE ERKLÄRUNG

AFFIDAVIT

ich erkläre an Eides statt, dass ich die vorliegende Arbeit selbstständig verfasst, andere als die angegebenen Quellen/Hilfsmittel nicht benutzt, und die den benutzten Quellen wörtlich und inhaltlich entnommenen Stellen als solche kenntlich gemacht habe. Das in TUGRAZonline hochgeladene Textdokument ist mit der vorliegenden Masterarbeit identisch.

I declare that I have authored this thesis independently, that I have not used other than the declared sources/resources, and that I have explicitly indicated all material which has been quoted either literally or by content from the sources used. The text document uploaded to TUGRAZonline is identical to the present master's thesis.

Datum / Date	**Unterschrift / Signature**

Acknowledgment

First of all, I want to thank my supervisor Assoc. Prof. DI Dr. Gregor Trimmel for giving me the opportunity to work on this interesting topic as well as for supporting me during my master thesis.

Also I'd like to thank Assoc.Prof. Dipl.-Chem. Dr.rer.nat Bernhard Gollas for his help during the CV measurements and Ao.Univ.-Prof. Dipl.-Ing. Dr.techn. Karl Gatterer for his support during UV-Vis measurements.

Greats thanks to my colleagues at the institute, especially to Sebastian Dunst and Sebastian Höfler, who supported me with their time, skill and knowledge.

The biggest thanks go to my friends who always provided me with motivation, to my family who always supported me and who are my greatest role models and to my girlfriend who helped me turning my crazy language into something readable.

THANK YOU!

Zusammenfassung

Organische Halbleiter rücken immer mehr in den Blickpukt der Forschung aufgrund ihren vielseitigen Möglichkeiten einer Anwendung in der Elektronik und Photovoltaik. Der Hauptvorteil organischer Halbleiter ist die leichte Verarbeitbarkeit bei geringen Temperaturen. Dadurch können sie sowohl in flexiblen als auch in gedrucken Anwendungen verwendet werden. Die großen Nachteile der organischen Halbleiter sind die schlechte Luftstabilität und die geringe Ladungs-Transport-Mobilität.

Diese Arbeit untersucht die Eigenschaften von vier Wasserstoffbrücken-bildende Diamino-Anthrachinon-Farbstoffen in Solarzellen. Diese Farbstoffe besitzen eine ambipolare Leitfähigkeit was bedeutet, dass sie in der Lage sind sowohl positive als auch negative Ladungen zur gleichen Zeit zu transportieren. Diese Eigenschaft macht die Farbstoffe perfekt für den Einsatz in sogenannten Homojunction-Solarzellen.

Der erste Teil der Arbeit befasst sich mich der Charakterisierung der Farbstoffe, der Bestimmung der Bandlücken und mit der Kalkulation des entsprechend höchsten besetzen Molekül Orbitals (HOMO) und des niedrigsten unbesetzten Molelül Orbitals (LUMO). Dafür werden cyclovoltammetrische Messungen in Acetonitril und UV-Vis-Spektroskopie in Dünnfilm und Acetonitril verwendet.

Im zweiten Teil der Arbeit werden die vier Diamino-Anthrachinon-Farbstoffe in Solarzellen verbaut. Die Solarzellen werden dabei im Homojunction- und im Bulk-Heterojunction-Aufbau gebaut. Beim Bau der Bulk-Heterojunction-Solarzellen werden 1-[3-(Methoxycarbonyl)propyl]-1-phenyl-[6.6]C_{61} (PCBM[60]) als Akzeptor- und Poly(3-hexylthiophen-2,5-diyl) (P3HT) als Donor-Material verwendet. Als Lochleitungs-Schicht dienen Poly-3,4-ethylendioxythiophen: Poly(styrenesulfonate) (PEDOT:PSS) im normalen Aufbau und Molybdänoxid im inversen Aufbau. Außerdem wird Titanoxid als Elektronenleiter-Schicht im inversen Aufbau verwendet. Die Solarzellen werden mit Strom-Spannung-Messungen charakterisiert.

Der letzte Teil untersucht den Einfluss von selbst assemblierenden Monolagen (SAMs) auf die Solarzellen-Parameter. Die SAMs bestehen aus para-substituierten Derivaten der Benzoesäure und werden auf eine Titanoxid-Schicht aufgebracht. Die Beschichtung durch die SAMs wird mittels Kontaktwinkel-Messungen bestimmt. Dafür werden H_2O und CH_2I_2 als analytische Flüssigkeiten verwendet. Außerdem werden die Oberflächenenergien ermittelt. Im Anschluss werden die SAM-beschichteten Titanoxid-Schichten in inversen Solarzellen verbaut und mittels Strom-Spannung-Messungen charakterisiert.

Abstract

Organic semiconductors are in the focus of research due to the manifold possible applications in photovoltaics and electronics. Their main advantage over inorganic semiconductors is the easy processability and the low process temperature. This property enables organic semiconductors to be used in flexible as well as in print applications. However, organic semiconductors still suffer from low charge carrier mobility and little air stability.

This thesis investigates the semi-conductive behaviour of four H-bonding diamino-anthraquinone dyes in solar cell applications. These dyes are considered to be ambipolar, making them suitable for homojunction solar cells as they are able to transport positive as well as negative charge carriers at the same time.

The first part focuses on the characterization of dyes and the determination of their band gaps and the corresponding highest occupied molecule orbital (HOMO) and lowest unoccupied molecule orbital (LUMO) levels. Therefore, cyclovoltammetric measurements in acetonitrile as well as UV-Vis spectroscopy in thin film and acetonitrile are performed.

The second part investigates on the diamino-anthraquinone dyes being introduced into solar cells including homojunction and bulk-heterojunction setups. In bulk-heterojunctions, the dyes are used along with [6,6]-phenyl-C_{61}-butyric acid methyl ester (PCBM[60]) and Poly(3-hexylthiophen-2,5-diyl) (P3HT). All experiments are carried out in normal architecture, including Poly(3,4-ethylen dioxythiophen); Poly(styrenesulfonate) (PEDOT :PSS) as hole transport layer, and inverse architecture, where titanium oxide is used as electron transport and molybdenum oxide as hole transport layer. The solar cells are characterized by current-voltage measurements.

The last part examines the influence of self assembling monolayers (SAMs), consisting of five benzoic acids derivatives, on the solar cell parameters. The coating of SAMs onto TiOx is measured with contact angle measurement and H_2O and CH_2I_2 as analytical liquids. Additionally, the surface energy is calculated. Then the SAMs are introduced into inverse architecture solar cells and characterized by current-voltage measurements.

SUN'S RAYS TO DRIVE
Aerial Landing Field

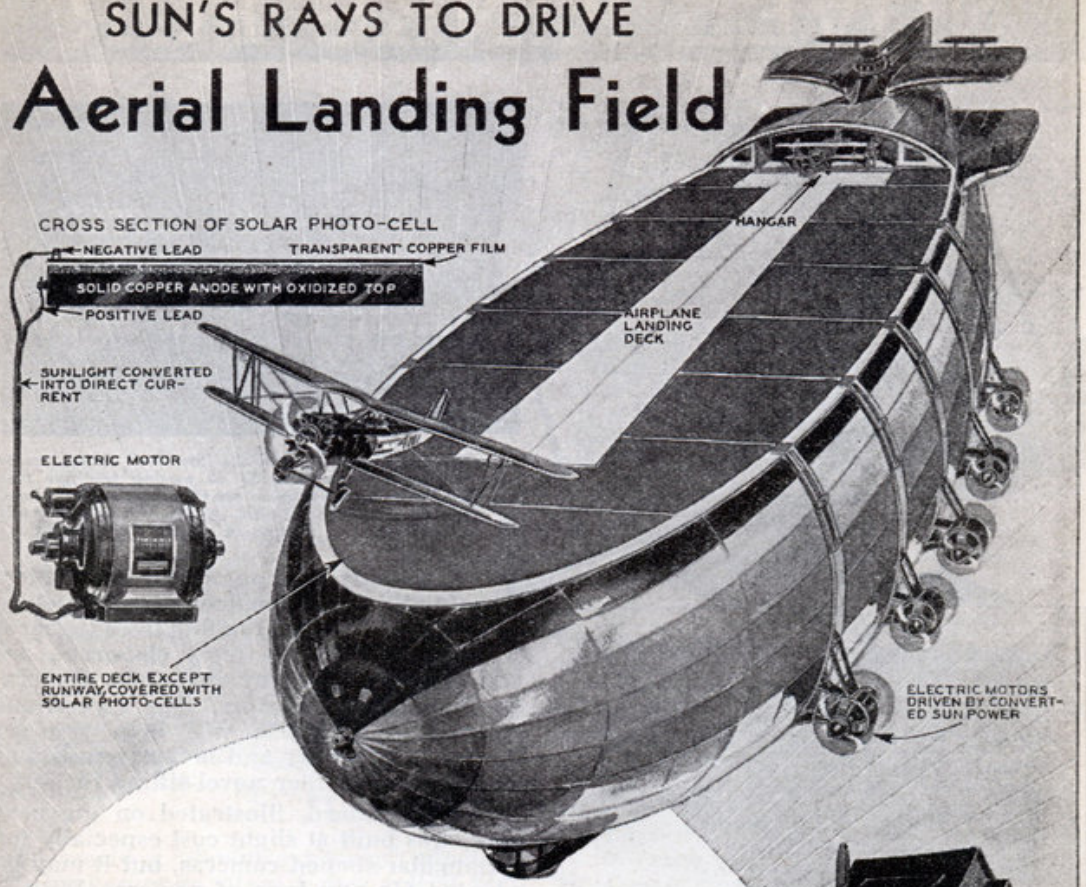

RECENT experiments in the conversion of the sun's rays into electric power have led to an unusual idea in aerial equipment. It is a dirigible that not only would get its power from the sun but also provide space for a landing field in the air.

The ordinary cigar-shaped dirigible would in effect have a slice taken from the upper half of the gas bag. This would provide a large deck on which could be mounted solar photo cells, an airplane runway, and a hangar. Planes could land on the dirigible, floating over the sea, to refuel for trans-ocean passenger service.

Another unusual feature of this design, in addition to the landing field, is the use of sun rays to power the motors of the dirigible. Scientists estimate that the sun can develop as much as 86,300 kilowatts or 115,000 horsepower per hour in an area of a square mile. Photo cells convert the sun's energy into electricity. When this can be done on a practical basis, the roof of an ordinary house can be used to develop electricity for the home.

ROOF SPACE OF ORDINARY HOME COVERED WITH SOLAR PHOTO-CELLS COULD DEVELOP CURRENT FOR APPLIANCES AND LIGHTS

MAXIMUM POSSIBLE ENERGY FROM SUN IS 86,300 KILOWATTS PER SQUARE MILE

© Modern Mechanix, Issue: Oct. 1934

TABLE OF CONTENTS

1 Introduction

Since life exists, there is the need for energy. The average energy needed to fuel a human body and its function is around 100 W, but to make life comfortable, in the way we do it nowadays, takes 30 times more energy [1]. Life, as we know it, is simply based on a processed form of solar energy. Plants like algae and photo bacteria directly process sunlight through photosynthesis into useful energy and are, therefore, the basis of all following life forms. It took over millions of years that a life form other than those is able to directly process sunlight: mankind. Since Alexandre Edmond Becquerel discovered that the illumination of one of two electrodes of the same material in a battery leads to an increased voltage (Becquerel effect) in 1839 [2], a lot of hard work and research led us to the current state of the art. Today, photovoltaic (PV) is already a basis in energy production and will become more and more important over the years in overcoming our dependency on fossil fuels.

1.1 World Energy Production

The usage of fossil fuels changed our world drastically. The possibility to generate heat and electricity on demand makes daily life very comfortable, but it comes for a very high price. Climate change and pollution, generated by burning of fossil fuel, are one of the most omnipresent topics when talking about energy and environment.

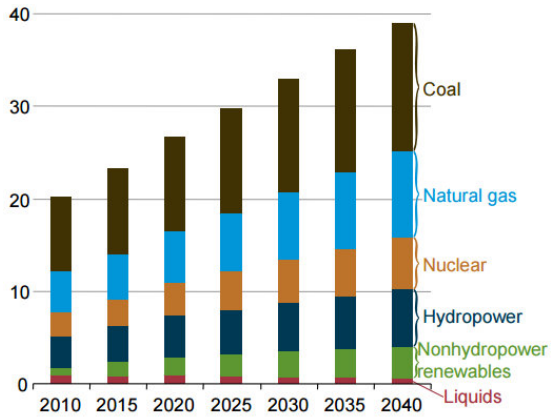

Figure 1: World net energy production by fuel in trillion kWh, provided by the EIA [3]

Nowadays, society started rethinking about the use of fossil fuel and the generation of anthropogenic greenhouse gases. Reducing carbon dioxide emissions and other greenhouse gases has become an important goal for many countries all over the world. Therefore, many initiatives try to promote and subsidise green energy sources in order to replace the existing fossil fuel sources.

In 2013, the U.S. Energy Information Administration (EIA) has presented a world energy outlook up to the year 2040 [3]. According to EIA, the world net energy generation will increase from 20.2 trillion kWh in 2010 to 39 trillion kWh in 2040 (see Figure 1). Considering the IEO2013 Reference case, one of the largest growths will be allocated in the sector of renewable energies.

However, it is not only the EIA that works on future world energy trends: The IEA has provided different scenarios for the future of renewable energy within their ETP 2014 analysis [4]. One of their scenarios is called 6DS meaning a raise of the mean temperature of the earth by 6°C through the current trend of energy production and consumption. That scenario leads to an increase in all sectors of energy production including fossil fuels to cover the increasing demand. The other two scenarios are called 2DS and hi-REN scenario. Both have the goal not to exceed the 2°C global mean temperature raise limit. This includes the raise in efficiency of the energy used and the reduction of fossil fuel to a bare minimum. However, the hi-REN scenario tries to archive the same energy level as 2DS but with 79% of the energy provided by renewable resources. For the hi-REN scenario the IEA provides a roadmap of the future PV-electricity generation and the total electricity generation (see Figure 2) [5].

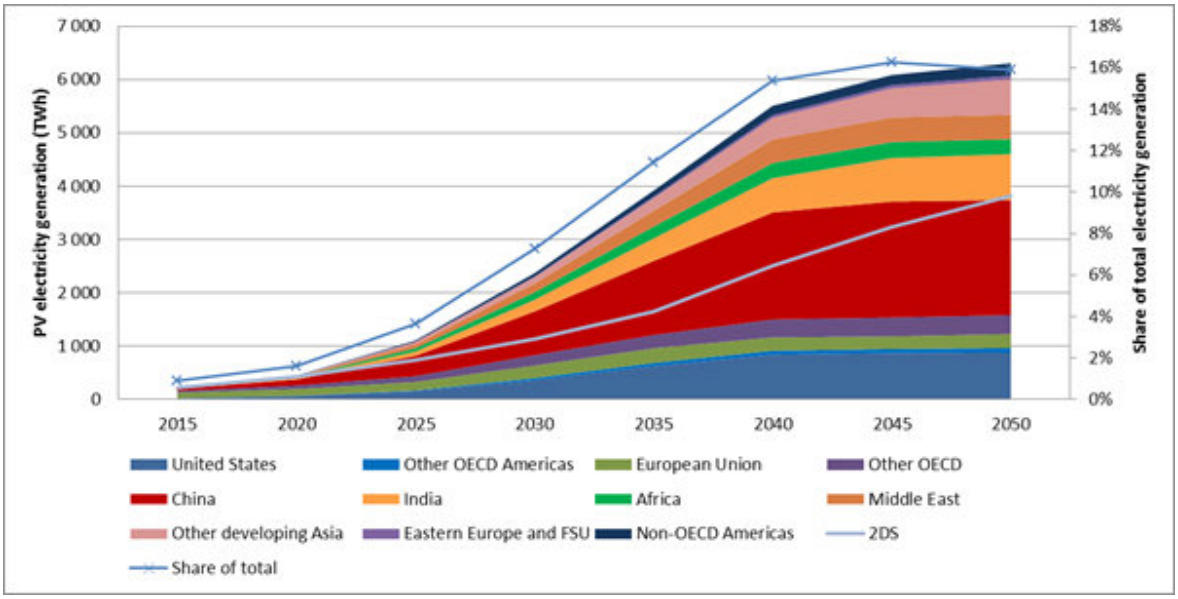

Figure 2: Roadmap of future PV-production according to the hi-REN scenario provided by the IEA [4]

1.2 Evolution of Photovoltaics

As already mentioned before, Alexandre Edmond Becquerel was the first to investigate on the influence of light on the electrical properties of batteries. Although this was performed in the mid 19th century, it still took more than 100 year to get to first solar cell as we know it today. It was William B. Shockley who provided the first theoretical concept for solar cells in his work “The Path to the Conception of the Junction Transistor” [6]. However, the first workable boron-doped silicon solar cell was built by D.Chapin, C.Fuller and G.Pearson at the Bell Laboratories in 1954 by bundling their cells into a panel [7].

The first real applications of solar cells were found in aeronautics and astronautics. During the oil crisis in the 70’s, the urge to become independent from fossil fuel came along. That marks the starting point to put more effort into this kind of technology.

Since this start, a lot of new PV technologies have emerged. Today, the predominant technology is still silicon-based but other crystalline systems like cadmium telluride (CdTe) [8] or copper indium gallium selenide (CIGS) [9] are commonly used too. Although Si-based technologies hold a market share of 91% whereby multi-crystalline Si accounts for 56%, thin film technologies like CIGS and CT already account for 9% of the total energy production [10].

Along all these well-established solar cell technologies, other branches like organic photovoltaics (OPV) try to find their way into the market of energy production. The estimated huge advantages of OPV are the highly reduced costs and their improved process capability. Although OPV possibly will never replace inorganic or hybrid systems in panels on rooftops und such, their main use can be found in intelligent textiles, roll to roll processes and flexible photovoltaics where ‘conventional’ PV does not meet the requirements needed like mechanic resilience for example.

Nevertheless, for the last six years a new technology has nearly overcome all other technologies: perovskite based solar cells. Starting with an initial efficiency around 3.8% in 2009 [11], the perovskite technology has found itself with a certified photon conversion efficiency of 20.1% in 2015 [12]. However, these very promising results still suffer from disadvantages. Perovskite solar cells are extremely sensible to moist which leads to a rapid degradation of the cell. Additionally, one of the main issues is lead on which the system is built. There are some efforts to replace lead with tin, but those systems suffer from severe efficiency losses [13].

As mentioned before, many technologies on photovoltaics have evolved and developed over the years. The National Renewable Energy Laboratory (NREL) has put together all technologies in one table to give an excellent overview on the evolution of photovoltaics from 1975 until now. All results from 2005 to 2015 shown in Figure 3 below are found in the work of M.A.Green et al. [14].

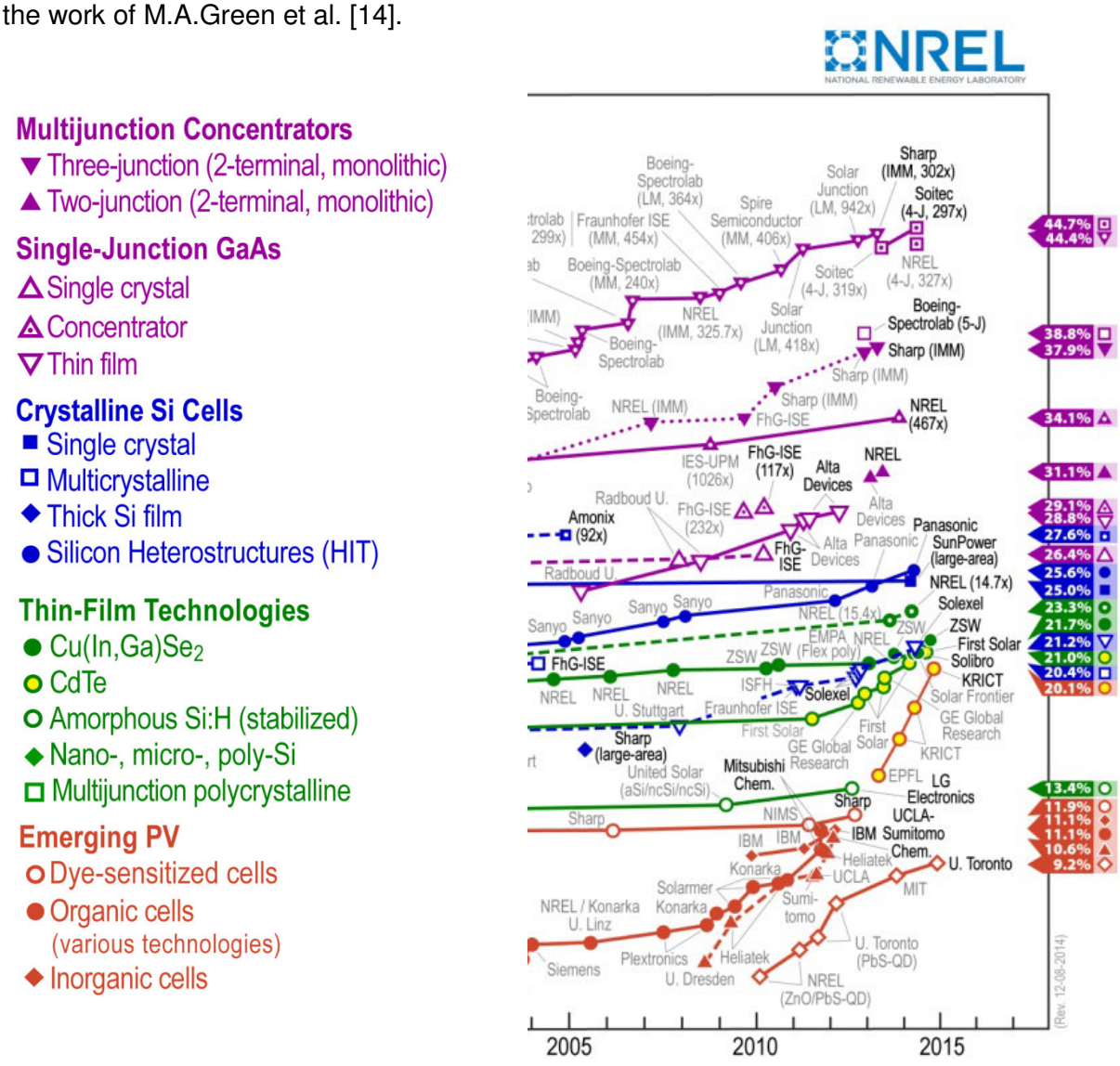

Figure 3: Best Research-Cell Efficiencies provided by NREL [15]

According to M.A.Green et al., the best organic cells reach efficiencies around 9-11% while thin-film technologies and perovskites are found between 20-23%. Crystalline Si-systems reach efficiencies up to almost 28%. The record of 44% can only be reached by triple-junction cells with concentrator array setting.

2 Basics

2.1 Light to Electricity

First of all, the general principle of the electricity generation in silicon-solar cells will be explained for a better understanding. All electronic processes within a Si-solar cell can be explained through the 'band'- model. Si is a semiconductor, whose valence band (VB) is filled with 'bonded' electrons, electrons which are not able to leave the core atom. Regarding the conduction band, energy- rich electron can be found here, free to move throughout the whole Si-lattice. These free electrons are considered to be delocalized. The gap between the valence and the conduction band is called 'bandgap'. This bandgap is very dependent on material properties, as well as on temperature and the amount of doping of the material used. If both, valence band and conduction band, are overlapping, the material is considered to be an electric conductor like metals. Materials where conduction band and valence band are far apart are electric insulators. Materials where conduction band and valence band are very close together are considered semiconductors. However, semiconductors are not neither good conductors nor good insulators. Therefore, to control and manipulate the electric conductivity it is very important to dope such materials [16,17].

To generate electricity from sunlight, photons of the energy of the band gap and above have to be absorbed by the material. These photons promote electrons from the valence band to the conduction band, leaving a positively charged 'hole' behind. This pair, the positive hole and the negative electron, build up an exciton pair who are still bound through coulombic forces. To split them apart, an electric field has to be applied. This is achieved through an n-doped (electron rich) and a p-doped (electron poor) area. Through the difference in electron density between these two areas an electric field occurs. If the electric field is strong enough and the coulombic force between the exciton pair is weak enough, they can be separated and each electron and hole moves to their electrode, where they contribute to the electric circuit. This process is shown below in the Figure 4 [18].

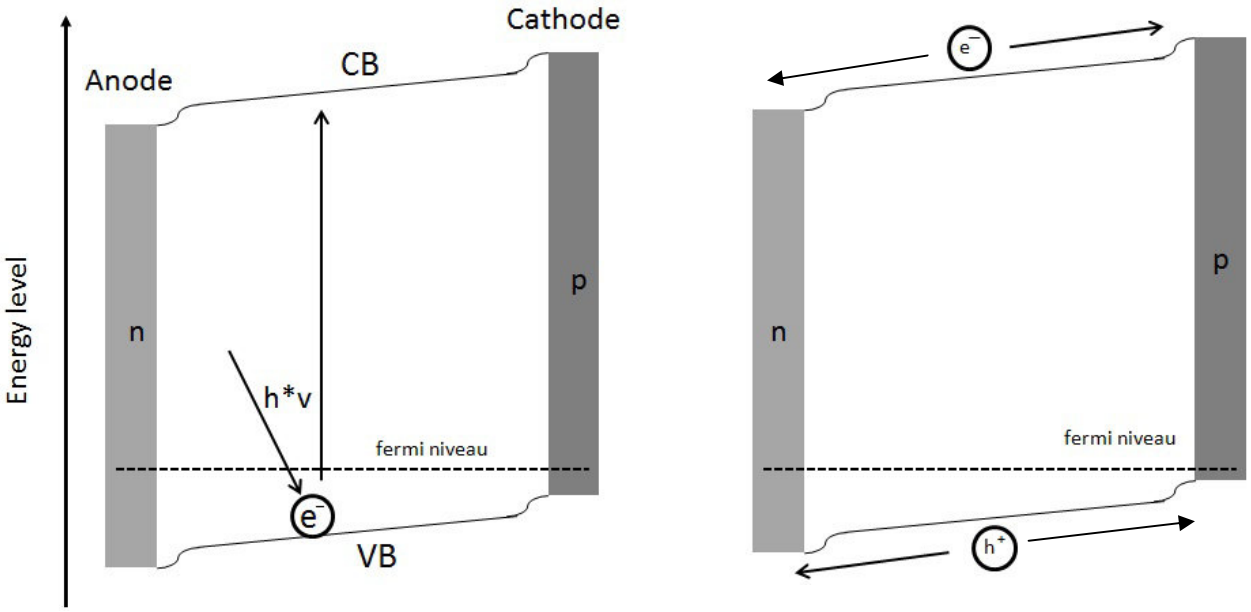

Figure 4: Exciton generation in a Si-solar cell

2.2 Organic Photovoltaics (OPV)

Organic molecules and polymers with a π-conjugated aromatic backbone, including those with hetero atoms, are capable of transporting holes and electrons like an inorganic semiconductor. Additionally, they can absorb light easily. Therefore, these systems can be used as semiconductors in opto-electronic systems like inorganic materials. Such organic molecules are easy to modify making it easy to adjust functional properties [19].

In OPV it is very important to have molecules with overlapping π-orbitals in order to have high electron mobility. As most of the used materials have a high permittivity and therefore a high binding energy of the excitons, a second semiconductive material is commonly introduced to facilitate the splitting of excitons. The concept of having using two or more materials is called heterojunction [20]. In a heterojunction the excitons are generated closed to the borders of these two materials. Through the difference in their energy levels, the splitting of electrons and holes as well as their transport towards the corresponding electrodes is increased. Figure 5 shows this process within a heterojunction. Materials which support the transport of electrons are called ‘acceptor’, therefore, materials which support the transport of holes are called ‘donor’. Regarding the energy levels, donors have a higher highest occupied molecular orbital (HOMO) and lowest unoccupied molecular orbital (LUMO) than the acceptor. If the difference of those energy levels is high enough, excitons can be split apart [21].

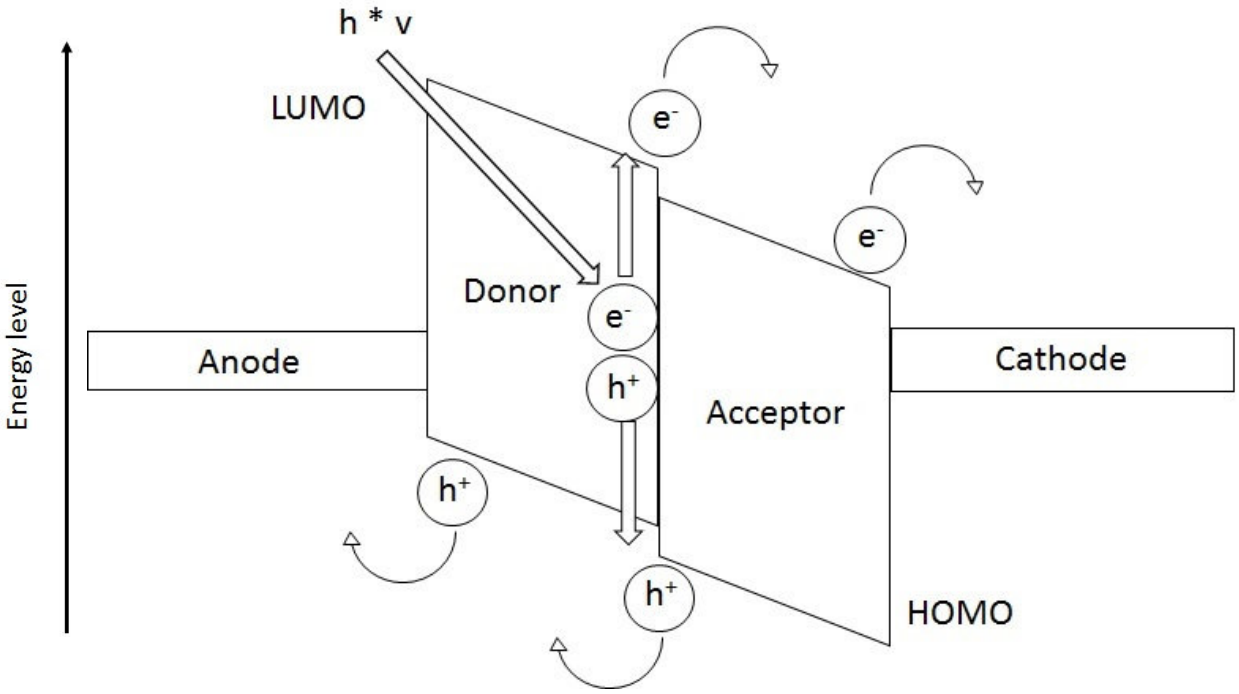

Figure 5: Schematic of exciton splitting in a heterojunction

As seen in Figure 5 photons with energy equal or larger than the band gap of acceptor or donor generate an exciton. While the electrons move along the acceptor towards the cathode, the generated holes move along the donor material up to the anode.

Over the course of time, two main types of architecture for heterojunctions have been established. The bilayer-heterojunction consists of the donor and acceptor material on top of each other in planar layers. Between those two materials an electric field is generated, capable of splitting excitons. One of the main issues of this system is that the diffusion length of the generated excitons is between 10 to 20 nm. However, to be able to move the excitons to the interface area and to split them into charge carriers, the film thickness has be around the same size as the diffusion length. Nevertheless, most polymers and organic molecules need a film thickness of at least 100 nm to absorb enough light. Therefore, only a small amount of excitons reach the interface before they recombine. [22-25]

A more efficiency system is the bulk-heterojunction. Here both materials, donor and acceptor, are blend together into one layer and as a result, a large interface area between donor and acceptor is generated. Therefore, it becomes very easy and likely for the excitons to reach the interface area and get split into the corresponding charge carriers. One of the issues about this kind of system is the problem of building ‘islands’ within the system. Islands are either donor or acceptor areas which are fully surrounded by the opposite material leading to an increased rate recombination due to a lack of possibility to

move the charges to the electrode. The following Figure 6 shows the schematic architecture of both systems.

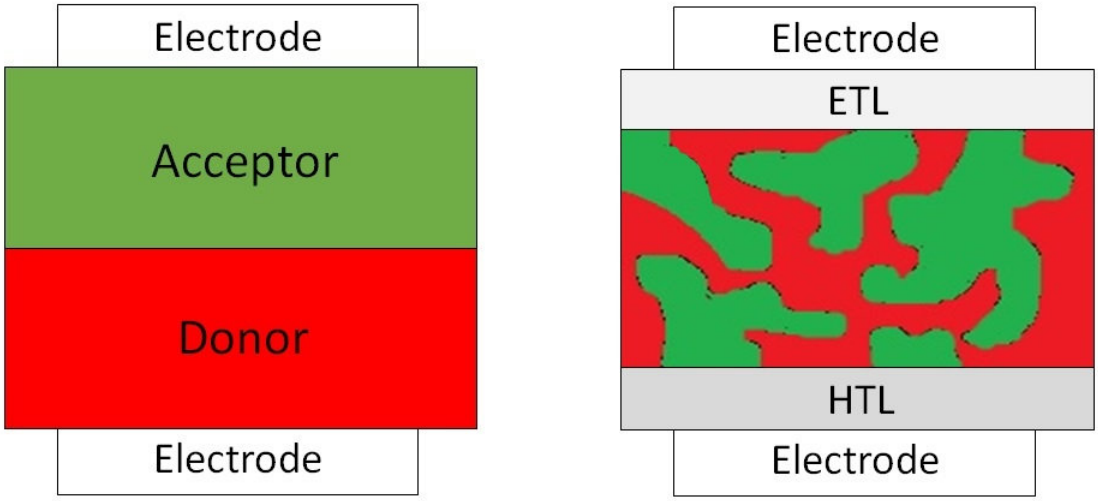

Figure 6: Left: schematic bilayer-heterojunction, Right: schematic bulk-heterojunction

To build organic solar cells, usually the active material is brought onto a transparent conducting oxide (TCO) by spin coating or doctor blading onto a glass or transparent polymer. This transparent oxide functions as the electrodes which faces the sun later on. Due to the excellent electrical and optical properties as well as the easy processability of indium-tin-oxide (ITO), it is used as TCO in most cases. However, as ITO is expensive and a non-environmental friendly compound experiments on cheaper and earth abundant aluminium-zinc-oxide (AZO) are carried out to replace ITO [26].

As seen in Figure 6, an electron transport layer (ETL) as well as an hole transport layer (HTL) is commonly introduced. These layers do not only have the task to increase the corresponding charge carrier extraction, they also prevent the opposite charge carrier from passing through that layer leading to a recombination which decreases the efficiency. Additionally they smooth the edges of the electrodes towards the active layer. That reduces possibilities of current peaks along the edges which could lead to a spark that damages the active layer and furthermore causes short circuits. Examples of electron transport layers are mainly n-type oxides like TiO_2 or ZnO but also salts like LiF. These oxides are easy to manufacture and are extremely stable towards temperature and light. Additionally those oxides can influence the morphology of the active layer which can result in higher efficiencis [27-29]. Examples of hole transport layers can be found in p-type oxides like MoO_3, WO_3 and NiO or polymers like Poly(3,4-ethylen dioxythiophen); Poly(styrenesulfonate) (PEDOT :PSS) as well as graphene compounds[30-32].

2.3 Cell architectures in OPV

As shown in the chapter before, heterojunctions can be built in two different ways but, they can also be built in two different directions called either normal architecture or inverse architecture.

2.3.1 Normal architecture

In normal architecture, ITO is used as anode and the metal electrode functions as cathode. In some cases, the ETL can be neglected as the metal electrode is an ideal electron collector. The schematic concept of a normal architecture solar cell is shown in Figure 7 below:

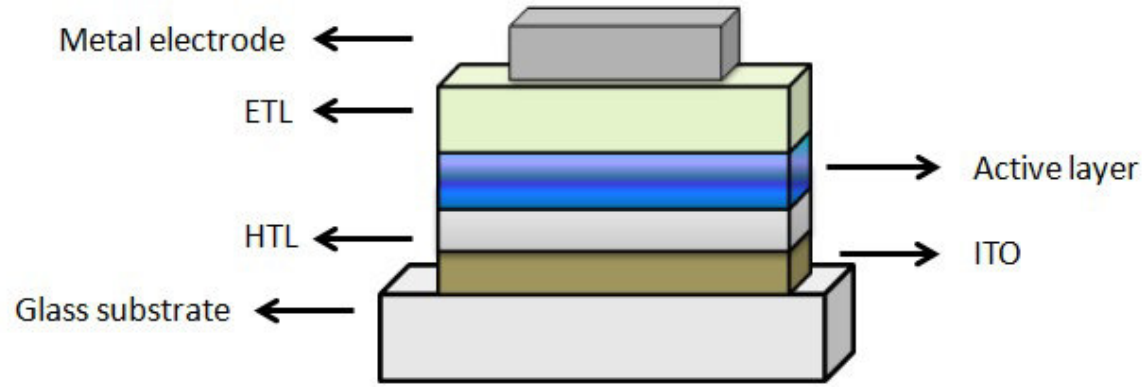

Figure 7: Scheme: normal architecture

2.3.2 Inverse architecture

In comparison to normal architecture, inverse architecture must use both, an ETL and a HTL to function properly. Also, the electrical poles are switched. Therefore the metal electrode functions as anode and the ITO functions as cathode. The scheme of inverse architecture is shown in Figure 8 below:

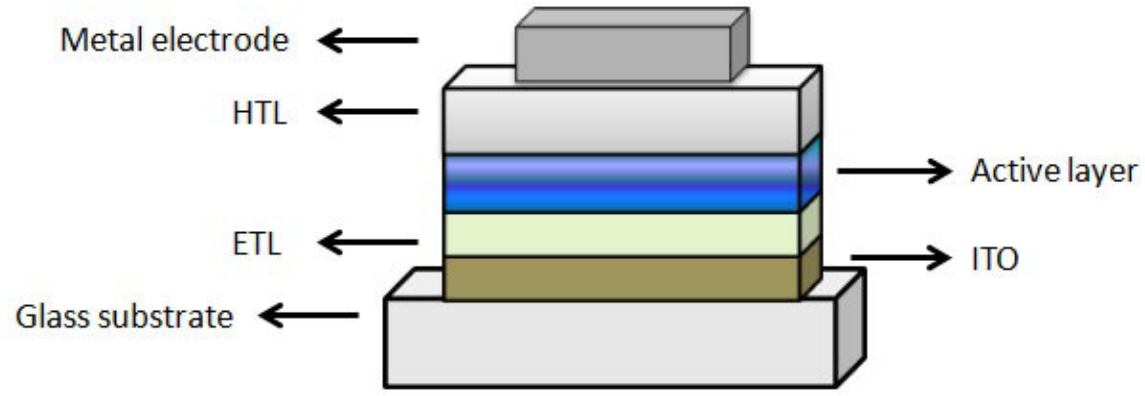

Figure 8 Scheme: inverse architecture

2.4 Dye Sensitized Solar Cell (DSSC)

When talking about dyes and OPV, it is important to take DSSC into account. In 1991 Michael Grätzel introduced the DSSC (today also called Grätzel cell), a solar cell system with an initial conversion efficiency of 7.9% [33]. In comparison to OPV, where electricity is generated through the separation of excitons, in DSSCs the light absorption and free charge carrier transport are separated.

The original Grätzel cell consists of two planar glass electrodes. Both electrodes are coated with an electrical conducting layer for example Fluorine doped Tin Oxide (FTO). The layer thickness of these conducting layers is usually around 0.5 µm. Then, a 10 µm thick TiO_2 nano-porous layer is applied on the anode. Through dipping of the TiO_2 layer into a dye solution a monolayer of dye gets adsorbed on the TiO_2 surface. The dye is a ruthenium-based molecular dye (molecular sensitizer [34]). On the other side, a thin film of electrolyte containing KI is applied on the catalyst, mostly a thin layer of platinum on top of the FTO electrode. The two plates are then pulled together and sealed to prevent the KI electrolyte from leaking out of the cell construction. The following Figure 9 shows the mechanism principle of the Grätzel cell.

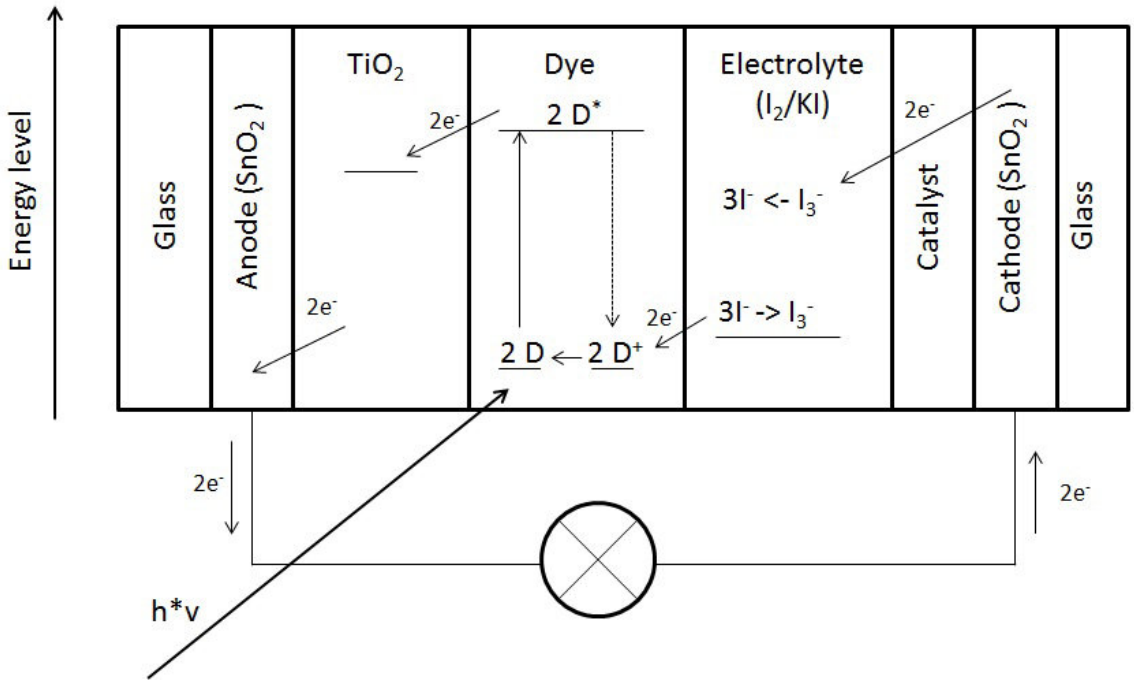

Figure 9: Function principle of a DSSC

The principle of the DSSC can be summed up in following steps:

- Light passes through the layers and gets absorbed by the dye. As a result electrons get exited into a higher energy level.

- As the energy of the electrons is higher than the energy level of TiO_2, electrons move from the dye to the conducting band of TiO_2 leading to an oxidation of the dye.

- At the same time, iodide is oxidized to triiodide and the resulting free electrons reduce the oxidized dye back to into the ground state.

- Meanwhile the free electrons from TiO_2 move into the circuit. The move to the anode where they reduce the triiodide back to Iodide.

The advantages of this technology are their low-production cost in comparison to Si-based PV systems. Additionally, only the transport of electrons through the system is of importance. Still, it is possible for the electrons to recombine with the dye, but it is very unlikely as the dye receives electrons from the electrolyte much faster. Also, it is possible for the recombination to happen between TiO_2 and the dye, but the rate is slow too. However, that means that it is very important for the catalyst to provide fast electron transfer to the electrolyte [35].

Due to these kinetically properties, DSSCs are not only able to work with low-light but also with diffuse light, making them very attractive for low light regions as well as for indoor use. Additionally, the architecture of DSSCs is making them more stable towards environmental stress. However, the DSSCs also have their disadvantages: The electrolyte, for example, is very sensitive to temperature. Too high temperatures lead to an expansion which could damage the sealing. On the other side, too low temperatures can cause the electrolyte to stop working due to freezing. Also, the Ru-based sensitizers as well as the Pt-based catalysts are still very expensive [36].

However, most of the inorganic-PV is integrated into heavy and environment-resistant boxes to prevent them from any harm. The result is a raise of internal temperature, which decreases the efficiency of the semiconductors. The light architecture of DSSCs enables the modules to release more heat out of the cell, keeping the internal temperature lower. This property is very beneficial for the efficiency of DSSCs.

2.5 Hydrogen-bonding Dyes

As already mentioned before, dyes are already used for photovoltaics in DSSCs. Recently, the group of Glowacki et al. has shown that H-bonding dyes like quinacridones show high field-effect mobility, almost in the same range as pentacene. Additionally, they found that photo induced charge generation in single-layer diodes is more than a hundred times more efficient than in pentacene diode devices [37].

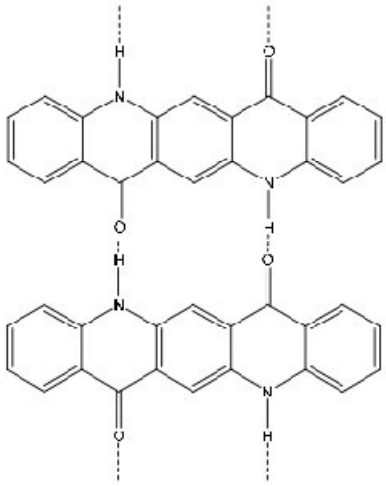

Figure 10: H-bonding Quinacridone

H-bonding dyes build up a long-rang order network held together by H-bonds. This leads to the advantage that intermolecular π-π interactions are beneficial to the free charge carrier transport increasing the conductivity of the dye [38]. Materials, which can transport electrons as well as holes, are called ambipolar. This property is very important as it is a prerequisite to build a homojunction solar cell with those dyes. In addition, the long-range order leads to lower exciton binding energies what makes them very suitable for further OPV applications. Additionally, those dyes often have a high absorption coefficient which is closely connected to high quantum efficiencies [39].

As they are already in use as pigments and dyes in other fields than OPV, as far as the dye itself is concerned, the advantage over commonly used OPV active materials is, of course, the cheap and easy synthesis in industrial scale. Also, they are light stable and resistant to environmental and thermal stress [40].

2.6 Solar Cell Parameters

To characterize solar cells, the current-voltage (I-V) characteristics are recorded under illumination and under dark conditions. The standardized procedure to measure solar cells is under illumination by light with an air mass 1.5 spectrum (AM 1.5, see Figure 11), which represents the sun's rays travelling through the earth atmosphere under an angle of 48.2° due to the earth tilt [41]. To fit the same radiation intensity on the cell as on the earth's surface, the power input is set to 1000 W/m².

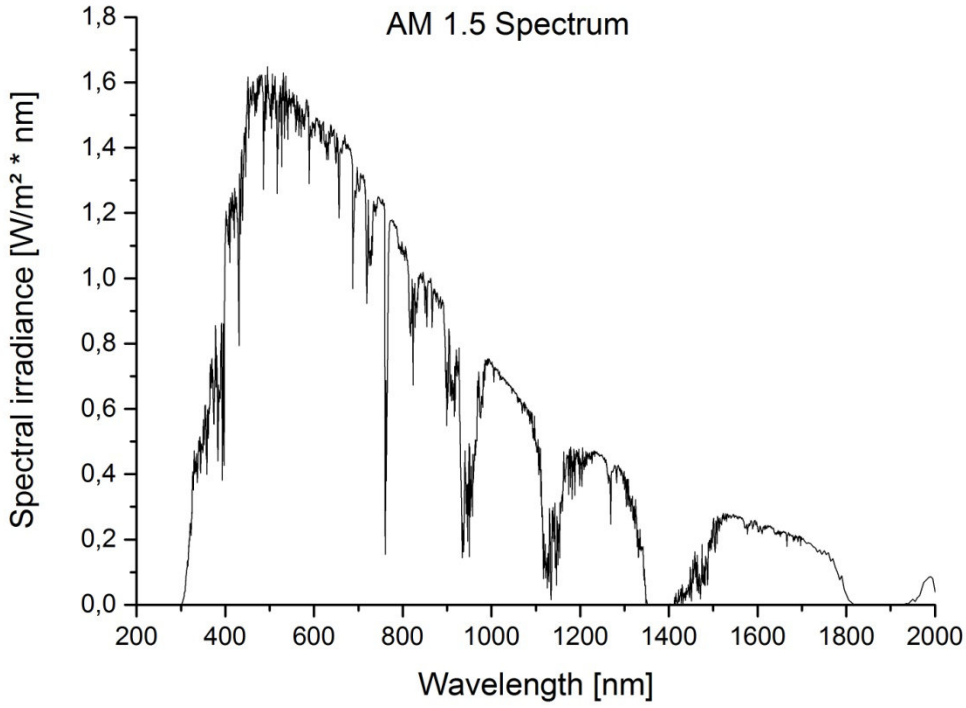

Figure 11: AM 1.5 Spectrum according to NREL [42]

The efficiency of a solar cell is determined by four main parameters:

- Open Circuit Voltage (Voc)

  The Voc is the voltage remaining at zero current. In OPV this parameter is mainly determined by the difference of the donors HOMO level and the acceptors LUMO level [43]

- Short Circuit Current (Isc)

  Alike the Voc, the Isc is the current density at zero voltage. It strongly depends on the charge carrier mobility and the charge density through photo induction and therefore on the incoming light intensity. Additionally, the Isc is also influenced by the morphology of each layer [44] and the size of the solar cell. For a better

comparability, this work uses the short circuit current density (Jsc) where the Isc is divided by the active cell area.

- Maximum Power Point (MPP)

  The electrical power is defined by the equation:

$$P = U * I \qquad \text{Eq. 1}$$

  Regarding at the power characteristics in Figure 12, the point of maximum power is determined by the voltage V_{mpp} and the current I_{mpp}.

- Fillfactor (FF)

  V_{mpp} * I_{mpp} shows the maximum achievable power of the solar cell. The ratio of the resulting rectangulars of Voc * Isc and V_{mpp} * I_{mpp} is called the fillfactor. This fillfactor is a proof of quality for a solar cell.

$$FF = \frac{Vmpp*Impp}{Voc*Isc} \qquad \text{Eq. 2}$$

- Power Conversion Efficiency (PCE, η)

  This is actually the most crucial parameter as it shows the ratio between the incoming power of the light and the power output.

$$\eta = \frac{P_{out}}{P_{in}} = \frac{Voc*Isc*FF}{P_{in}} \qquad \text{Eq. 2}$$

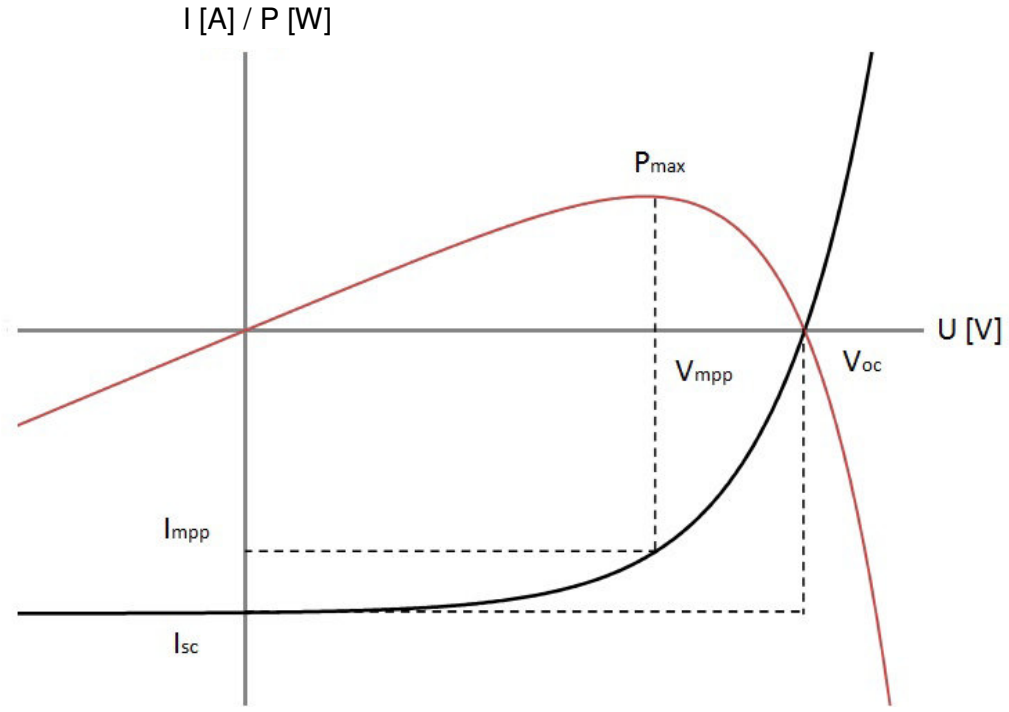

Figure 12: I/V curve of a solar cell, red: under illumination, black: dark measurement

2.7 Shockley-Queisser Limit

As mentioned before, HOMO and LUMO levels in solar cells are the key to separate charges and to generate electricity. The gap between those two levels is called the band gap and predetermines the maximum efficiency of the solar cell used.

In 1961, Shockley and Queisser proposed the limits of an ideal p-n junction diode when illuminated by a black body at a temperature of 6000K. Through losses, including spectral losses, blackbody radiation and radiative recombination, they found a maximum conversion efficiency of 30% at a band gap of about 1eV [45]. In Figure 13, M.A. Green shows that the Shockley-Queisser Limit for an isotropic photon converter at 300K. Here, the maximum efficiency in AM 1.5 sunlight can reach up to 34% [47,48].

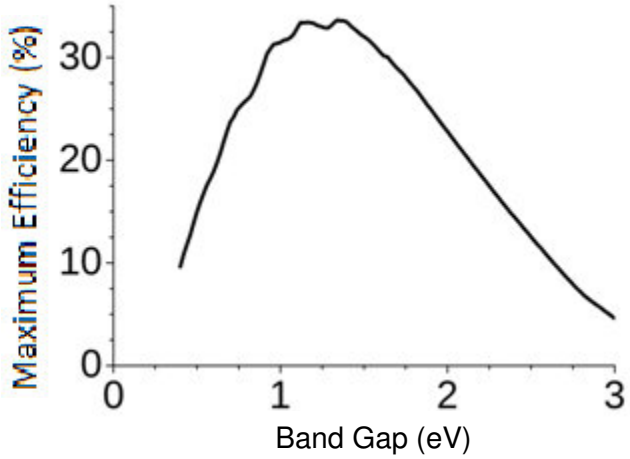

Figure 13: Shockley Queisser Limit according to reference [48]

However, those limits can be exceeded when different techniques for building solar cells are applied. Using tandem cells, by building solar cells on top of each other in series circuit, may extend the maximum up to 42 % for two cells, 49% for three cells and finally up to 68% using an infinite amount of cells. Additionally, if using concentrated light, this limit can be extended to 86% [46].

Another way of increasing photovoltaic efficiencies is the impurity photovoltaic (IPV) effect where sub-bandgaps contribute to the absorption of photons smaller than the band gap. A.S. Brown and M.A. Green showed in their calculation for such a device an impressing efficiency of 77.2% [49].

As already said before, radiative recombination is an important factor regarding the maximum efficiency of a solar device. The following Figure 14 shows the losses of efficiency depending on the external radiative efficiency (ERE). Looking at single junction crystalline solar cells, EREs are found to be between 0.01 – 1 % and therefore, maximum efficiencies between 22% and 28% are possible. However, organic solar cells depend on the separation of the generated exitons whereas the recombination of free charge carriers is a nearly non-radiative recombination (ERE~10^{-7}%). Considering this, the maximum efficiencies of organic solar cells is expected to be around 15% [50].

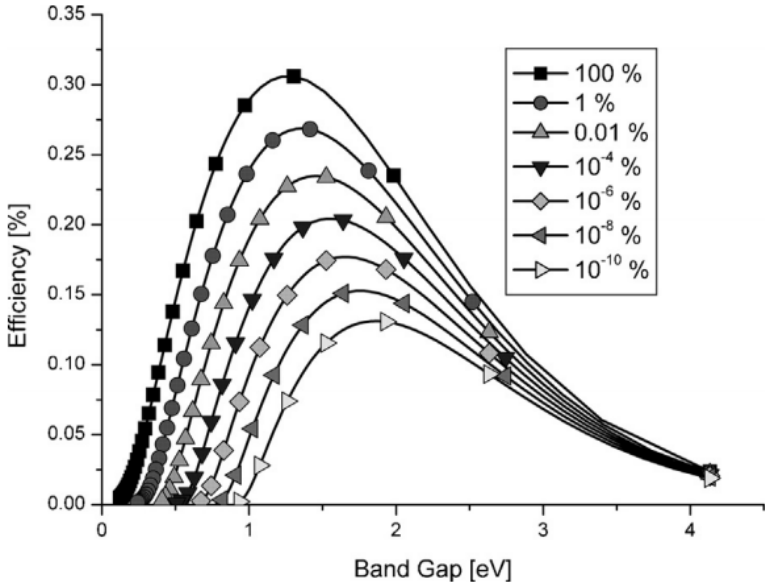

Figure 14: Shockley Queisser Limits for different radiation recombination characteristics of solar cells according to reference [45,51].

2.8 Self-Assembling Monolayers [SAMs] in OPV

SAMs consists of molecules with the ability to spontaneously build monolayers on suitable surfaces. This behaviour is caused by the strong affinity of the head group of the molecule to the surface. Usually, the SAM building characteristic belongs to surfactant molecules, but also molecules from other groups like carboxylic acids, phosphonic acids, thiols and trichloro-silanes can form SAMs on appropriate surfaces [57-62].

There are various ways to prepare SAMs on surfaces: Common ways of preparation are either dipping the surface into a solution containing the SAM molecules or dropping a solution onto the surface and spread it via spin coating. Further methods are organic molecular beam epitaxy and gas phase deposition [63, 64].

However, SAMs are excellently suitable for modifying surface properties. In OPV, SAMs can directly manipulate electrodes as well as intermediate layers like ZnO or TiO_2. Through the introduction of a dipole moment, the workfunction of the corresponding layer can be either increased or decreased [65]. Figure 15 shows, how a SAM influence the dipole.

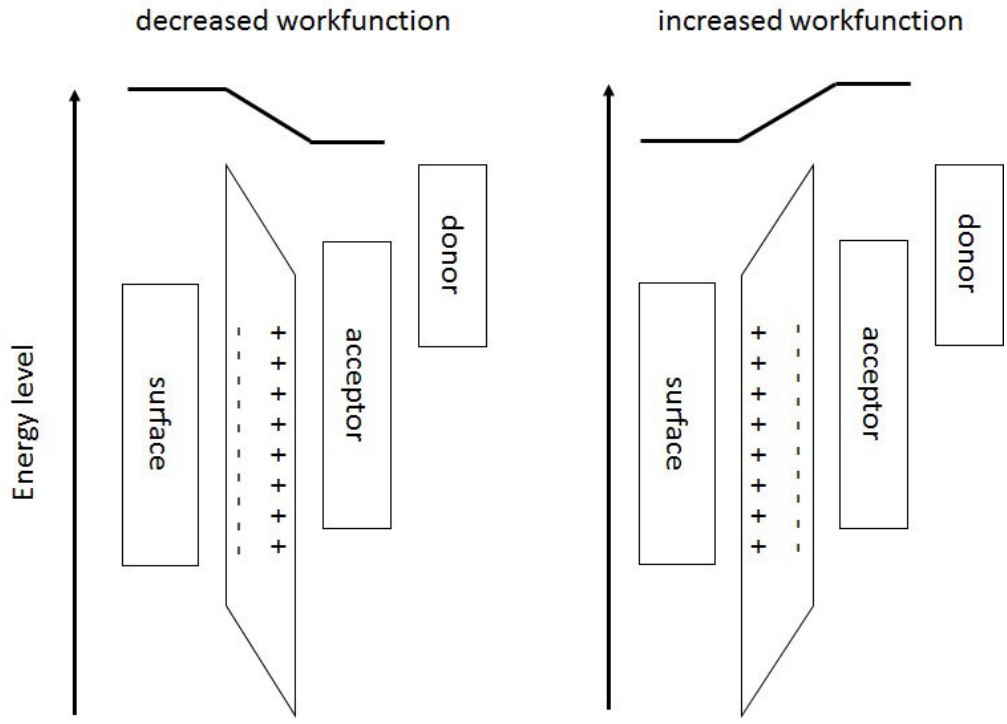

Figure 15: Influence of the dipole moment on the workfunction

To introduce either a negative or a positive dipole moment, the molecules have to have either an electron drawing or an electron pushing group, depending on the corresponding surface.

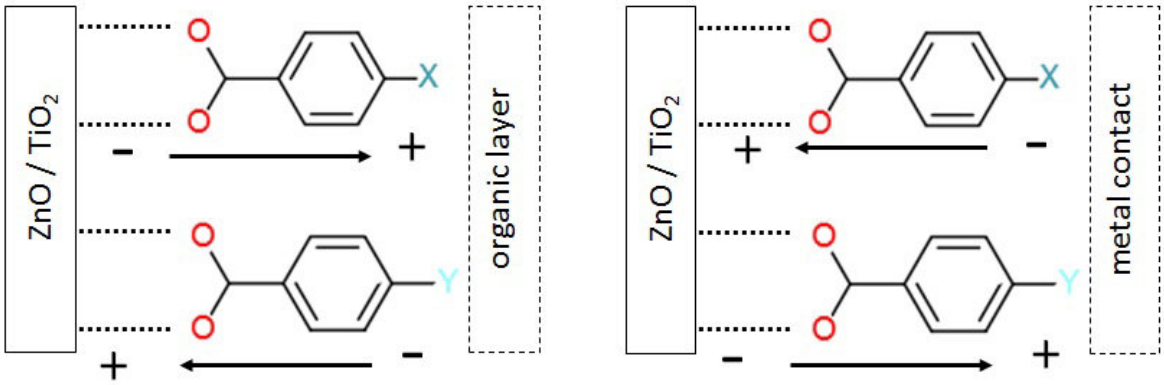

Figure 16: Difference in net dipole moment, X: electron pushing, Y: electron drawing

As seen in Figure 16, the effect of positive net dipole moment for organic layers results in the opposite effect for metal contacts. A net dipole moment towards the metal contact results in an ohmic contact which leads to an increase of the Voc. A net dipole away from the metal contact leads to a tuning of the conductive band of either ZnO or TiO_2, but increases the effect of a Schottky barrier, which results in a decrease of the Voc. In this work, SAMs will only applied between TiO_2 and the active organic layer, thus electron drawing SAMs should lead to an increase of the solar cell performance.

Furthermore, Hau et al. showed not only that SAM enhanced TiO_2 surfaces in inverted solar cells led to higher performances, they also led depending on the functionality of the SAM to an improvement of the contact resistance as well as the charge transfer. Additionally the overlayer distribution of phases, the morphology and the crystalline order were improved [66].

2.9 Aim of this thesis

Photovoltaic applications are now on the market since nearly 30 years; however, the energy input for the production of classical silicon based solar cells is quite high, which gives rise to the research on cheaper alternatives. One of the best candidates to archive low-cost production prices is OPV. Although OPV bulk-heterojunctions will never beat the efficiency of crystalline PV-systems due to the Shockley-Queisser limit as shown before, the price for production and materials can be lowered dramatically. That could lead to a lower $\$/W_p$ price than already available PV-modules, making them attractive for commercial use. Still, the prices for OPV are very high, as the best results were archived with high-tech polymers and molecules like PCBM [60] and P3HT. However, a solution can possibly found in ambipolar dyes which are not only potent for electrochemical reasons but also they are easy to synthesise in industrial scale. Therefore, this work focuses on the following four H-bridging diammino-anthraquinone dyes seen in Figure 17-20:

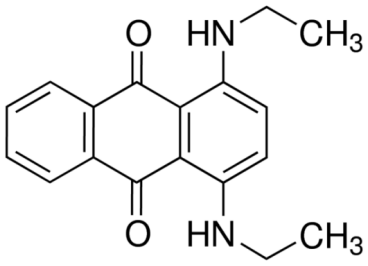

Figure 17: Structure of Sudan Blue I (SB I) [1,4-Bis(ethylamino)-9,10-anthraquinone]

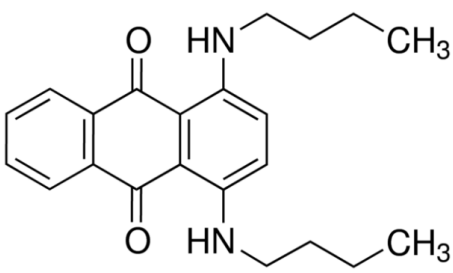

Figure 18: Structure of Sudan Blue II (SB II) [1,4-bis(butylamino)-9,10-anthraquinone]

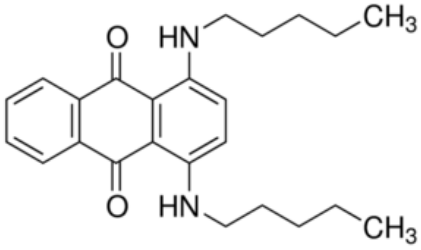

Figure 19: Structure of Oil Blue N (OBN) [1,4-bis(pentylamino)-9,10-anthraquinone]

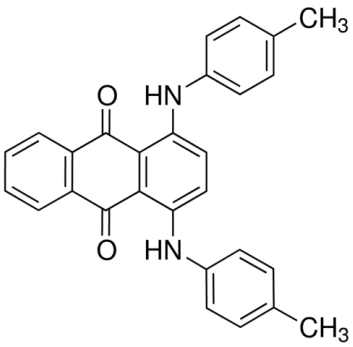

Figure 20: Structure of Solvent Green 3 (SG 3) [1,4-bis[(4-methylphenyl)amino]-9,10-anthraquinone]

The first part of this thesis focuses on the characterization of these four diammino-anthraquinone dyes. For the determination of the band gap cyclic voltammetry (CV) as well as UV-Vis measurements will be used. Additionally, layer thicknesses of the active layer will be determined by profilometry measurements and analysed through optical microscopy. For the characterization of SAMs, contact angle measurements using H_2O and CH_2I_2 will be performed. The following Figures 21 – 23 show the benzoic acids used for SAM preparation as well as the acceptor material PCBM[60] and donor material P3HT.

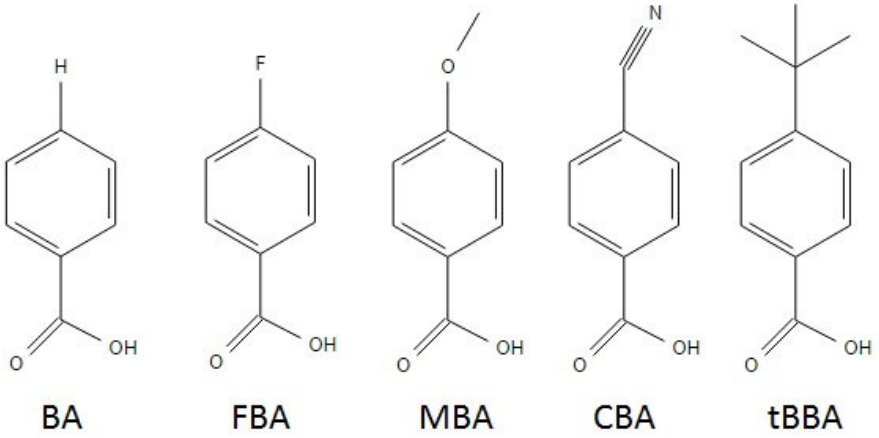

Figure 21: Benzoic acids used as self-assembling molecules

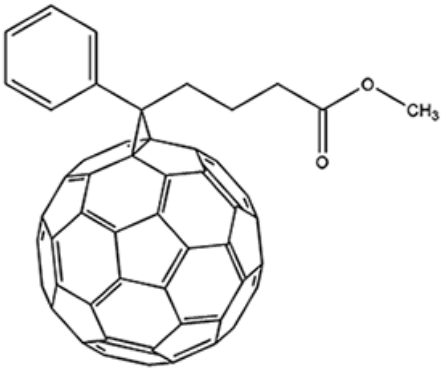

Figure 22: Structure of PCBM[60]

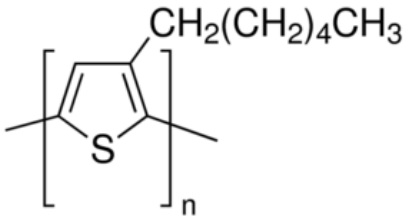

Figure 23: Structure of P3HT

The aim of the second part of this thesis is to investigate the ambipolar behaviour of those diammino-anthraquinone dyes through integration into a bulk-heterojunction solar cell as well as into homojunction solar cells. If the dyes work in homojunction architecture, it can be assumed that they exhibit ambipolar behaviour. In bulk-heterojunction they will be used as donor material in combination with the acceptor material [6,6]-phenyl-C_{61}-butyric acid methyl ester (PCBM[60]) and they will be tested in acceptor position together with Poly(3-hexylthiophen-2,5-diyl) (P3HT) as donor. All solar cells will be built in normal as well as in inverse architecture where TiO_2 will be used as ETL. In addition, the influence of SAMs on the I-V characteristics of the solar cells is investigated, consisting of benzoic acid and para-substituted derivatives of benzoic acids chemically bound to TiOx.

3 Results and Discussion

3.1 Characterization of Dyes

All dyes are characterized through UV-Vis and cyclic voltammetry (CV) in order to receive the corresponding band gaps. Through these band gaps the HOMO and LUMO levels can be calculated.

3.1.1 UV-VIS-spectroscopy

UV-Vis measurements have been performed in two different media: First all dyes are measured in solution. As acetonitrile is used as solvent for CV measurements the same solvent is used for UV-Vis measurements. The second medium is in thin film where any influences of the solvent are excluded. However, through the forming of crystals other effects might appear.

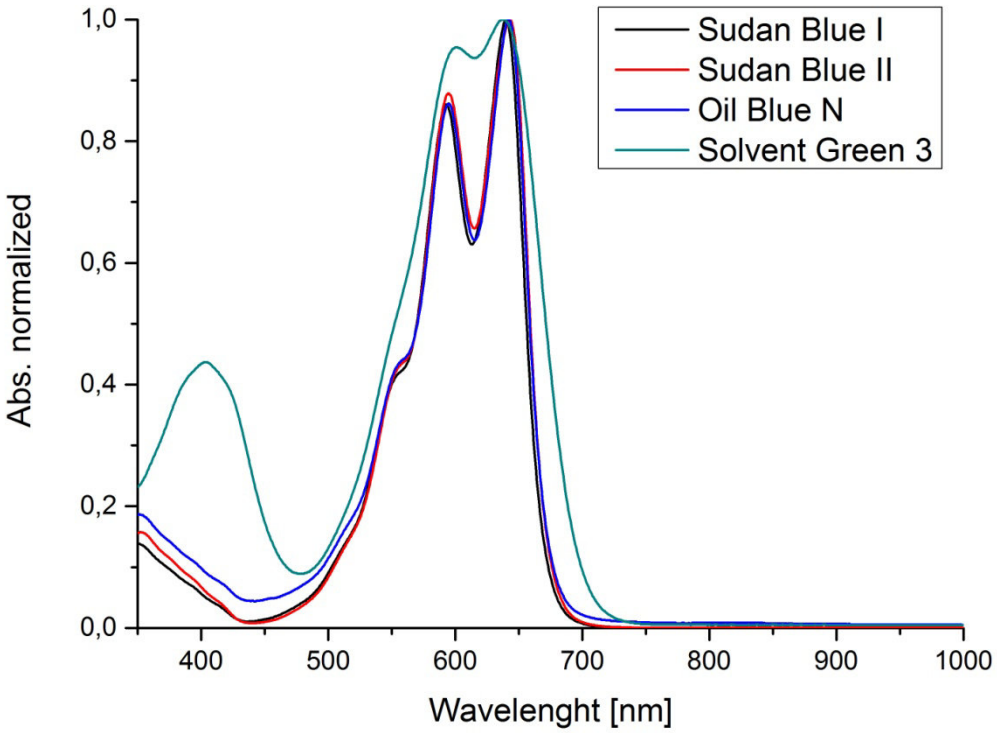

Figure 24: UV-Vis spectra of the dyes in ACN

As seen in Figure 24, the spectra of all dyes lie very close together. The two absorption maxima are found around 590 and 640 nm. Additionally all dyes slightly absorb in the UV-range due to the aromatic ground structure. Only SG 3 shows an increased absorption at 400 nm due to the benzylic groups which form the side chains. These values fit to the values found by Marzec for similar anthraquinone dyes measured in chloroform [69]. Additionally, Marzec showed a high absorption for these dyes in the range of 230 nm.

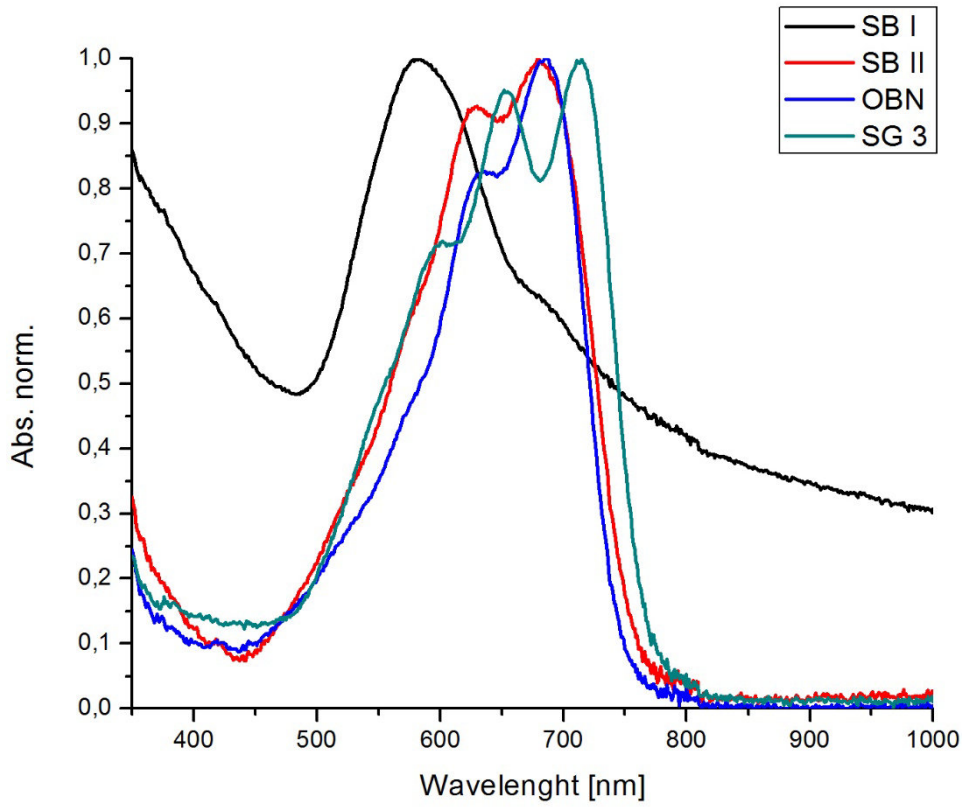

Figure 25: UV-Vis spectra of the dyes in thin film

Interestingly, the spectra gained from thin films with thicknesses in the range of 80 to 100 nm are strongly shifted towards higher wavelengths. This includes the absence of H-bonds in solution but a presence of H-bonds in thin films. The first maximum is found around 630 nm and the second maximum is found at 690 nm for SB II and OBN and 720 nm for SG 3. Only SB I shows a hypsochromic shift and a broad absorption over the whole spectrum. Additionally, in comparison to the other dyes, SB I just shows one absorption peak at 570 nm and a light shoulder at 680 nm. However, the absorption maximum of SB I is found at the lowest wavelength while the absorption maximum of SG 3 is found at the highest wavelength similar to the absorption behaviour in solution. Therefore, the fact that all dyes nearly overlap in solution but differ more in bulk, the crystal structure as well as the capability to build hydrogen bonds must be significantly different for each dye.

3.1.2 Determination of the optical band gap

To determine the optical band gap of the dyes the Tauc Plot is used [52]. For the absorption coefficient α, a direct relationship to the energy of photons $h * \upsilon$ is stated in the equation below:

$$\alpha = \frac{A}{h*\upsilon} * (h * \upsilon - Eg)^n \qquad \text{Eq.1}$$

in which A is a constant and n an exponential factor between 0.5 and 2, depending on the type of transition [53]. In this case the type of transition is a direct transition and therefore n has to be 0.5. Thus, following equation applies:

$$\alpha = \frac{A}{h*\upsilon} * \sqrt{h * \upsilon - Eg} \qquad \text{Eq. 2}$$

When resolved to

$$(\alpha * h * \upsilon)^2 = A^2 * (h * \upsilon - Eg) \qquad \text{Eq.3}$$

a linear connection between $(\alpha * h * \upsilon)^2$ and $h * \upsilon$ can be found and therefore be plotted.

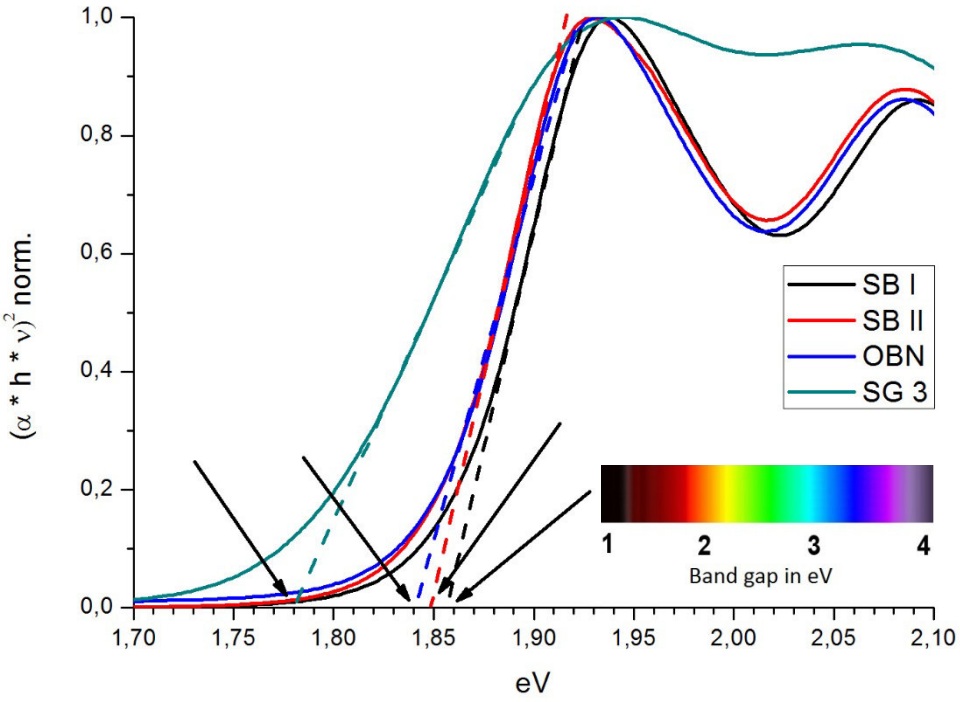

Figure 26: Optical band gap from dyes in ACN; normalized Tauc-Plot

The intersection of the linear part of $(\alpha * h * \upsilon)^2$ with the x-axis results in the band gap energy representing the optical band gap. Figure 26 shows that the band gaps of SB I, SB II and OB N lay very close together at 1.84, 1.85 and 1.86 eV, indicating that a longer side chain leads to a decreasing band gap. Hence, SG 3 with its benzyl-groups has the lowest band gap of 1.78 eV.

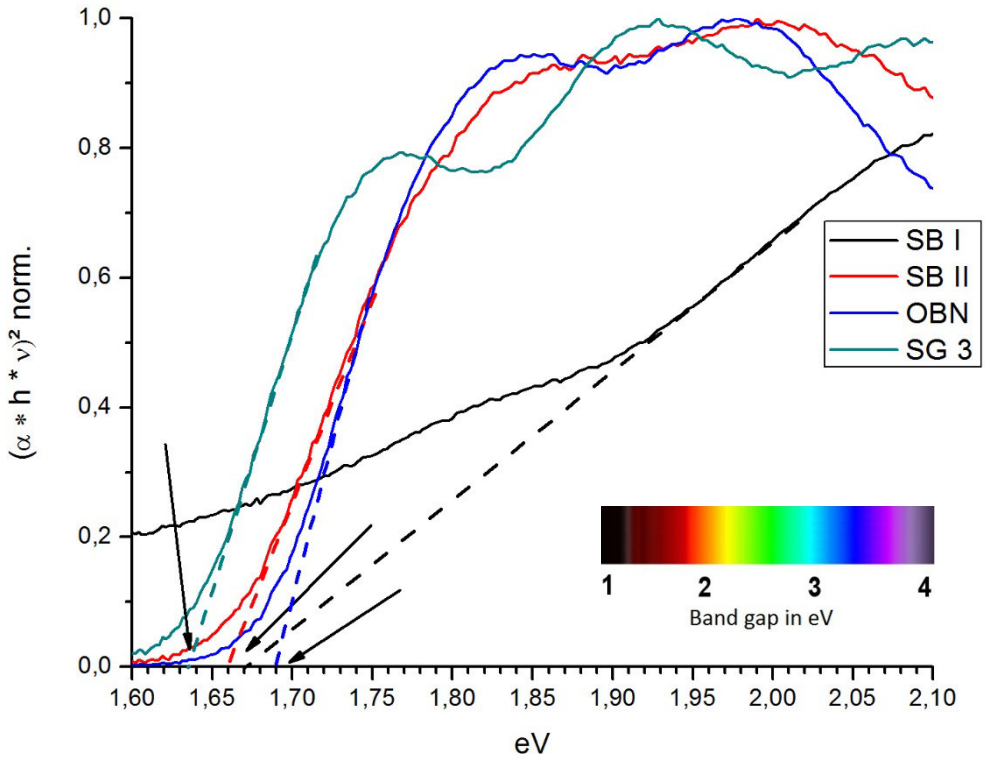

Figure 27: Optical band gap from dyes in thin film; normalized Tauc-Plot

As expected, the band gap in thin film is significantly lower in thin films than in solution. The only surprising value is found for SB I as it lies between those of SB II and OBN. However, the band gaps of the dyes used in thin films can be found at 1.63 for SG 3, 1.66 for SB II, 1.67 for SB I and 1.69 eV for OBN.

3.1.3 CV measurements

The CV measurements are used to determine the reduction potential E_p^{red} and the oxidation potential E_p^{ox}. Also they show the amount of electrons needed for a red/ox reaction and whether the reaction is reversible or irreversible. Figure 28 shows the scheme to determine these properties.

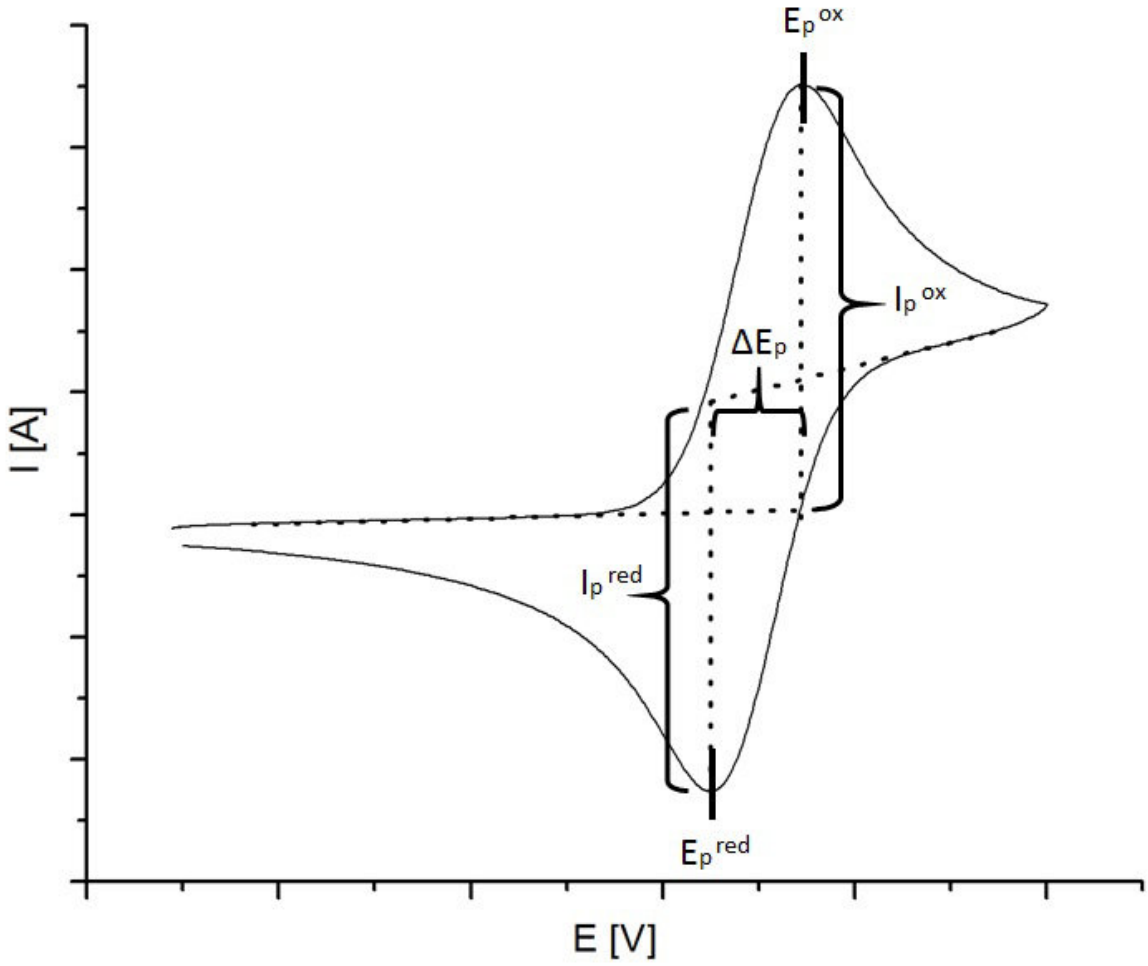

Figure 28: Scheme of a CV measurement

To find the numbers of electrons (n) needed for the reaction $\frac{\Delta Ep}{n} \approx 59\ mV$ Eq. 4

A reaction can be considered reversible when $\frac{I_p^{ox}}{I_p^{red}} \approx 1$ Eq. 5

Intersecting the linear part of the first peak of either reduction or oxidation with the x-axis leads to the onset of E_{red}^{on} and E_{ox}^{on}. Both parameters are needed to further determine the HOMO and LUMO distribution of the dyes used.

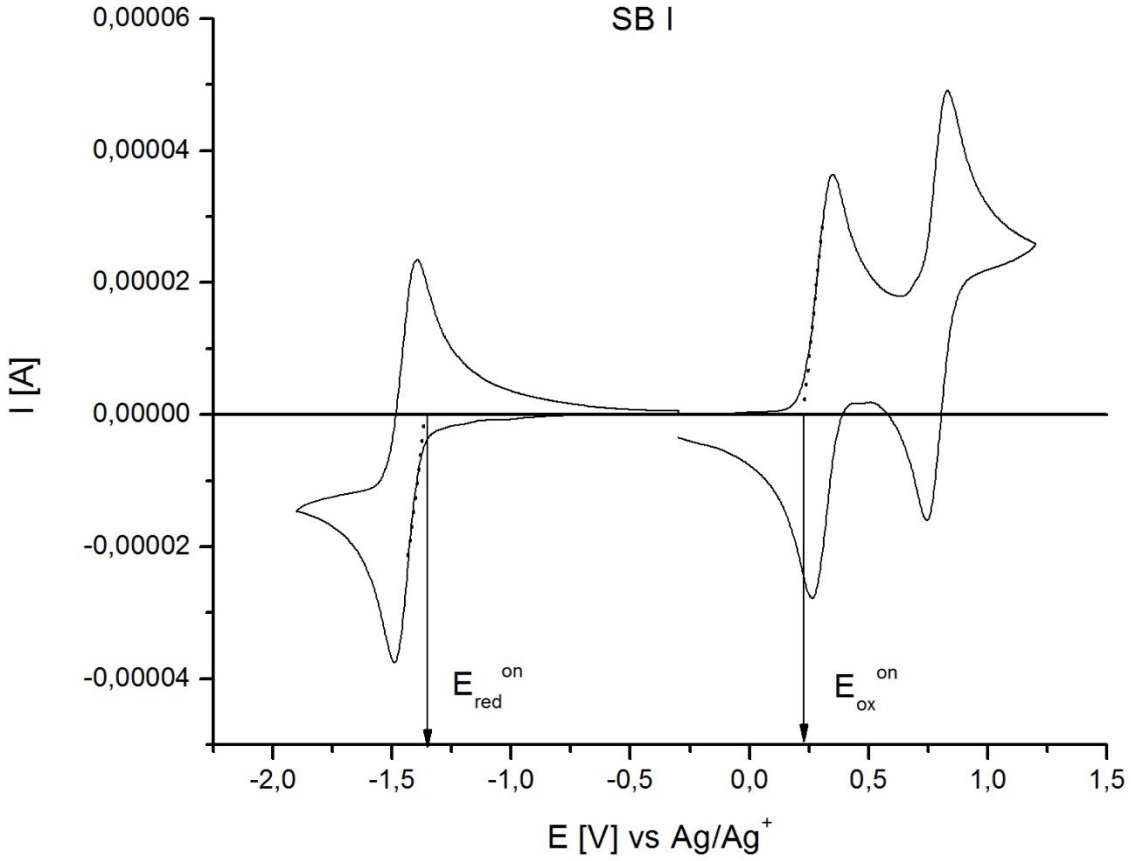

Figure 29: CV of SB I

CV-measurements in Figure 29 show two fully reversible reactions for the oxidation of SB I at 0.33 and 0.82 V. The onset E_{ox}^{on} is found at 0.22 V. The reversible reduction takes place at -1.49 V with an onset E_{red}^{on} of -1.37 V. All reactions are one-electron reactions.

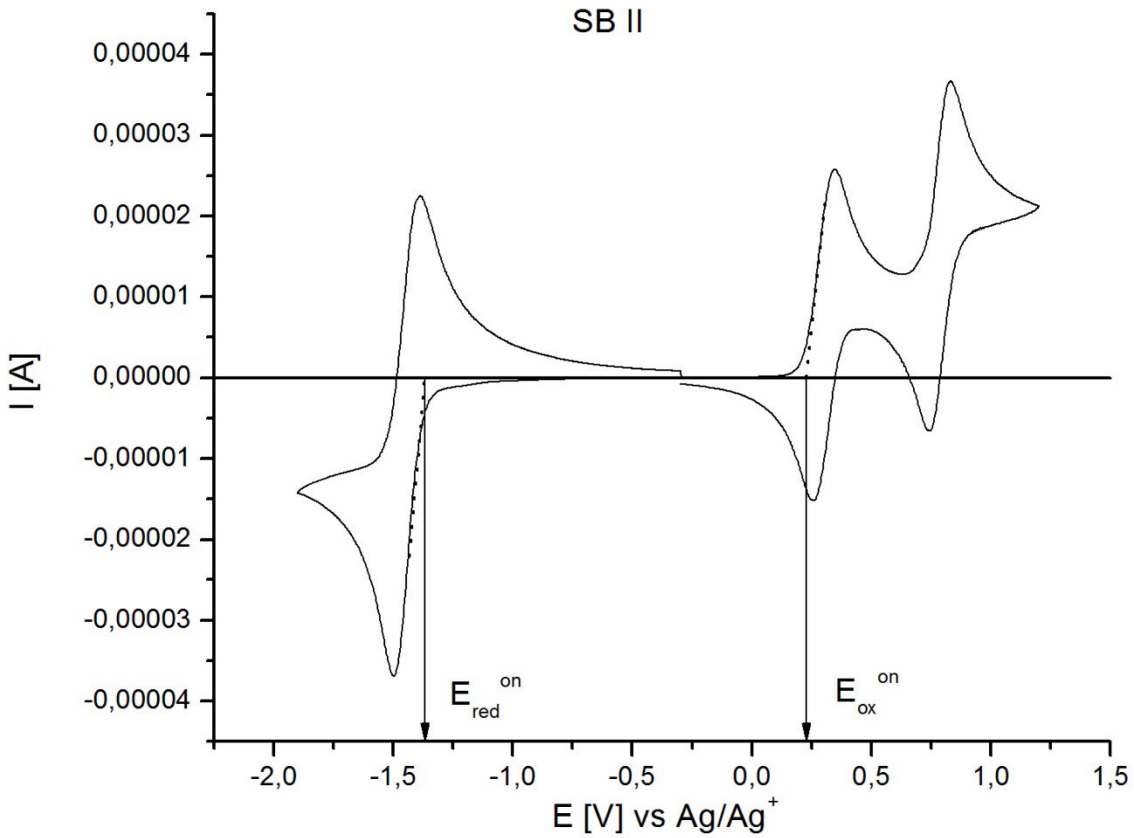

Figure 30: CV of SB II

Similar to SB I CV-measurements in Figure 30 show two fully reversible reactions for the oxidation of SB II at 0.32 and 0.81 V. The onset E_{ox}^{on} is found at 0.21 V. The reversible reduction is found at -1.50 V with an onset E_{red}^{on} of -1.38 V. All reactions are one-electron reactions.

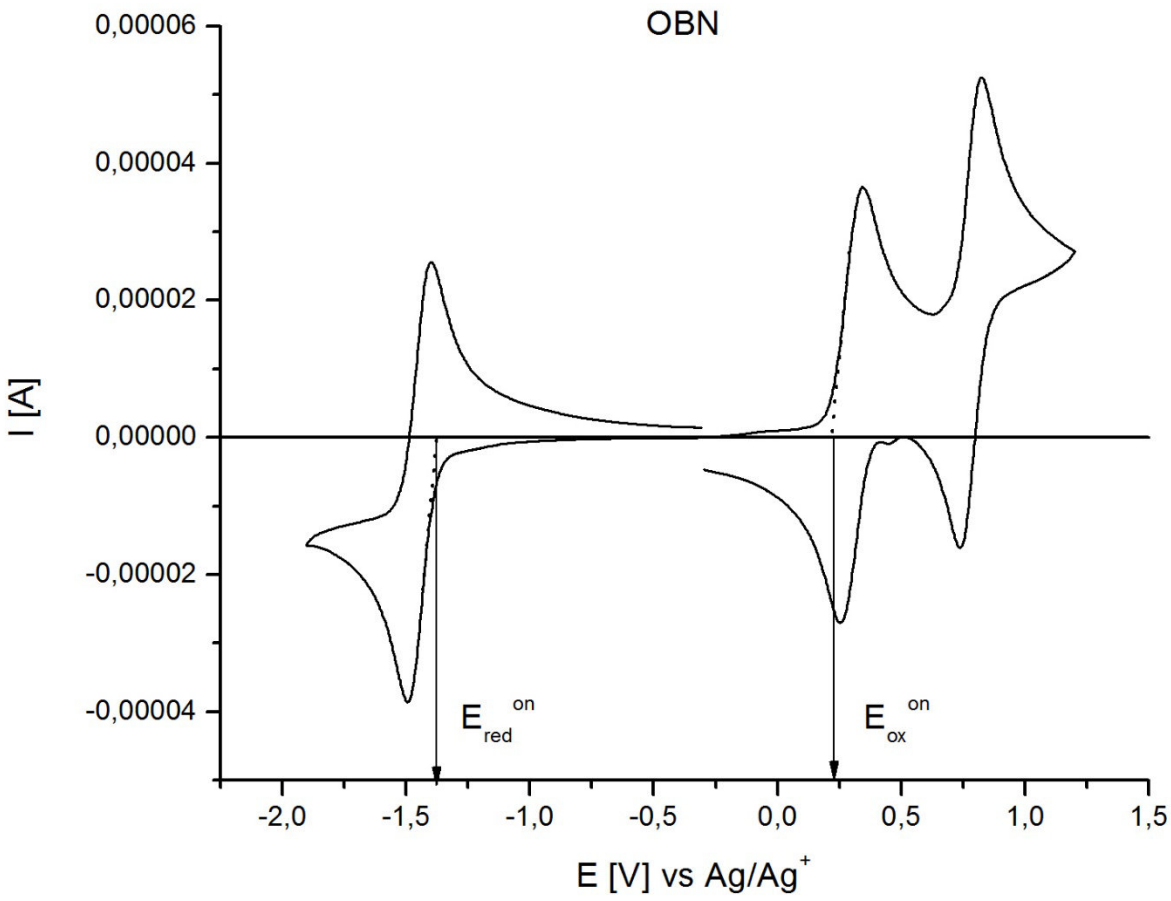

Figure 31: CV of OBN

Like the other dyes before, Figure 31 shows two reversible one-electron reactions for oxidation too at 0.36 and 0.81 V with an onset E_{ox}^{on} at 0.22 V. The reduction appears at -1.50 V with an onset E_{red}^{on} at -1.37 V and also is a one-electron reaction.

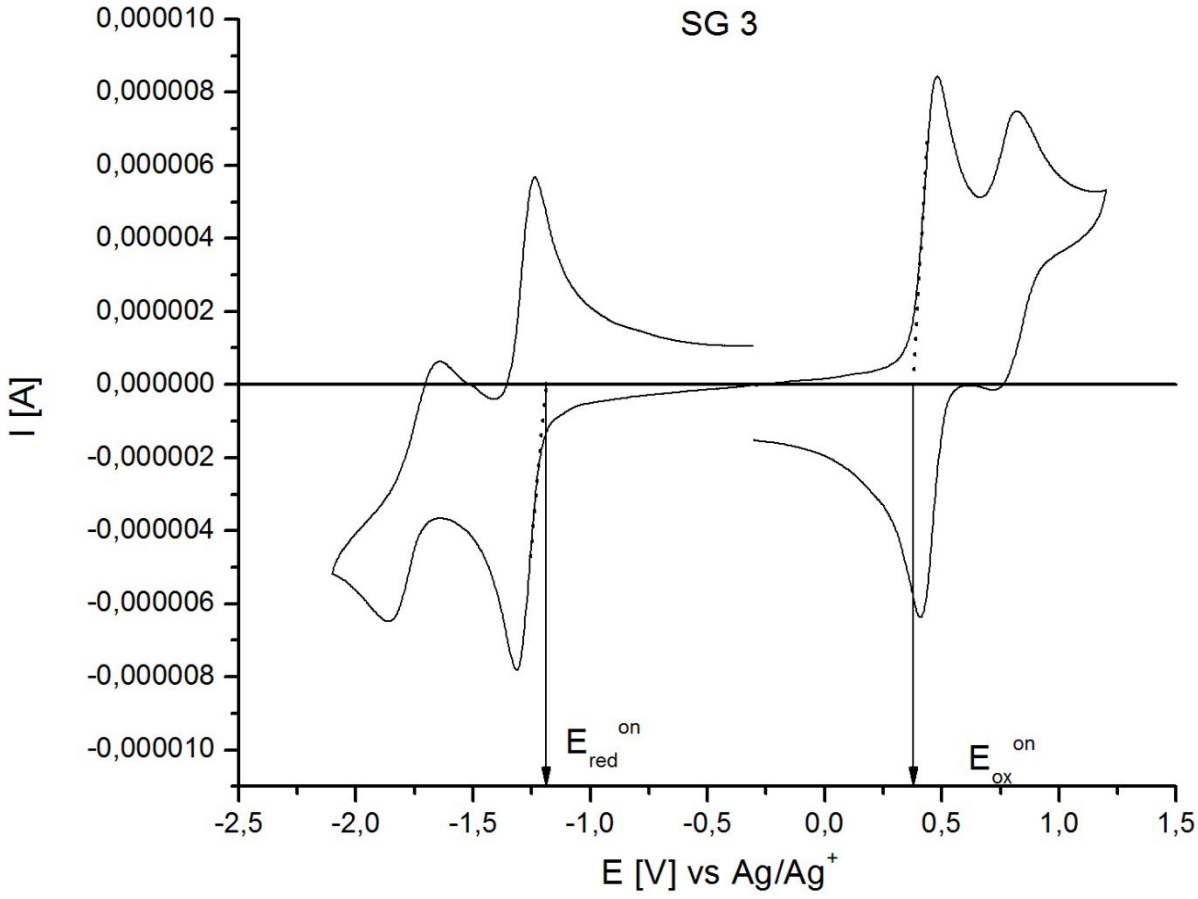

Figure 32: CV of SG 3

Unlike the other dyes, Figure 32 shows two reversible reactions for reduction at -1.3 and –1.82 V and an onset E_{red}^{on} of -1.19. This does not exclude the other dyes from having a second reduction peak, but they could not be found within the stability window of the solvent used. E_{ox}^{on} can be found at 0.37 V and oxidation peaks at 0.49 and 0.82 V. All reactions are one-electron reactions.

Due to the similarity of the chemical structure and the red/ox potentials of the dyes, it is assumed that during oxidation the two amino-groups are oxidized. Under reductive conditions, the oxygen of the two keto-groups will be reduced.

3.2 HOMO and LUMO from CV and UV-Vis

To determine the HOMO and LUMO from those anthraquinone dyes, the method of Veldmann et al. and Beverina et al. is used [54,55] where $E_{1/2}$ of Ferrocene is used for the purpose of correction. Therefore, the following equation is used:

$$E_{HOMO} = \frac{1}{2}\left(E_g^{CV} - E_g^{opt}\right) - E_{ox} - (5.23 + E_{1/2}) \quad \text{Eq. 4}$$

$$E_{LUMO} = \frac{1}{2}\left(E_g^{CV} - E_g^{opt}\right) - E_{red} - (5.23 + E_{1/2}) \quad \text{Eq. 5}$$

The following table sums up all gathered results from CV and UV-Vis-spectrum measurements in thin film (TF) and in solution (sol) as well as the results from HOMO and LUMO calculations.

Dye	$E_{1/2}$ [V]	E_{ox}^{on} [V]	E_{red}^{on} [V]	E_g^{CV} [V]	$E_g^{TF,opt}$ [V]	$E_g^{sol,opt}$ [V]	HOMO [eV]	LUMO [eV]
Sudan Blue 1	0,08	0,22	-1,37	1,59	1,67	1,84	-5,57	-3,98
Sudan Blue 2	0,08	0,21	-1,38	1,59	1,66	1,85	-5,56	-3,97
Oil Blue N	0,08	0,22	-1,37	1,59	1,69	1,86	-5,58	-3,99
Solvent Green 3	0,06	0,37	-1,19	1,56	1,64	1,78	-5,70	-4,14

Table 1 Electrochemical characterisazion of the dyes used

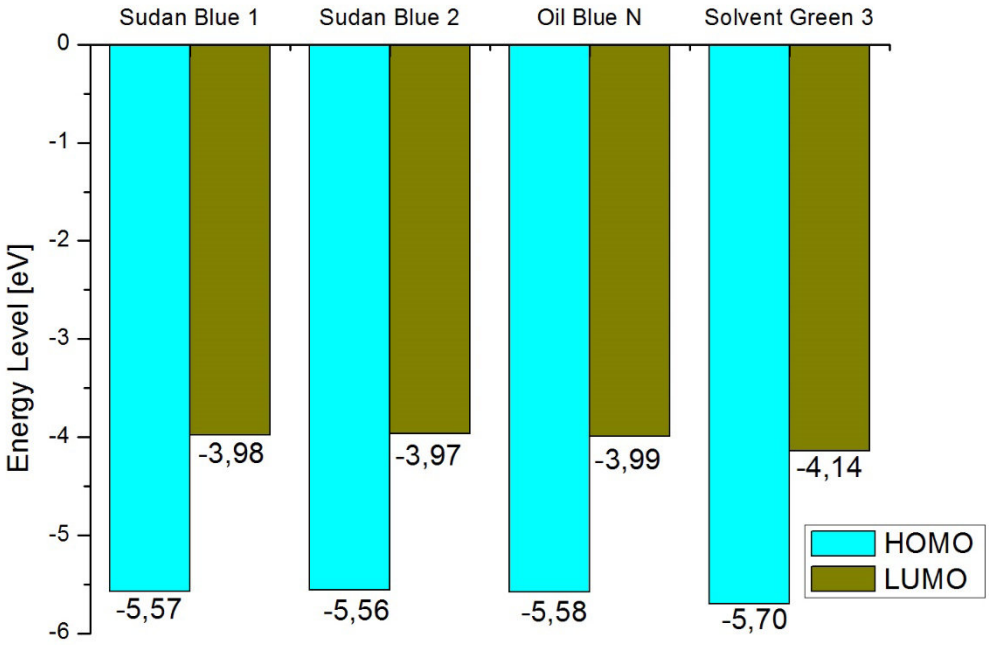

Figure 33: Calculated HOMO and LUMO levels of the dyes used

Comparing the band gap of SB 1 and SG 3 to the results gained by Kim et al. [70], the band gaps are found to be 0,2 - 0.3 lower than those of Kim et al. . The difference of the

band gaps can be explained through the use of a glassy carbon working electrode instead of a platinum disc electrode as well as the use of a different conduction salt. Additionally a different approach for the calculation of the HOMO and LUMO levels is used. A comparison can be made between SG 3 and the CV results from Solvent Blue used by Marzec, which is a SG 3 derivative with a pentyl group instead of a methyl side group. These results show similar oxidation and reduction peaks around 0.59 and -1.17 eV. The difference in potential is caused by the use of a different solvent [69]. The fact that $E_g^{CV} < E_g^{TF,opt}$ is caused by the higher permittivity in solution than in thin films [54]. Also, $E_g^{sol,opt}$ is 0.2 eV higher than $E_g^{TF,opt}$ which can be explained through a solvation effect and its influence on the intermolecular H-bonds. In CV, electrons are either added or removed directly to or from the according energy level. In optical measurements, electrons are promoted from the HOMO to the LUMO level. As n-π* transitions are very unlikely due to their forbidden nature, the optical transition in solution is a π- π* transition, which does not confer to the direct transition from the HOMO to the LUMO level [72]. Therefore, the band gap measured in solution is not connected to the band gap in thin film as the difference is probably caused by the H-bonds which do not occur in solution but in thin film. However, Veldmann et al. show that the max. Voc attainable is the lowest optical band gap E_g^{opt} minus 0.6V. Therefore, the maximum Voc is predicted to be around 1 V [54].

3.3 Solar Cell Production

This chapter shows the materials and architecture used for solar cell production.

3.3.1 Normal architecture

The schematic concept of a normal architecture solar cell is shown in Figure 31 below:

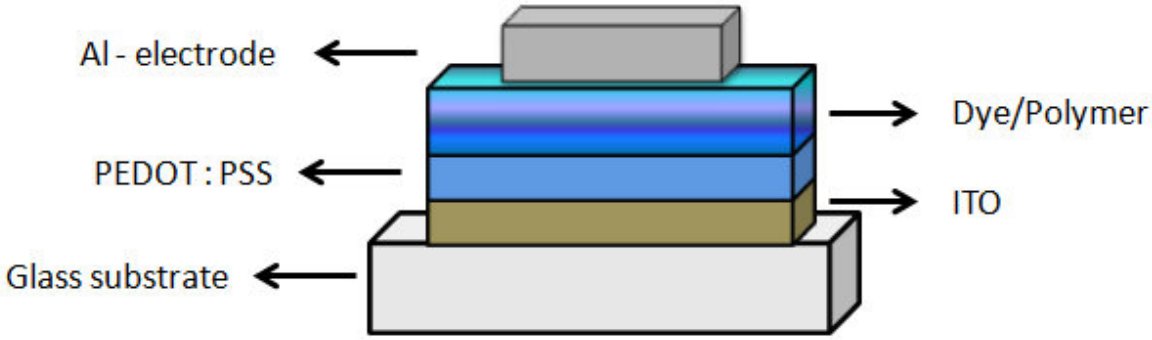

Figure 34 Scheme: normal architecture

Including the HOMO and LUMO levels gained by CV and optical experiments, the distribution of the HOMO and LUMO levels throughout the cells architecture are shown below:

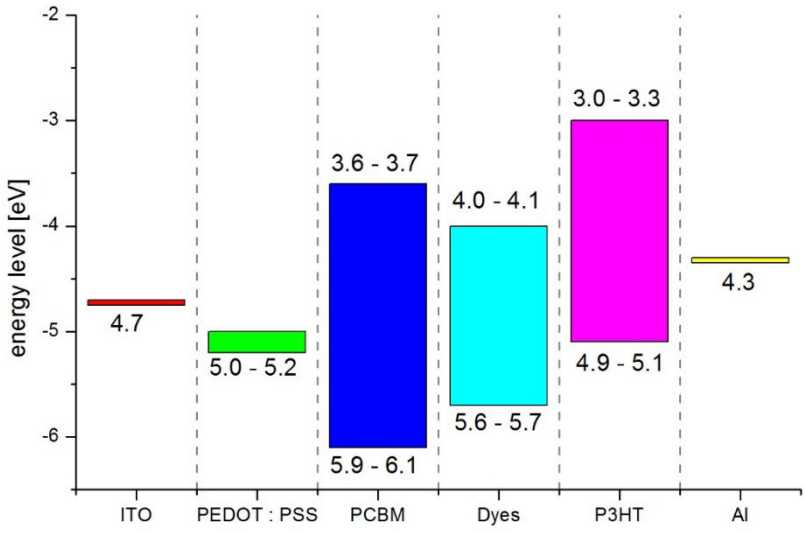

Figure 35: Energy levels in normal architecture

3.3.2 Inverse architecture

In comparison to normal architecture, inverse architecture offers an additional TiOx layer covering the ITO layer. The scheme of inverse architecture is shown in the figure below:

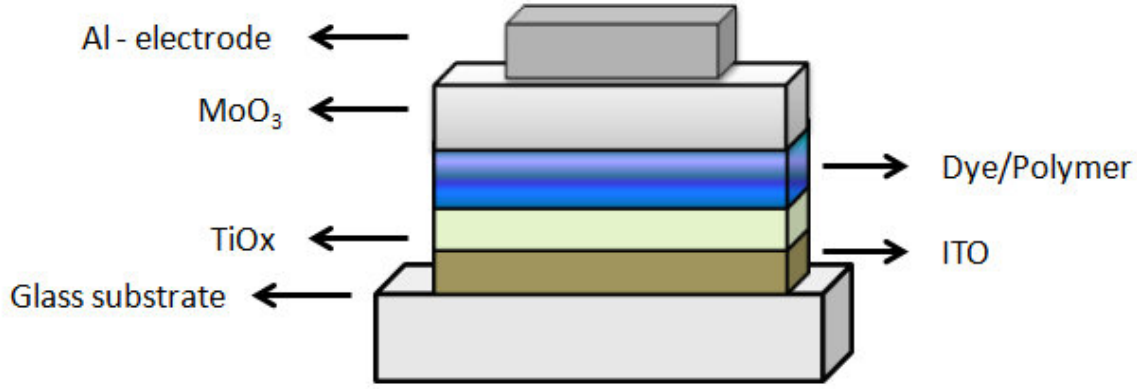

Figure 36 Scheme: inverse architecture

As it is already shown for normal architecture, the HOMO and LUMO level distribution for inverse architecture is shown in Figure 34 below:

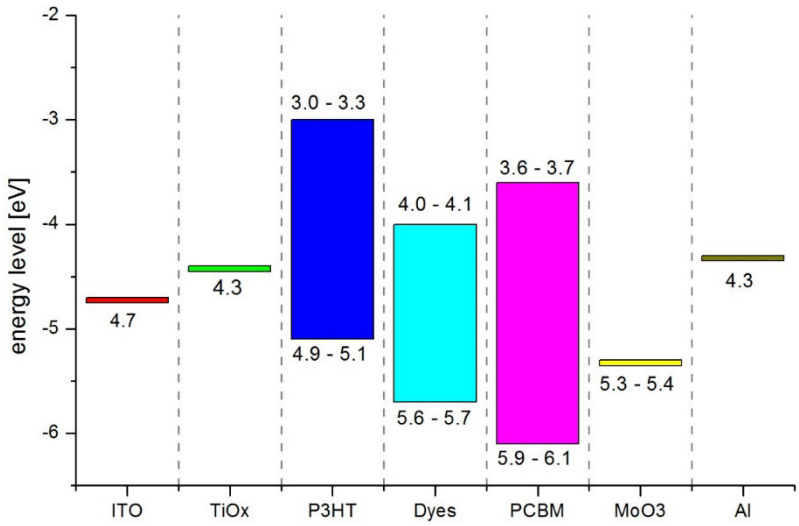

Figure 37: Energy levels in inverse architecture

When looking at the energy levels of the dyes compared to P3HT and PCBM shown in Figure 36 and 37, the dyes are expected to work better with P3HT than with PCBM.

3.4 H-bridging Dyes in OPV

This chapter focuses on the integration of dyes in solar cells. First, each dye is built into a homojunction solar cell. Then the dyes are introduced into a bulk-heterojunction system as donor material along with PCBM[60] and as acceptor material along with P3HT. All setups used are found in the experimental section.

3.4.1 Sudan Blue I [1,4-Bis(ethylamino)-9,10-anthraquinone]

Throughout the variety of setups, different film thicknesses from 50 to 200 nm and no functioning homojunction solar cell were achieved. The reason for the short circuited solar cell can be easily found in Figure 40: SB I forms crystals rods in the range of 10 – 25 µm. As they are loosely packed, they allow the current to bypass the crystals which leads to short circuits.

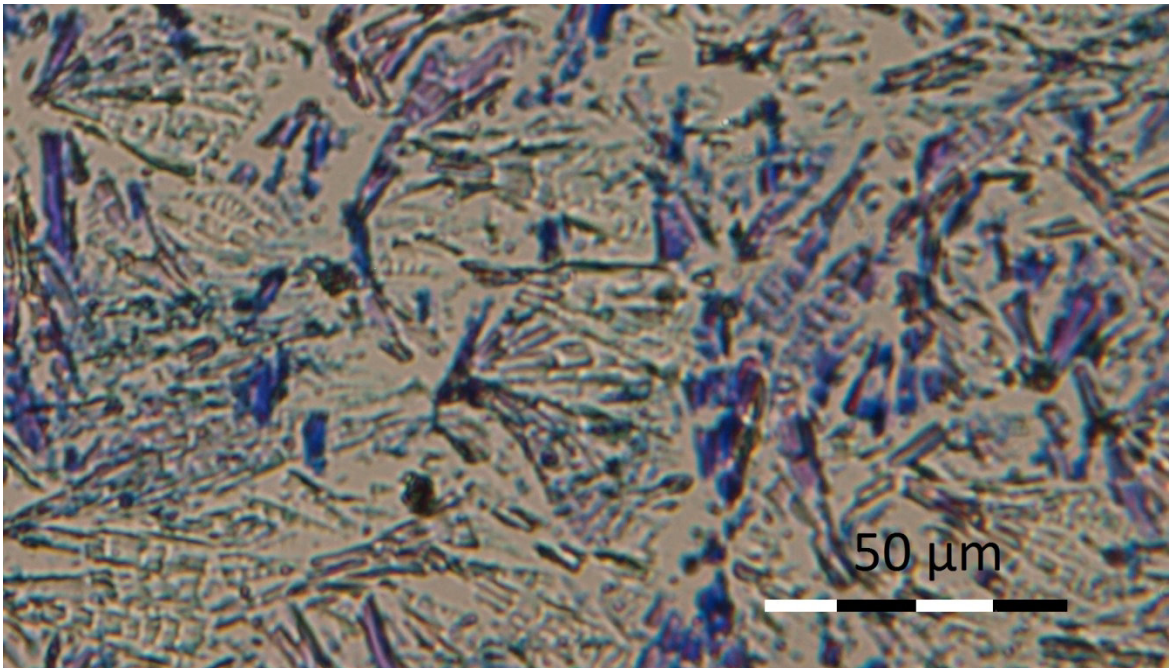

Figure 38: Light-microscopy of an inverse Sudan Blue I homojunction solar cell

When building bulk-heterojunctions, no functioning inverse PCBM [60] solar cell was achieved. The following Figures 39 and 40 show the J/U-curves as well as the overall performances of the SB I Bulk-heterojunctions.

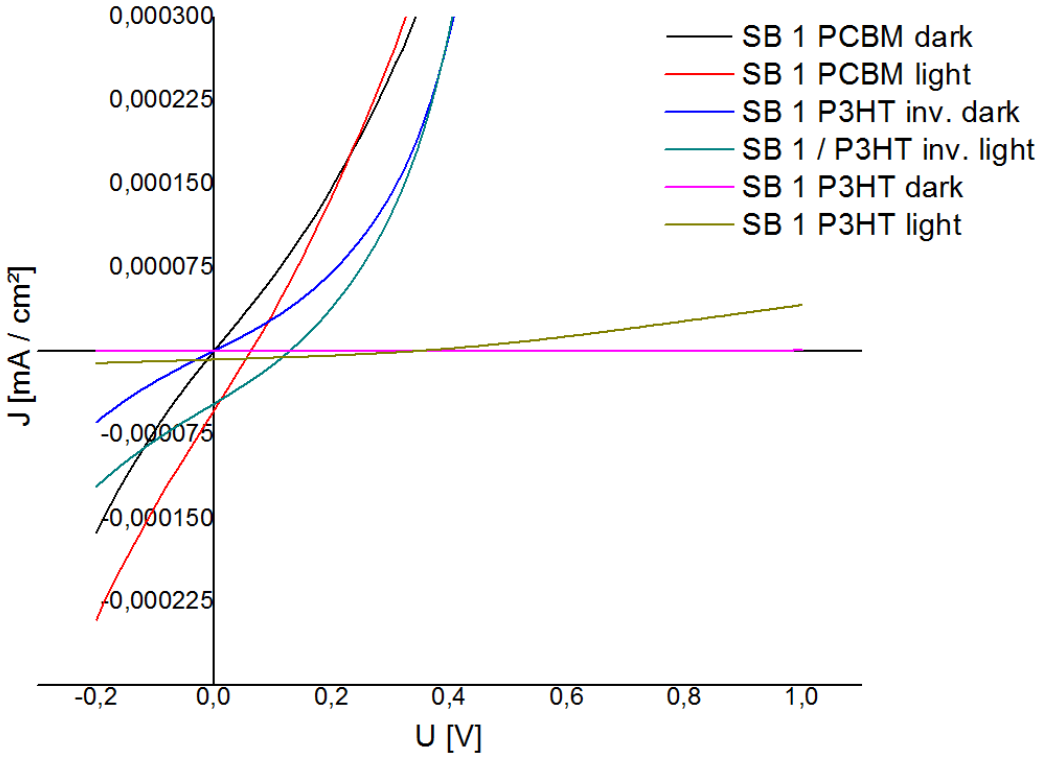

Figure 39: J/U-curves of SB I setups

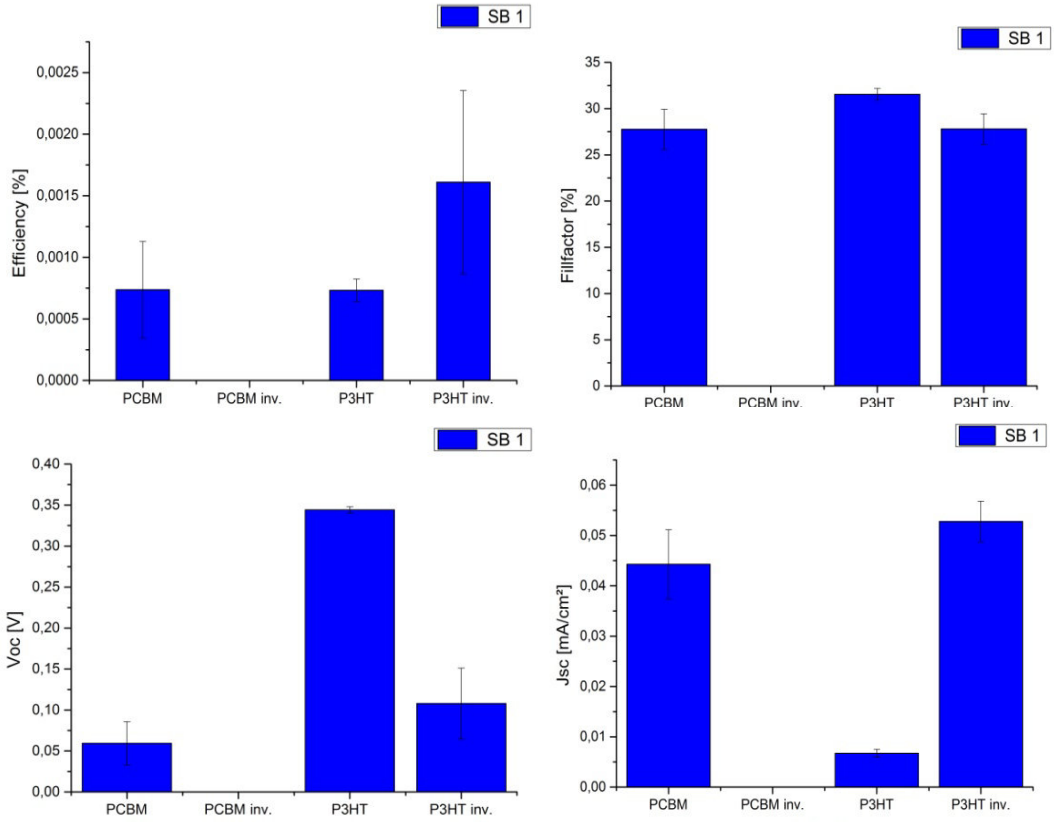

Figure 40: Solar cell parameters of SB I

As shown in Figure 38, inverse P3HT enhanced SB I cells exhibit highest efficiencies and current densities over all setups used, while having slightly reduced fillfactor and highly reduced voltage. Besides the strong scattering of the efficiencies, the average value circles around **1.5 x 10^{-3} %.** Cells built in inverse-architecture with PCBM only resulted in short-circuit. Still, SB I works as donor as well as acceptor in the same range of efficiency. However, Figure 37 shows the I-V curve of an average inverse SB I / P3HT solar cell. All attempts to build SAM-enhanced Sudan Blue I cells failed due to bad coating of the dye which only resulted in short circuits.

3.4.2 Sudan Blue II [1,4-bis(butylamino)-9,10-anthraquinone]

Like for Sudan Blue I, all attempts to build a functioning homojunction solar cell resulted in short-circuited solar cells. The optical microscopy in Figure 41 shows two different areas for SB II. Half of the covered are consist of a smooth oil-like phase (light blue areas), the other half builds a poly crystalline network. As the optical structure of OBN will show, the crystalline phase of SB II might be responsible for the short circuits.

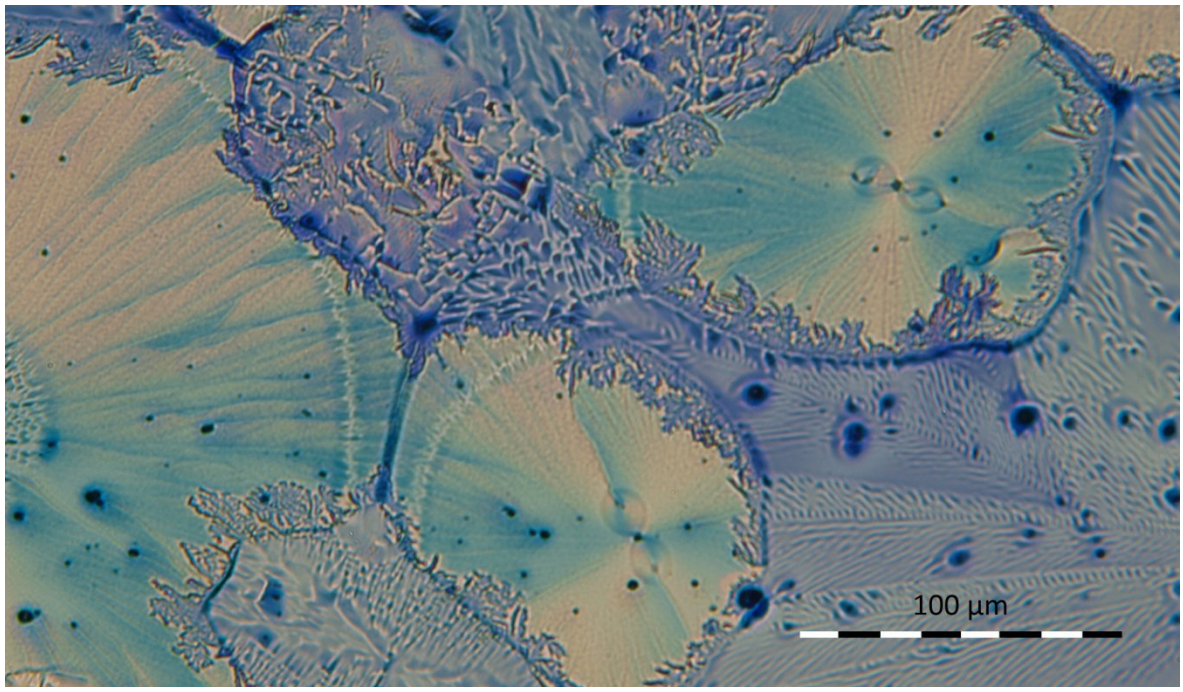

Figure 41 Light-microscopy of an inverse Sudan Blue II homojunction solar cell

Figure 42 and 43 show the J/U-curves and the solar cell parametes of the SB II Bulk-heterojunctions.

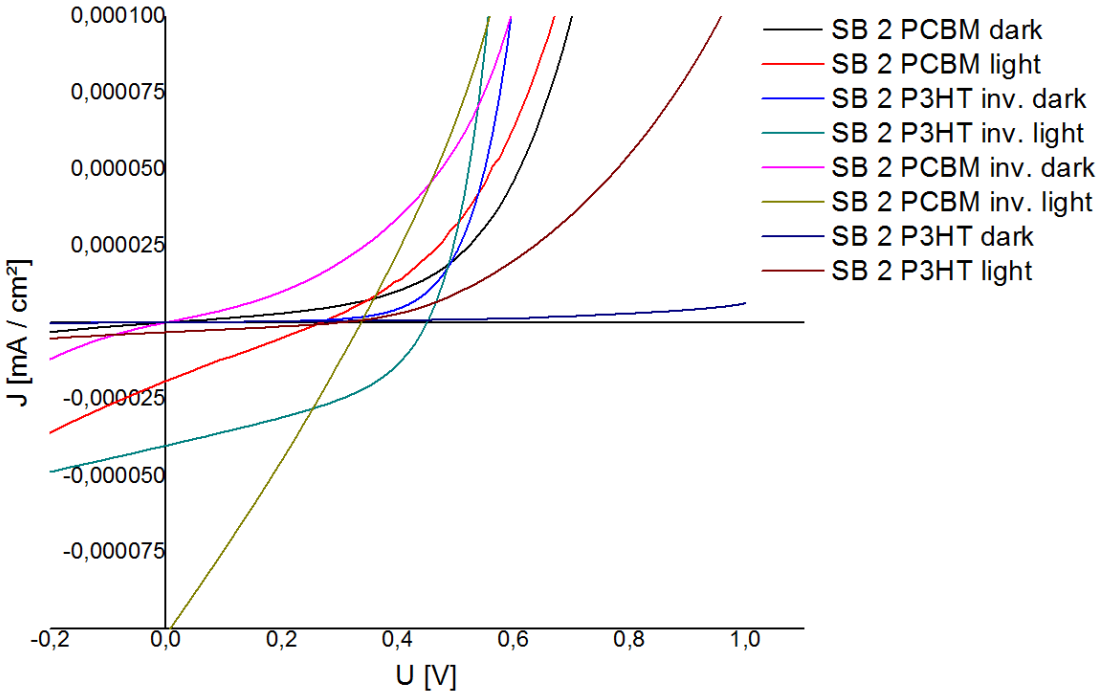

Figure 42: J/U-curves of SB II setups

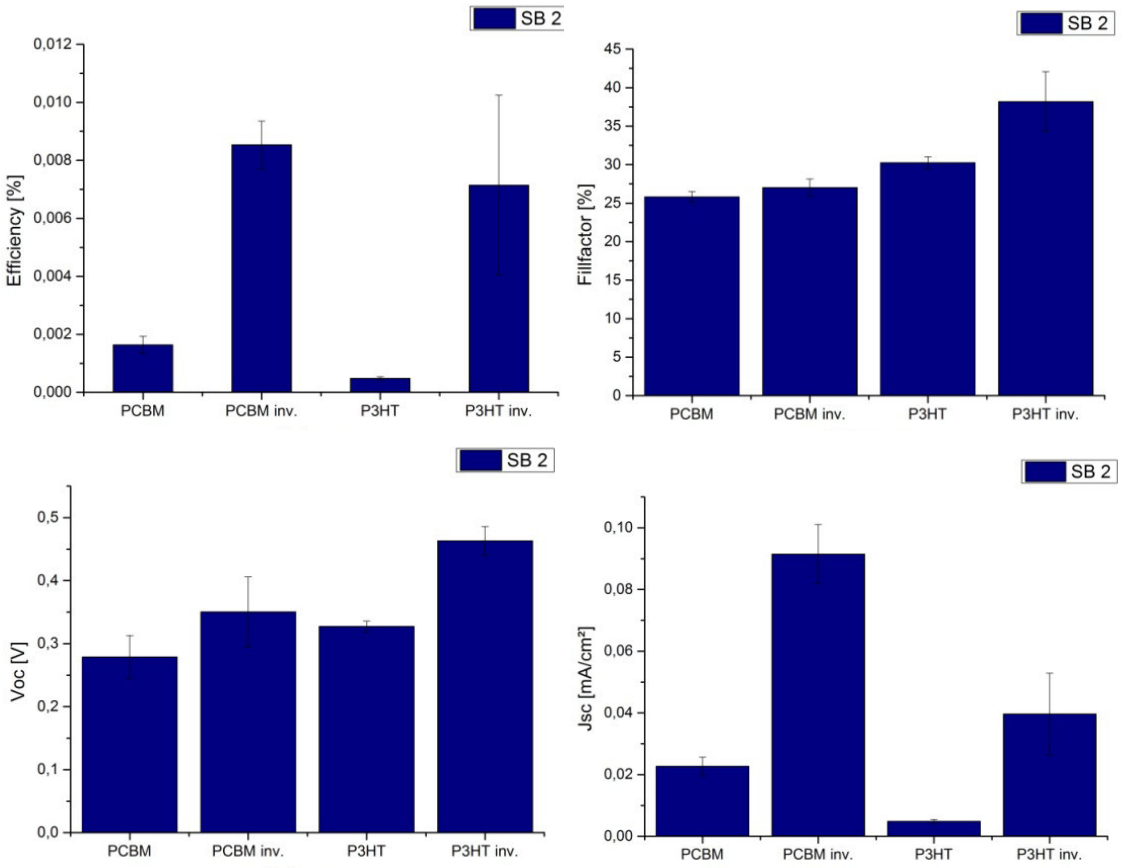

Figure 43: Solar cell parameters of SB II

In comparison to Sudan Blue I, the best results for Sudan Blue II shown in Figure 41 were archived with inverse-architecture and PCBM[60] showing an average value of **8 x 10^{-3} %**. Although fillfactor and Voc for PCBM[60] are lower than for inverse-architecture with P3HT, the Jsc is significantly higher than in all other setups, resulting in higher efficiencies. However, cells built in inverse architecture show better overall performances und show that SB II can work as donor as well as acceptor. The performance of an average inverse SB II / PCBM solar cell is shown in Figure 41. All attempts to build SAM-enhanced Sudan Blue II cells failed due to bad coating of the dye making it impossible to finish the cells properly.

3.4.3 Oil Blue N [1,4-Bis(pentylamino)-9,10-anthraquinone]

OBN is the first dye to successfully function properly in homojunction setup by forming a homogeneous layer. Regarding the crystal structure of OBN seen in Figure 44 it can be said, that SB II already shows the transition to similar crystallization behaviour as OBN when building large areas of a smooth oil-like phase meaning the absence of crystal boundaries. Still, the areas in Oil Blue N are in the range of 200 µm and more.

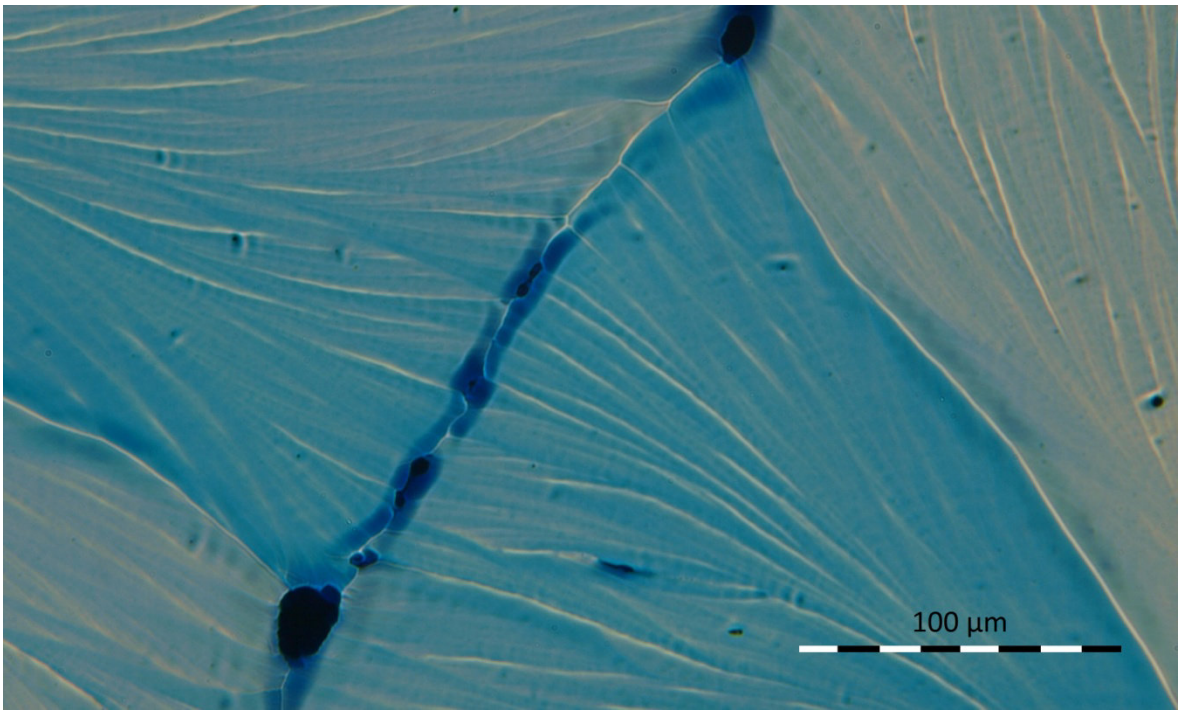

Figure 44: Light-microscopy of an inverse Oil Blue N homojunction solar cell

In comparison to SB I and SB II, the homojunction can be directly compared to the Bulk-heterojunction. Figure 45 and 46 show the J/U-curves and the solar cell parametes of the OBN homojunction and Bulk-heterojunctions.

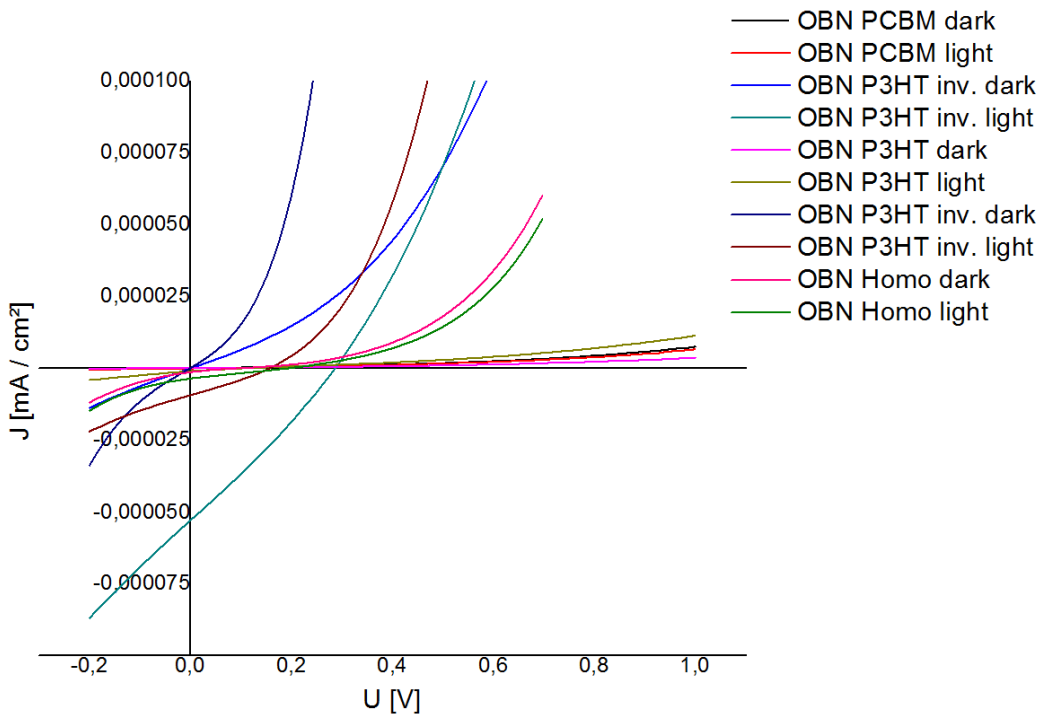

Figure 45: J/U-curves of OBN setups

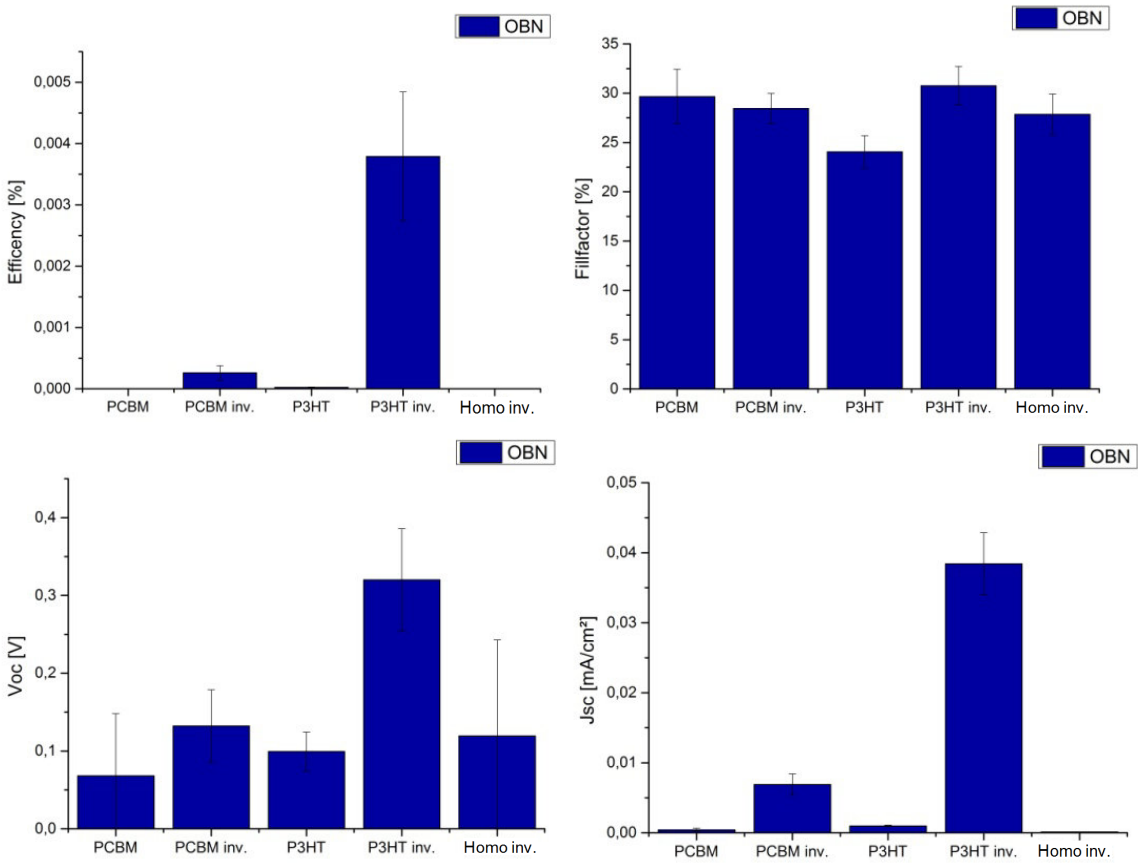

Figure 46: Solar cell parameters of OBN

Although a homojunction setup worked for OBN, it suffers of a worse current density which leads to a very poor efficiency. Figure 37 clearly shows that P3HT enhanced OBN solar cells have the highest Voc and Jsc in comparison to all other setups. Additionally, the inverse architecture archive better results than normal architecture cells. Thus, the highest efficiencies are found around **3.5 x 10^{-3} %.** However, comparing the Voc of blank OBN with normal architecture bulk-heterojunction shows that the main issue for building solar cells is the electron mobility of the active layer which corresponds to the current gained. Therefore, an average solar cell of the best performing setup is shown in Figure 44. Still, SAM-enhanced OBN cells only worked for homojunction solar cells described in the following chapter.

3.4.4 Solvent Green 3 [1,4-bis[(4-methylphenyl)amino]-9,10- anthraquinone]

From all dyes used, SG 3 is the easiest dye to process in terms of solar cell production. Additionally, most of the cells worked without short circuits. Compared to the other three dyes, the reason for the 'high performance' of SG 3 might lie in the crystalline structure. SG 3 forms a densely packed multi-crystalline way, including small grains of 10 µm and crystal areas of 20 µm shown in Figure 47.

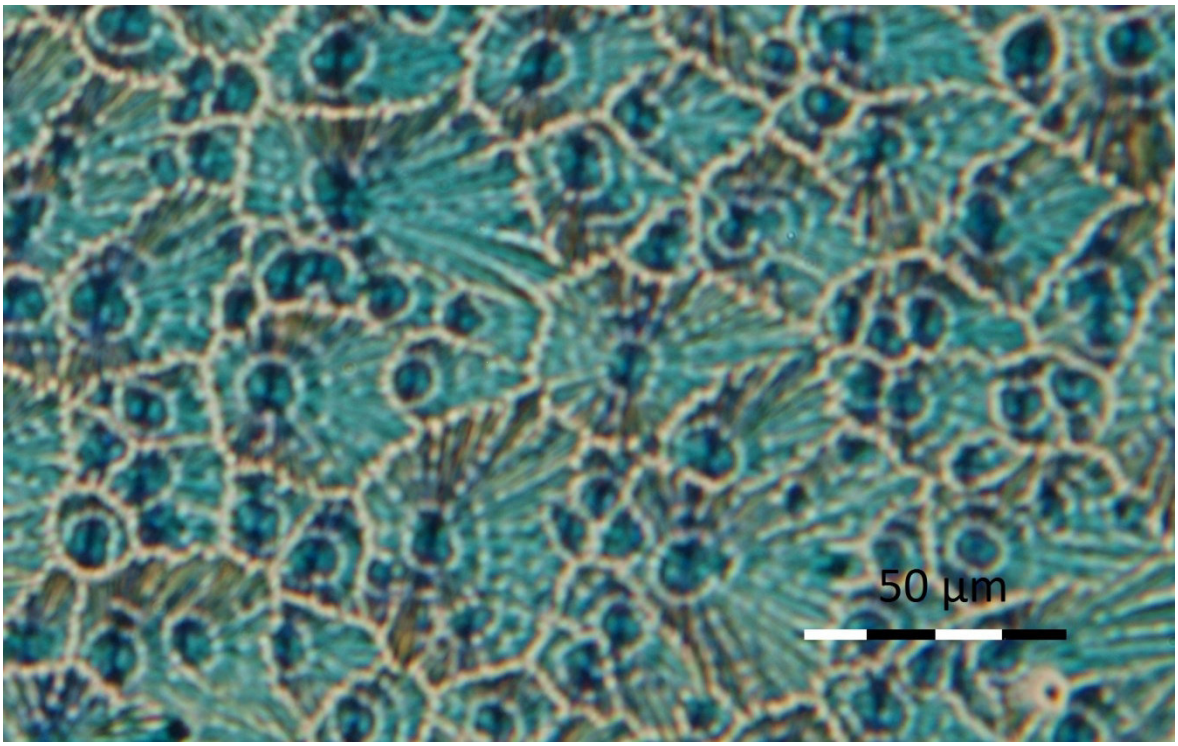

Figure 47: Light-microscopy of an inverse Solvent Green 3 homojunction solar cell

Figure 48 and 49 show the J/U-curves and the solar cell parametes of the SG 3 homojunction and Bulk-heterojunctions.

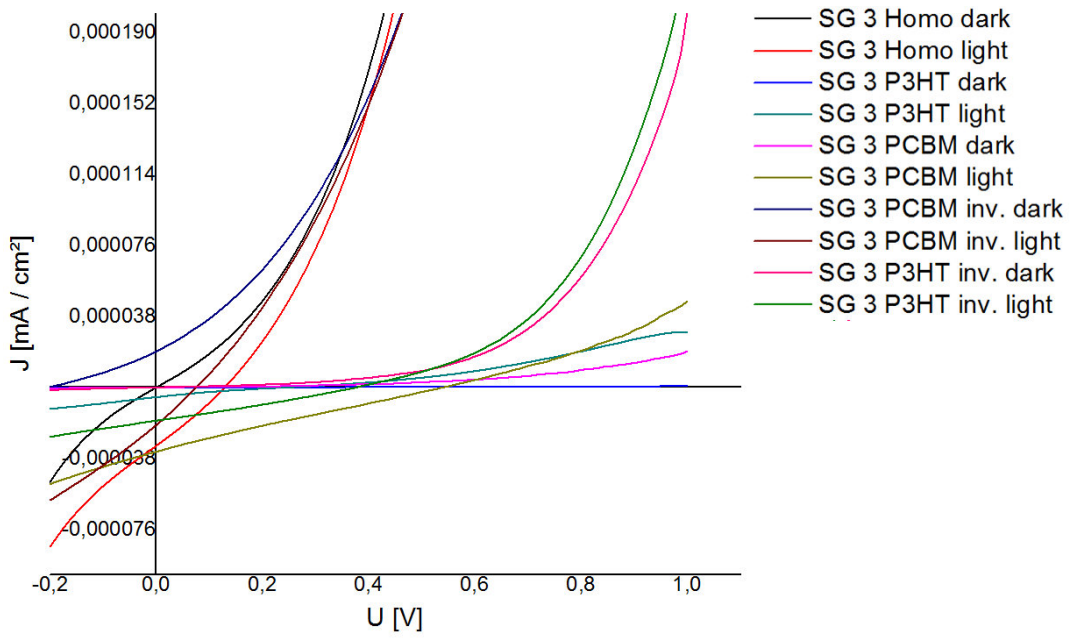

Figure 48: J/U-curves of SG 3 setups

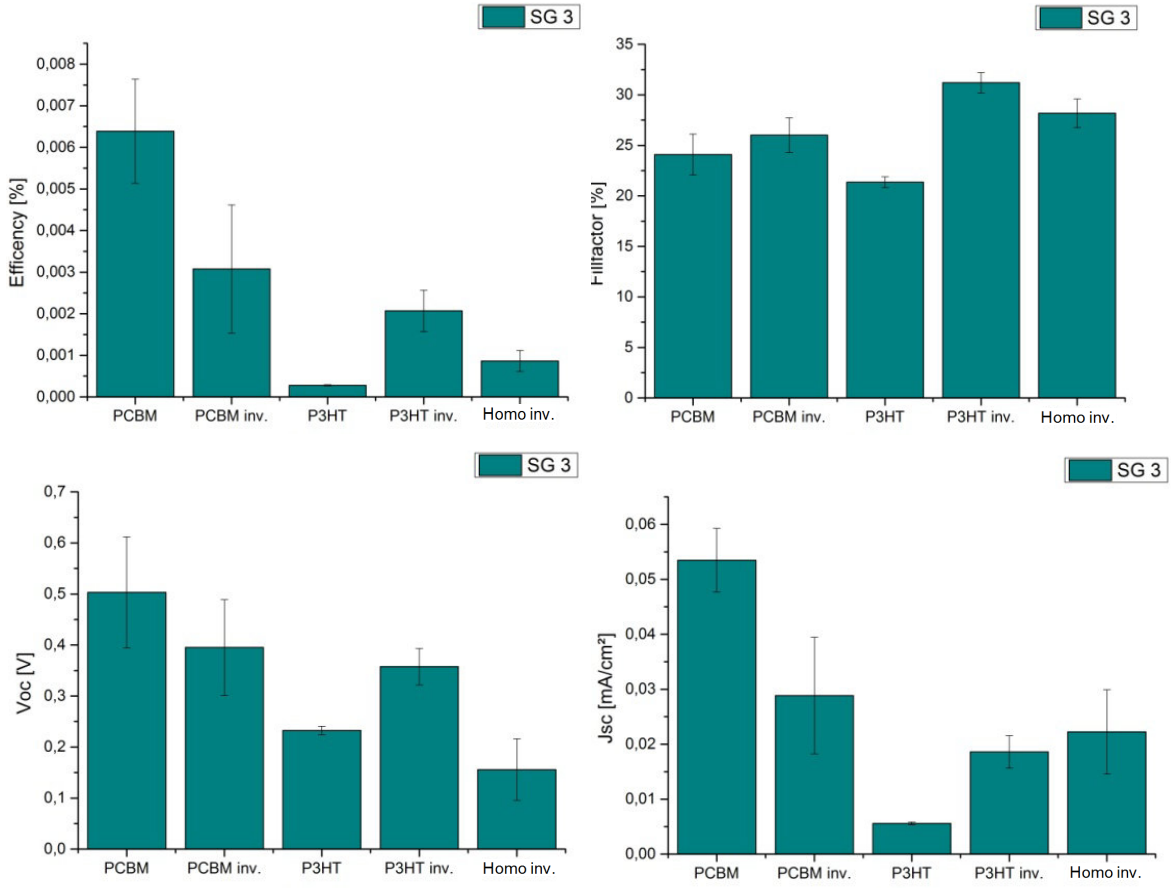

Figure 49: Solar cell parameters of SG 3

In comparison to all other dyes presented before, SG 3 shows a clear trend towards working as a donor regarding the setup given. Still, it works for both, PCBM and P3HT,

indicating that SG 3 has ambipolar properties, but it receives higher voltages and currents along with PCBM. Efficiencies received with PCBM are found in the range of **6 x 10^{-3} %.** An average regular SG 3 / PCBM[60] solar cell is shown in Figure 47. Additionally, the blank homojunction shows quite reasonable photovoltaic characteristics being in the same range as the Voc and Jsc of the bulk-heterojunction setups. Building SAM-enhanced SG 3 cells only successfully worked with PCBM and the results are given in the next chapter.

3.4.5 All Blue

When looking at the crystal structure of SG 3 and regarding the fact that SG 3 gives the best results for the homojunction solar cell an attempt is made to receive an even smaller crystal structure to increase the performance. Therefore a solution is formed from all dyes used before by mixing them up 1:1:1:1, named for this purpose “All Blue”. Figure 50 shows a smaller a tightly packed crystal structure for All Blue. The grains as well as the rods are about 5 µm wide.

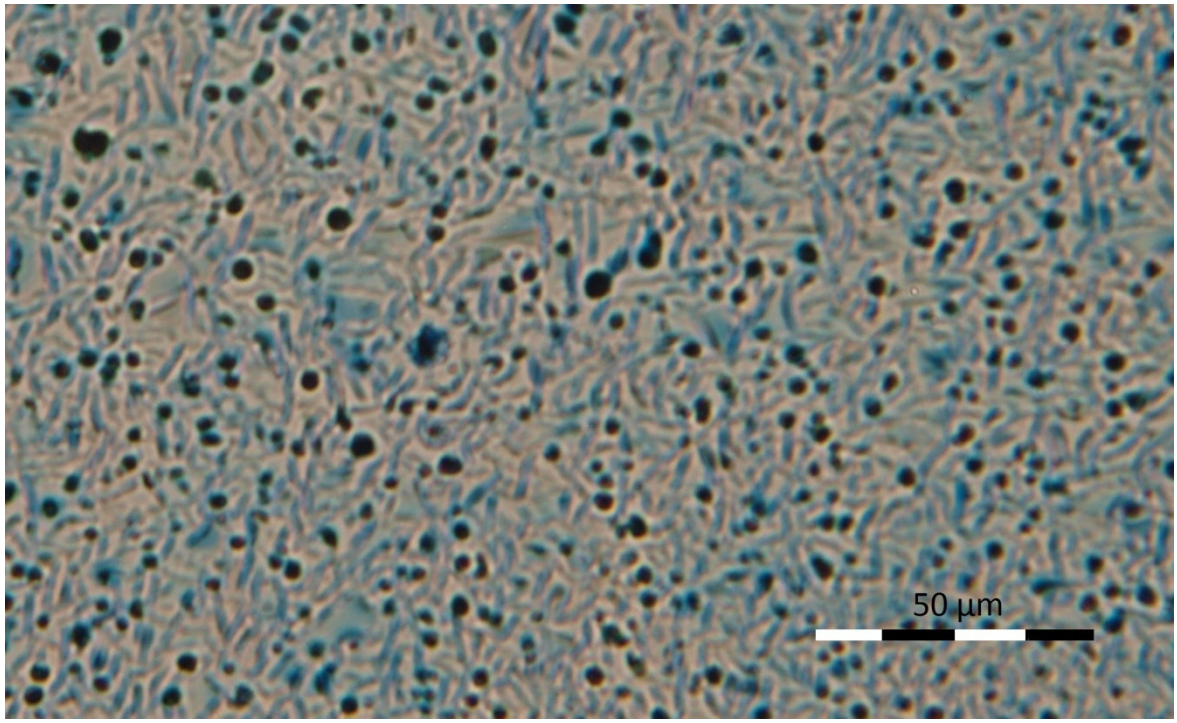

Figure 50 Light-microscopy of an inverse All Blue homojunction solar cell

As the overall results of the dyes used prefer inverse architecture over the normal architecture, only inverse type solar cells are built. Figure 51 and 52 show the J/U-curves and the solar cell parametes of the All Blue homojunction and Bulk-heterojunctions.

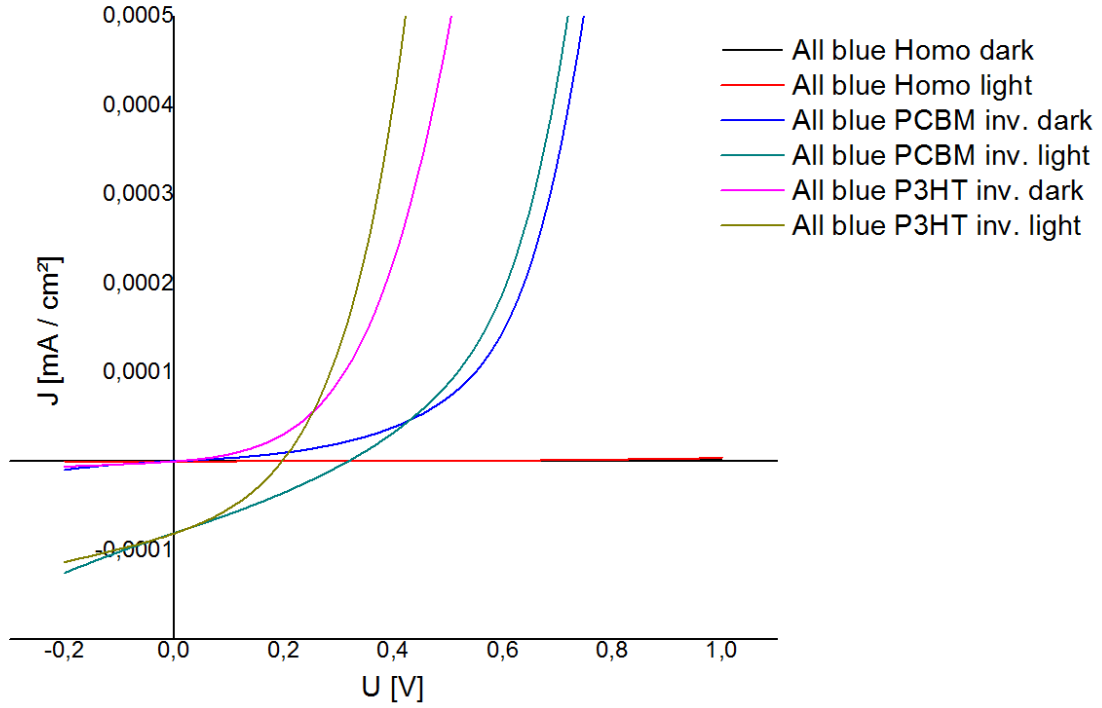

Figure 51: J/U-curves of All Blue setups

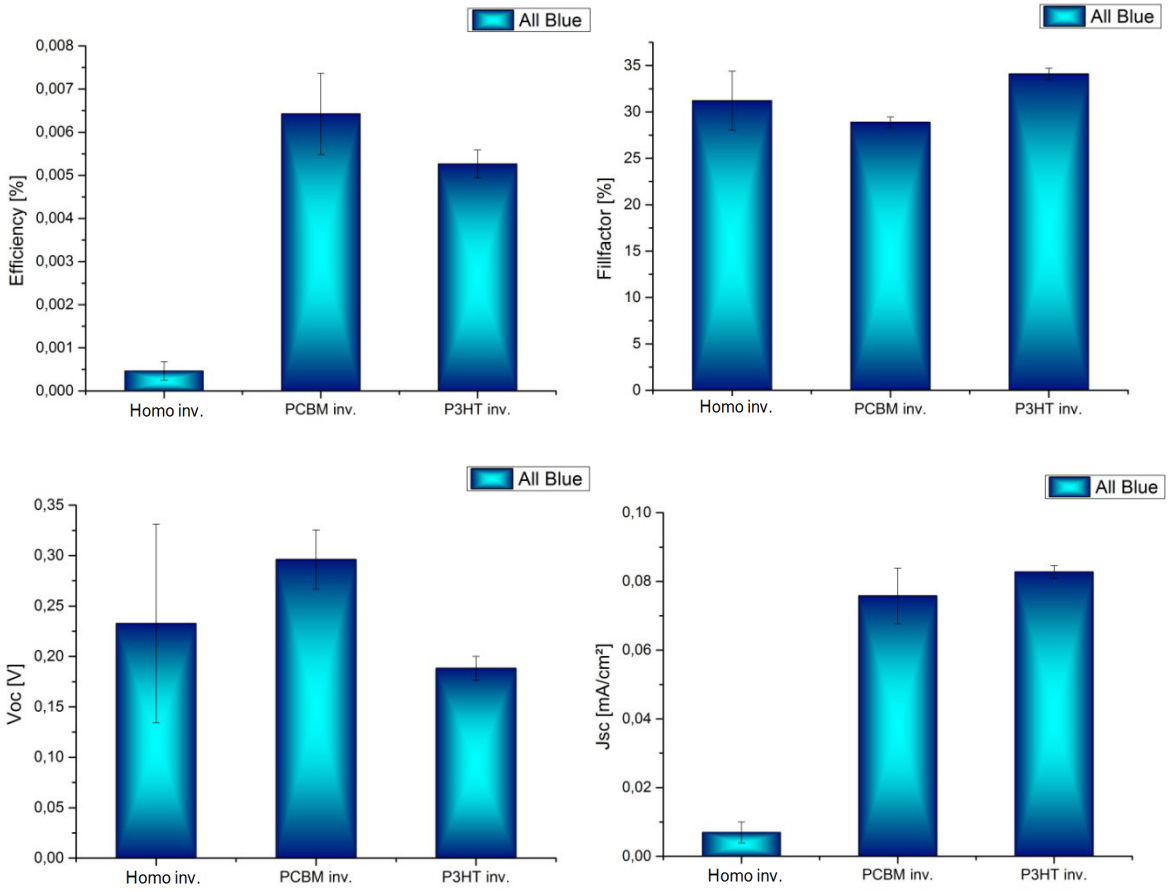

Figure 52: Solar cell parameters of All Blue

Regarding the results received from All Blue, the highest efficiency of **6.5 x 10^{-3} %** does not surpass the efficiencies of the SB II / PCBM or those of SB II/P3HT. Also, the blank homojunction leads to a lower efficiency than the SG 3 homojunction. However, as the best results are achieved with inverse PCBM[60] it can be derived that SB II played the major role in terms of efficiency.

3.5 Overall comparison

In this section, the most efficient setup from each dye, as well as All Blue, are compared with each other. The following Figure 53 shows a clear overview over the photovoltaic properties of these setups made during the course of these experiments.

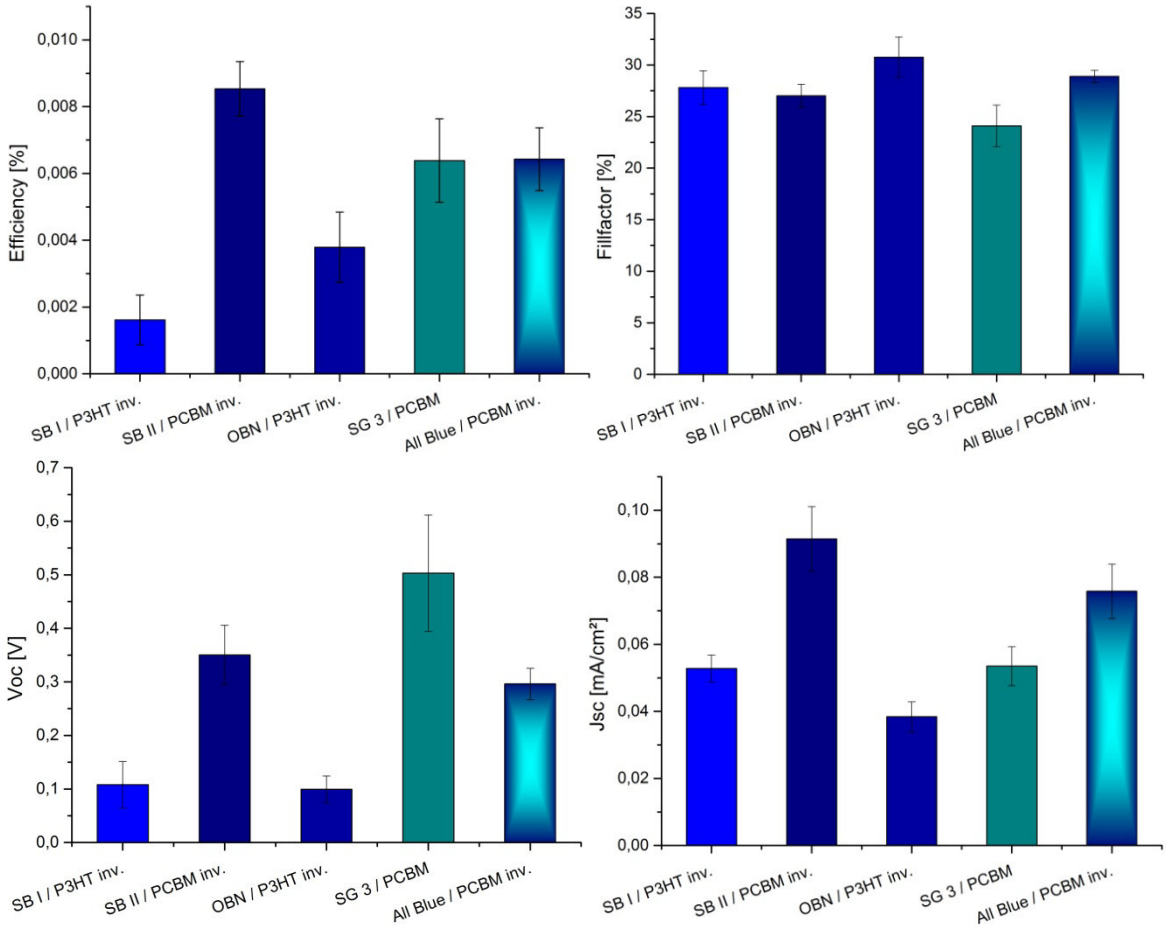

Figure 53: Overall comparison

First of all it can be seen, that three of five of the best setups are made of dye in combination with PCBM. These setups show an up to three times higher Voc and an up to two times higher Jsc than setups with P3HT. However, four out of five setups are built in inverse architecture. Comparing the architectures it can be said that inverse architecture leads to better currents while regular architecture gives a higher voltage.

The overall most efficient setup is SB II in combination with PCBM in inverse architecture. Although the Voc of SB II is still below the Voc of SG 3, the received Jsc for SB II is nearly double as high as those from all other dyes except for All Blue. As a result, SB II shows the best efficiency of **8 x 10^{-3} %**. Additionally it can be seen that all setups lead to a similar fillfactor in the range of 25 to 30%. Regarding the standard deviation of all parameters the deviation is quite low for all setups pointing out that the process used to build the solar cells leads to a homogeneous layer throughout the doctor blading step.

However, to be able to evaluate the results received blanks from sole PCBM and P3HT are built in inverse and normal architecture. Unfortunately, only cells built with P3HT worked properly. Therefore, the following Figure 54 compares the best P3HT setup of all dyes used with a plain P3HT solar cell in regular and inverse architecture.

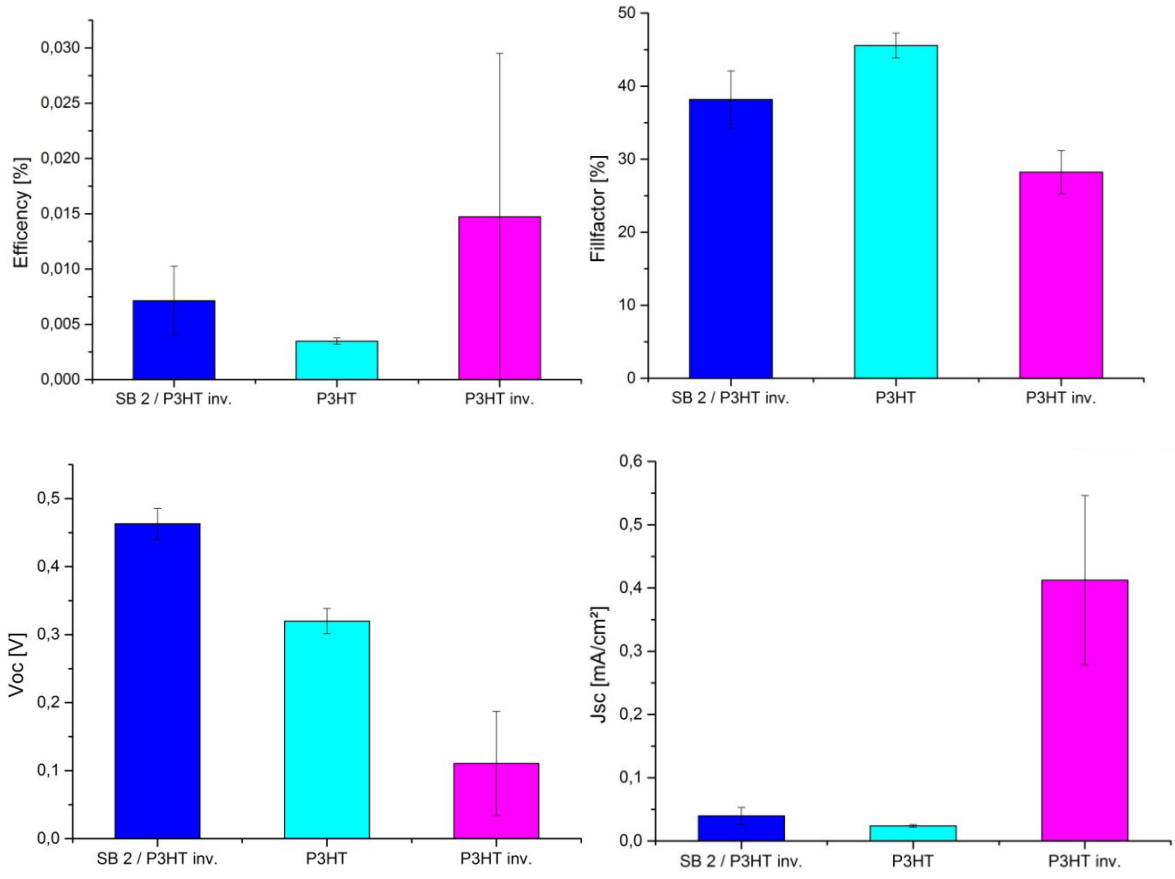

Figure 54: Comparison of solar cell parameters of SB 2 / P3HT and P3HT only

As the best result in combination with P3HT is achieved with SB 2, this dye is used for reasons of comparison. It can be clearly seen in Figure 54 that P3HT alone in inverse architecture leads to higher efficiencies than the best dye in combination with P3HT. This leaves the question what leads to a higher efficiency of P3HT and what leads to a decrease in efficiency when combined with a dye. Regarding the difference of Jsc of the

setups shown, it becomes clear that the sole P3HT in inverse architecture benefits from the high current density which means high electron mobility. Although the Voc is far higher for the dye, the current density is severely reduced including a lowered efficiency.

As already mentioned before, plain PCBM[60] cells did not function, however, they worked in combination with dyes. PCBM[60] slightly absorbs light leading to a photovoltaic current, but not as much as P3HT does. Therefore, the dye still participates in the electricity generation what can be seen in the results gained by SB II in combination with PCBM [60]. In contrary to the expected acceptor behaviour deducted from the HOMO-LUMO calculations, the best results are achieved in combination with PCBM, suggesting increased donor properties. This coincides with the initial assumption that all dyes used show ambipolar behaviour.

However, it can be said that the introduction of diammino-anthraquinone dyes into a bulk-heterojunction system does not lead to an improved system due to the lack in electron mobility but still, a functioning solar cell can be built. Additionally, these dyes are able to generate photovoltaic current in homojunction solar cells although the efficiencies gained can be neglected in comparison to common photovoltaic technologies.

3.6 SAM-enhanced Solar Cells

In this section, SAMs are introduced onto the TiOx layer to modify the electric properties of inverse solar cells. First, five different benzoic acid derivatives are coated onto the TiOx layer and measured via contact angle measurements. Additionally the surface energy will be calculated. In the second step, the SAM coated TiOx layers are used for solar cel production and afterwards compared to the non-SAM coated solar cell.

3.6.1 Contact Angle Measurements

Contact angle measurements are used to give a qualitative statement on the wetting properties of a liquid on a surface. Generally it can be said that a lower contact angle means better wettability while a wider angle means lower wettability. Here, the contact angle Θ is closely connected to the surface energy Ϭ of the corresponding interfaces as given in Equation 4 according to Young and seen in Figure 55 [67]. However, the contact angle is not only dependent on the surface energy but also on the morphology of the surface. A common effect of the morphology of the surface on the contact angle can be seen in the lotus effect [68].

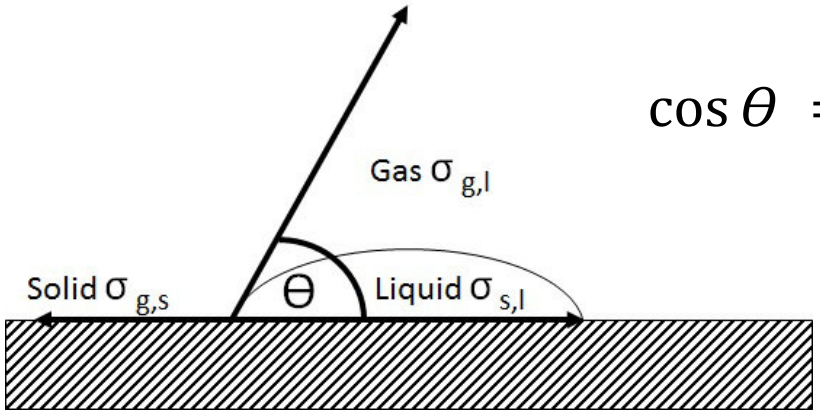

$$\cos\theta = \frac{\sigma_{g,s} - \sigma_{s,l}}{\sigma_{g,l}} \qquad \text{Eq. 4}$$

Figure 55: Contact angle measurments

To show the quality of the SAM-coating, two different analytical liquids, H_2O and MeI_2 are used to determine their corresponding contact angle. The method static contact angle measurement is used where a sessile of liquid is dropped on the surface and a picture is immediately taken. As mentioned in the experimental section, two approaches are used to prepare the SAM-layers, however, using approach #1 only gave vales around 40-50° for all SAMs and blanks used, meaning that the surface is not sufficiently covered by the SAM-molecules. Therefore, only results from approach #2 are presented.

3.6.2 H_2O measurements

In order to determine a reliable mean of contact angles, all measurements are carried out 10 times per substrate and using three different substrates. The following Figure 56 shows the angles received with five different benzoic acids as well as a blank for the purpose of comparability.

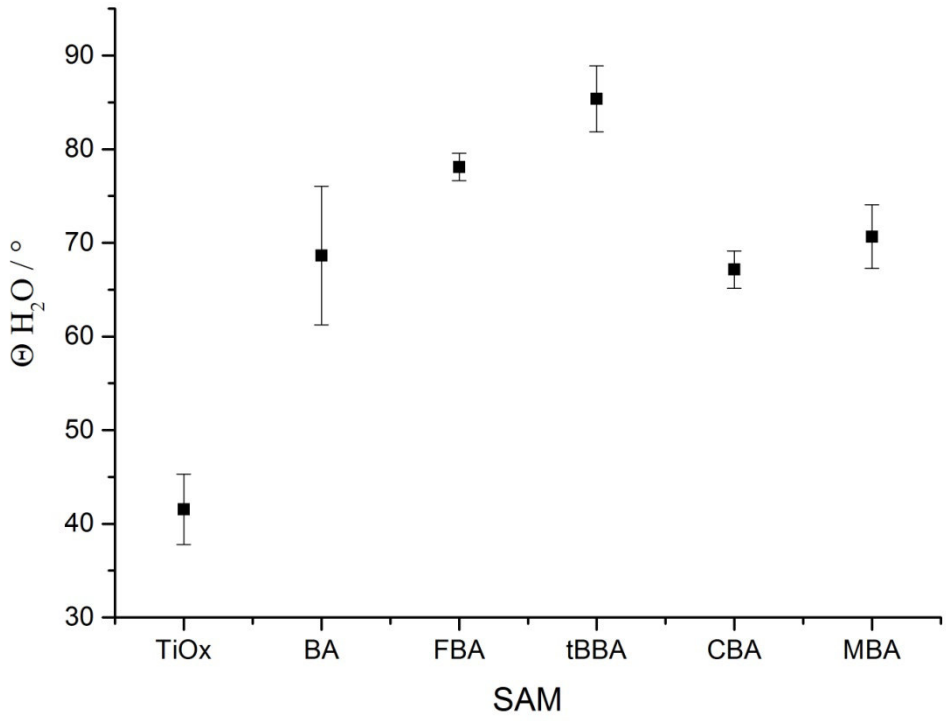

Figure 56: Comparison of the H_2O angle of different benzoic acids on TiOx

All results are shown in Table 2. Regarding the vales given, all benzoic acids lead to a more hydrophobic surface. When comparing to the values from Six[56], it is noticed that tBBA leads to a higher contact angle than FBA which is supposed to be the most hydrophobic benzoic acid used. Therefore, the difference might be related to the surface topography.

3.6.3 CH_2I_2 measurements

The measurements with CH_2I_2 are carried out in the same way as for H_2O. The results are shown in Figure 57 below.

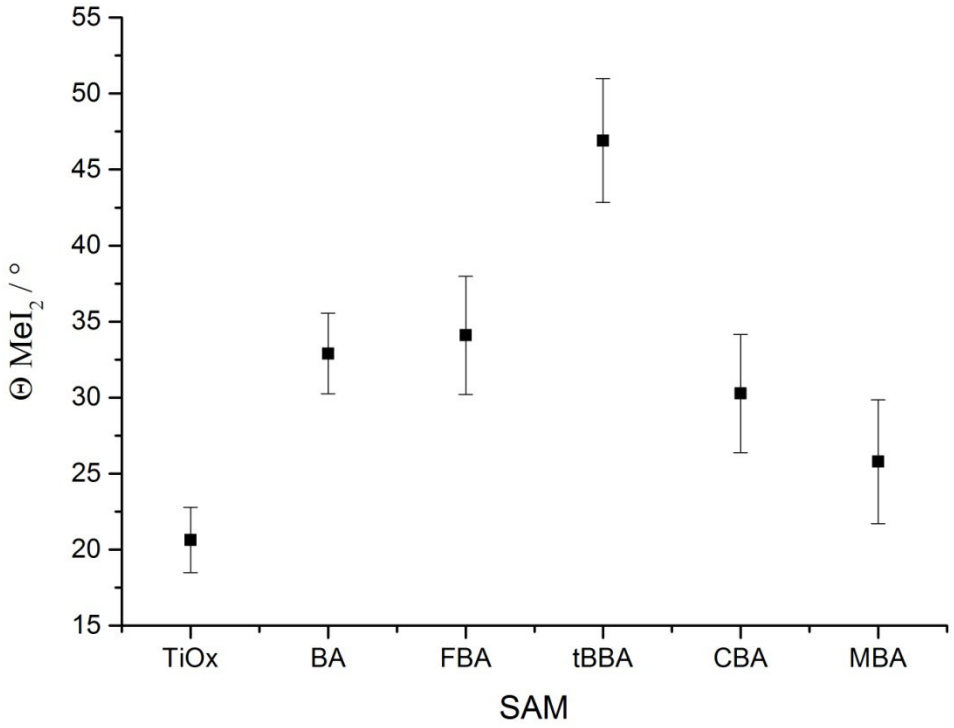

Figure 57: Comparison of the methyliodide angle of different benzoic acids on TiOx

All results are found in Table 2. The contact angles of CH_2I_2 are far lower than those of H_2O, supporting the assumption of an increase in hydrophobicity of the SAM-enhanced TiOx-layers. Still, as seen in the results of H_2O, the contact angle of all SAMs is higher than the angle of blank TiOx. This indeed indicates a strong impact of the surface topology on the contact angle.

	Θ H_2O		Θ CH_2I_2		Free Surface Energy σ	σ_s^D	σ_s^P
	[°]	±	[°]	±	[mN/m]	[mN/m]	[mN/m]
TiOx	41,5	3,8	20,6	2,1	60,75	35,64	25,11
BA	68,7	7,4	32,9	2,7	45,63	36,71	8,92
FBA	78,1	1,5	34,1	3,9	42,95	38,60	4,35
tBBA	85,4	3,5	46,9	4,1	36,21	33,18	3,03
CBA	67,1	2	30,3	3,9	46,99	37,54	9,45
MBA	70,7	3,4	25,8	4,1	47,33	40,44	6,89

Table 2 Contact angles and Surface Energies

As two different liquids, a polar and an apolar liquid, with known surface energies are used for contact angle measurements, the free surface energy of the SAM-coated TiOx can be calculated. Therefore, the method after Fowkes is used [71]:

$$\sigma_{sl} = \sigma_s + \sigma_l - 2(\sqrt{\sigma_s^D * \sigma_l^D} + \sqrt{\sigma_s^P * \sigma_l^P}) \qquad \text{Eq.5}$$

σ_s^D and σ_l^D describe the disperse parts of the surface energy of the liquid and the solid whereas σ_s^P and σ_l^P describe the polar parts of the surface energy. The following Figure 58 shows the impact of the used SAMs on the surface energy of the TiOx layer.

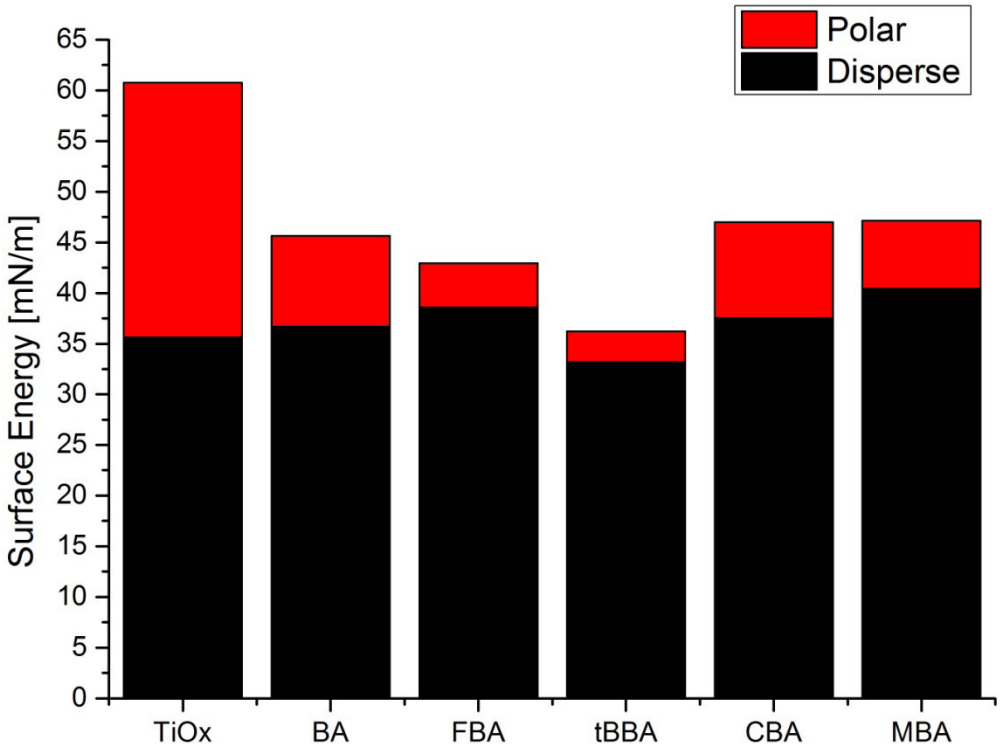

Figure 58: Surface Energy of SAM-coated TiOx

However, Figure 58 shows that the introduction of SAMs decreases the overall surface energy. The lowest surface energy is found with tBBA-SAM where the energy is reduced from 61 to 36 mN/m. This reduction is mainly caused by the reduction of the polar parts. The disperse parts only change slightly.

Although introducing a SAM-layer is supposed to modify the electric properties of the solar cell, it still causes a severe problem when assembling the solar cell. As the wettability changes too, creating a homogenious layer has become very difficult. Therefore, only results are presented which fulfil the requirements of being reproducible. For both, homojunction and bulk-heterojunction, only one experimental setup each succeeded: an OBN homojunction and a SG 3 / PCBM[60] bulk heterojunction, in particular.

3.6.4 SAM-enhanced homojunction

Throughout the homojunction experiments, OBN always showed the least efficient cells. However, they were the most reproducible but still quite inhomogeneous cells. Any cells using BA as SAM were all short-circuited.

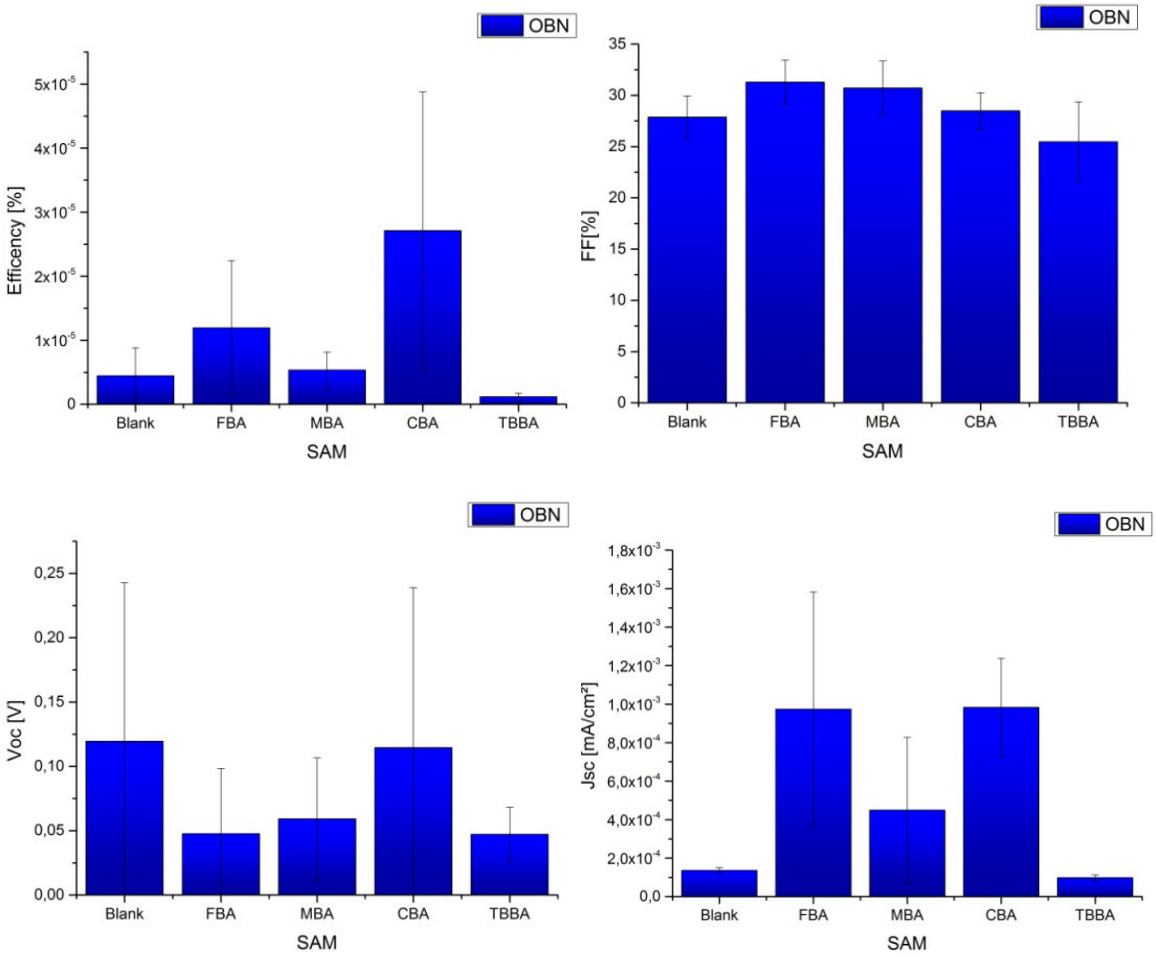

Figure 59: Solar cell parameters of SAM enhanced OBN

This experiment shows that introducing SAMs influence the electric properties of the solar cells. As seen in Figure 58 three of five SAMs raised the efficiency, especially CBA raises the efficiency up to three times higher than without any SAM. Comparing Voc and Jsc it becomes clear that this increase in efficiency derives from an increased Jsc although Voc has been slightly decreased. This can be seen as an acceptable trade-off, as the current is the limiting factor regarding the efficiency of solar cells. However, these cells are very inhomogeneous what can be seen in the standard-deviation given in Figure 58.

3.6.5 SAM-enhanced bulk-heterojunction

For the purpose of bulk-heterojunction, only SG 3/PCBM solar cells could be reproducibly built. In comparison to the OBN-based cells, SAM-enhanced cells built with SG 3/PCBM are more homogeneous and therefore show less deviation on all properties.

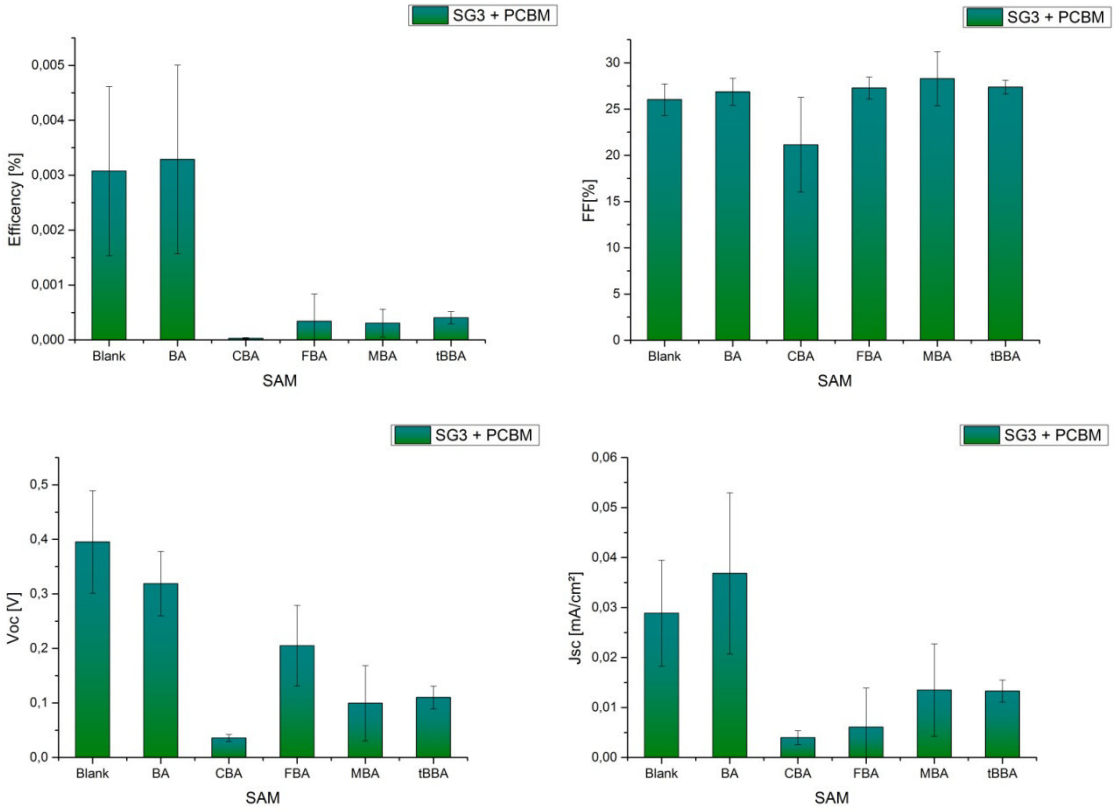

Figure 60: Solar cell parameters of SAM enhanced SG 3 with PCBM

Although CBA, FBA and MBA increased the OBN-based solar cell, these SAMs strongly decrease the properties of the SG 3/PCBM cells. Only BA-enhanced solar cells lead to an increase of efficiency over the non-enhanced SG 3/PCBM cell. As already seen for OBN, the trade-off of increasing Jsc and decreasing Voc leads to an improved efficiency.

According to Yip et al., electron drawing groups lead to an ohmic contact between the organic and the TiOx layer [65]. This can be verified by the SAM-enhanced OBN homojunction where all three electron drawing benzoic acids lead to higher currents. This still leads to the question what lead to the increase of current with BA in the SG 3 bulk-heterojunction. Hau et al. described in his work that morphology and crystalline order also play a role on the solar cell performance [66]. Therefore, it is assumed that the improved current with BA derives from PCBM[60] where the aromatic side group of PCBM[60] aligns with BA. Hence it is not the change in dipole moment which leads to the improvement of the current but the interaction between these two aromatic groups.

4 Experimental

The following table shows all chemicals and solvents used for the experiments. None of those chemicals has received further treatment or purification.

Chemicals	Purity grade	Supplier
Acetone	≥ 99%	Sigmar Aldrich
Methanol	99%	Sigmar Aldrich
Chloroform	≥ 99.9%	Sigmar Aldrich
Isopropanol	99%	Sigmar Aldrich
Chlorobenzene	≥ 99%	Sigmar Aldrich
BA	99%	Fluka
CBA	99%	Sigmar Aldrich
FBA	98%	Sigmar Aldrich
MBA	99%	Sigmar Aldrich
tBBA	99%	Sigmar Aldrich
P3HT	RR	Rieke
PCBM [60]	99.5 %	Solenne
SB I	2x crystallized	Joanneum Research
SB II	2x crystallized	Joanneum Research
OBN	2x crystallized	Joanneum Research
SG 3	95%	Sigmar Aldrich
TBAP	99%	Sigmar Aldrich

4.1 UV-Vis measurements

All UV-Vis spectra are taken with a Perkin Elmer Lambda 35 in the range from 350 to 1000 nm. For the measurement, a 10 g/L solution of dye in chloroform has been doctor bladed onto a supersonic cleaned and oxygen etched glass substrate at a speed of 5 mm/s and at 60°C. In order to minimize light scattering effects by using the glass-dye transition instead of the air-dye transition, the glass substrate is facing the light beam rather than the processed dye site.

4.2 CV measurements

For all CV measurements a three-electrode design is used where the working electrode (WE) is a platinum disc electrode and counter electrode (CE) is made of a platinum wire grid. As reference electrode an $Ag/AgBF_4$ in ACN is used. The measurements are performed in a 0.1M tetrabutylammonium perchlorate (tBAP) solution in ACN whereas tBAP functions as conducting salt and a dye concentration of 2 mmol. Ferrocene is added after the measurements as internal standard,

4.3 Solar cell preparation

In order to find the optimal setup for the solar cell constructions some parameters are varied:

- Cyclohexane, chlorobenzene, tetrahydrofurane and acetone are used as solvents.
- The doctor blading are carried out at either 40 or 60°C.
- Concentrations used are 5, 10, 15, 20 and 30 mg/mL
- Doctor blading speeds used are 5, 7.5, 10, 12.5 and 15 mm/s

The following chapters represent the best working setup.

4.3.1 Normal architecture

Substrate preparation:

First, the plastic foil on top of the ITO-substrate is removed and all particles are removed via a tissue paper. All ITOs are the cleaned in an isopropanol bath and supersonic treatment (VWR ultrasonic cleaner) for 30 min. The substrates are then dried in a nitrogen stream.

PEDOT:PSS-layer preparation:

Prior the preparation, the substrates undergo oxygen plasma etching for three minutes with an O_2 flow of 10 sccm (Diener Electronics). 1 mL of PEDOT:PSS is applied on the substrate via syringe and then spin coated (30s, 2500rpm, 300 rpm/s)

Homojunction active-layer preparation:

A 30 mg/ml solution of dye in $CHCl_3$ is prepared. 30 µL of the solution are taken and applied via doctor blading at 60°C and 7.5 mm/s.

Donor-enhanced bulk-heterojunction preparation:

At first a 20 mg/mL solution of P3HT in $CHCl_3$ is prepared and stirred for at least 1h. Additionally a 20 mg/mL solution of dye in $CHCl_3$ is prepared. To prepare the final solution, 80 µL of both solutions are mixed together in a 4 mL vial and mixed through fast drawing and withdrawing of the solution through a pipette for several times. Afterwards 30µL are used for doctor blading at 60°.

Acceptor-enhanced bulk-heterojunction preparation:

At first a 10 mg/mL solution of PCBM[60] in $CHCl_3$ is prepared and stirred for at least 1h. Additionally a 20 mg/mL solution of dye in $CHCl_3$ is prepared. To prepare the final solution, 80 µL of both solutions are brought together in a 4 mL vial and mixed through fast drawing and withdrawing of the solution through a pipette for several times. Afterwards 30µL are used for doctor blading at 60°C.

Metal Electrode deposition:

100nm of the aluminium metal contact are applied via physical vapor deposition (PVD) at $1x10^{-5}$ mbar in a thermal evaporation chamber (MBraun LABmaster glove box system)

4.3.2 Inverse architecture

The substrate preparation as well as the active layer preparation is performed in the same way as for normal architecture.

TiO_x-Layer preparation:

Prior to the preparation, the substrates undergo oxygen plasma etching for three minutes with an O2 flow of 10 sccm. When activated, the method used by Fradler [71] for the preparation of TiO_x-layers is used: 30µL of a 0.1M solution of titanium propoxid-bis-acetylacetonate is used for doctor blading (25 mm/s , 40°C, 100 µm) under ambient conditions. After annealing the precursor at 400°C for 15 min, a layer of TiO_x has formed.

Metal electrode and MoO_3 deposition:

15 nm of MoO_3 have been used for this experimental setup and 100nm of the aluminium metal contact. Both are applied via physical vapour deposition (PVD) at $1x10^{-5}$ mbar in a thermal evaporation chamber.

4.4 I-V-Characterization

I-V-characteristics:

To determine the electrical properties of the produced solar cells, I-V-characteristics are recorded. First, temperature and light intensity are measured through a photodiode on the measuring device. Then, the intensity is set to 100 mW/cm² whereas the solar spectrum is simulated by an AM 1.5 Dedolight lamp. In addition to every illuminated measurement, a dark measurement is taken too by covering up the measuring device. The effective area of 0.09 cm² of each solar cell is guaranteed by using a defined shadow mask.

Measurements are performed by a Keithley control unit. The control unit is run by a LabView program written by Lukas Troy. All characteristics are taken from -0.2 to +1 V.

Layer Thickness:

All layer thicknesses and roughnesses are recorded by a Bruker DektakXT Profilometer. To prepare the measurements, three areas are cut using a scalpel to remove the layer of interest. The difference of height between the remaining substrate and the active layer is measured by the profilometer needle. Each measurement is taken three times.

4.5 SAM-enhanced Solar cells

The following Figure shows the experimental setup for a SAM-enhanced solar cell:

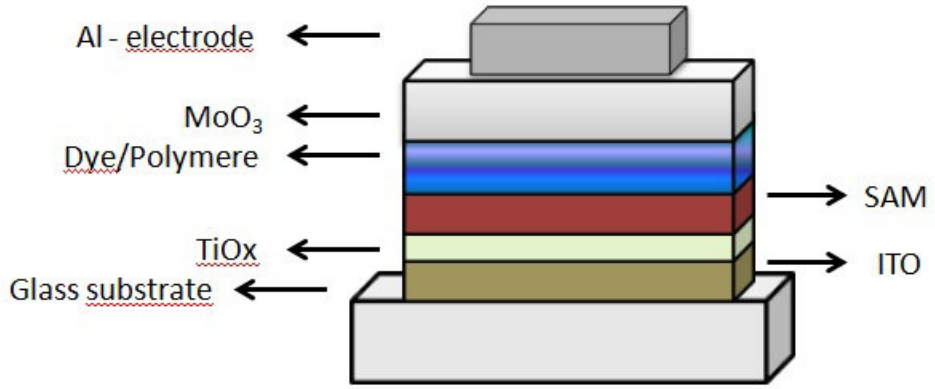

Figure 61 Scheme: inverse architecture including a SAM-layer

SAM preparation

The substrates are activated via oxygen plasma etching before the actual SAM preparation. For this preparation, two approaches have been used: Approach #1 and #2 use a two-step spincoating process according to Six[56]. For approach #1 and #2 , 0.5 mL of a 1 mg/mL solution of the benzoic acid or it derivatives in Methanol (apporach #1) or Acetone (approach #2) is applied on the TiOx layer and then spin coated (60 s, 300 rpm/s, 4000 rpm). To wash off the non-chemisorbed residue, 0.5 mL of pure Methanol (apporach #1) or pure Acetone (approach #2) is dropped on the substrate and then spin coated (30s, 300 rpm/s, 2500 rpm).

5 Summary and Outlook

Organic semiconductors have become more and more important in photovoltaics and electronics. Their main advantage over inorganic semiconductors is the easy processability and the low process temperature. This property enables organic semiconductors to be used in flexible as well as in print applications. However, organic semiconductors still suffer from low charge carrier mobility and little air stability.

This thesis investigates the semi-conductive behaviour of four H-bonding diamino-anthraquinone dyes in solar cell applications. These dyes are considered to be ambipolar, making them suitable for homojunction solar cells as they are able to transport positive as well as negative charge carriers at the same time.

First, the dyes are electrochemically analysed via CV and UV-Vis measurements to give the HOMO and LUMO levels of the diamino-anthraquinone dyes. CV measurements show one-electron reversible oxidations and reductions reactions for all dyes. The difference between the optical band gap in solution and in thin film is about 0.2 eV. Other experiments described in different papers show little dependence of the absorption maxima on the solvent. It is assumed, that the transition seen in solution is a π-π* which does not represent the HOMO-LUMO transition. Derived from these results, the crystal structure as well as the capability to build H-bonds in thin films have a strong impact on the band gap of these dyes. The levels of the four dyes range from -3.98 to -4.14 eV for HOMO and -5.57 to -5.70 for LUMO. Therefore, the dyes are expected to work better in acceptor-position along with P3HT than in donor position along with PCBM in bulk-heterojunctions.

The second part investigates the incorporation of the dyes into solar cells. Therefore, homojunction solar cells are built, but functioning homojunctions are only achieved with OBN and SG 3. They show very poor efficiencies around 10^{-5} % for OBN and 10^{-3} % for SG 3 and also the Voc of 0.15 V is far beneath the predicted maximum Voc of 1 V. This indicates that these dyes are not suitable for homojunction applications.

The dyes are also used in bulk-heterojunctions together with PCBM[60] and P3HT. The best efficiencies reached are $9*10^{-3}$ % and the best Voc reached is 0.6 V. Nevertheless, the efficiency results are not very promising in comparison to 5 % in a bulk heterojunction consisting of PCBM[60] and P3HT due to a lack in the current density. However, the Voc is almost the same for the dye bulk-heterojunction as it is for PCBM/P3HT.

At last SAMs are introduced into the solar cell system by coating the TiOx layer with five different benzoic acid derivatives. The SAMs are characterized by contact angle measurements which indicate that the morphology of TiOx/SAM overules the hydrophobicity. However, the introduction of SAMs onto TiOx drastically reduced the processability of the solar cell as the SAM prevents the active layer from homogeneously coating. Still, two setups successfully lead to functioning solar cells. For an OBN homojunction, CBA and FBA lead to higher efficiencies as they increase the Jsc by a factor of 10. In the SG 3/PCBM setup, only BA slightly increases the efficiency up to $5*10^{-3}$ through increasing the JSC while reducing the Voc.

Concluding can be said that many setups have already been tested and resulted in very poor efficiencies. However, other classes of H-bonding dyes or donor/acceptor combinations might lead to better results. Still, research on these diamino-anthraquinone dyes in OLED and transistor applications should be conducted.

6 Appendix

6.1 Abbreviations

ACN	Acetonitrile
AM	Air Mass
BA	Benzoic Acid
CBA	4-Cyano Benzoic Acid
ETL	Electron Transport Layer
EIA	U.S. Energy Information Administration
FBA	4-Fluoro Benzoic Acid
FF	Fillfactor
HOMO	Highest Occupied Molecular Orbital
HTL	Hole Transport Layer
IEA	International Energy Association
ITO	Indium-Tin-Oxide
IV	Current-Voltage
Jsc	Short Circuit Current Density
LUMO	Lowest Unoccupied Molecular Orbital
MBA	4-Methoxy Benzoic Acid
MeOH	Methanol
OBN	Oil Blue N (Solvent Blue 14)
OPV	Organic Photovoltaic
P3HT	Poly-(3-Hexyl Thiophene)
PCBM[60]	[6,6]-phenyl-C_{61}-butyric acid methyl ester
PEDOT:PSS	Poly(3,4-ethylen dioxythiophen), Poly(styrenesulfonate)
PV	Photo Voltaic
SAM	Self Assembling Monolayer
SB I	Sudan Blue 1 (Disperse Violet 14)
SB II	Sudan Blue 2 (Oil Blue 35)

SG 3	Solvent Green 3 (D & C Green No. 6)
tBAP	Tetra-Butyl Ammonium Perchlorate
tBBA	4-tert-Butyl Benzoic Acid
Voc	Open Circuit Voltage

6.2 Literature

[1] Peter Würfel, *Physics of Solar Cells: From Basic Principles to Advanced Concepts*, WILEY-VCH, **2009**

[2] J. Schubert: *Physikalische Effekte.* Physik-Verlag, 2. Auflage, **1984**

[3] www.eia.gov/forecasts/ieo/ pdf/0484(2013).pdf

[4] https://www.iea.org/media/freepublications/technologyroadmaps/solar/Launchsolarroadmaps2014_WEB.pdf (19.10.2015)

[5] https://www.iea.org/publications/freepublications/publication/TechnologyRoadmapSolarPhotovoltaicEnergy_2014edition.pdf (19.10.2015)

[6] W.B.Shockley, *The Path to the Conception of the Junction Transistor*, IEEE Transaction on electron devices, **1949**, 23, 7

[7] D.M. Chapin, C.S. Fuller, G.L. Pearson, *A new silicon p-n junction photocell for converting solar radiation into electrical power*, J. Appl. Phys., **1954,** 510-519

[8] J. Britt, C. Ferekides, *Thin-film CdS/CdTe solar cell with 15.8% efficiency*, Appl. Phys. Lett.,**1993,** 62, 22, 2851-2852

[9] Ingrid Repins, Miguel A. Contreras, Brian Egaas,Clay DeHart, John Scharf, Craig L. Perkins, Bobby To, Rommel Noufi*, 19.9%-efficient ZnO/CdS/CuInGaSe$_2$ solar cell with 81.2% fill factor,* Prog. Photovolt: Res. and Appl., **2008** ,16, 3, 235–239

[10] https://www.ise.fraunhofer.de/en/downloads-englisch/pdf-files-englisch/photovoltaics-report-slides.pdf (19.10.2015)

[11] Kojima Akihiro, Teshima Kenjiro, Shirai, Yasuo, Miyasaka Tsutomu, *Organometal Halide Perovskites as Visible-Light Sensitizers for Photovoltaic Cells,* J. Am. Chem. Soc.,131, **2009** ,6050–6051

[12] S.Collavini, S. F.Völker, J. L. Delgado, *Understanding the Outstanding Power Conversion Efficiency of Perovskite-Based Solar Cells*. Angew. Chem. Int. Ed., **2015**, 54, 9757–9759

[13] Nakita K.Noel, Samuel D. Stranks, Antonio Abate, Christian Wehrenfennig, Simone Guarnera, Amir-Abbas Haghighirad, Aditya Sadhanala, Giles E. Eperon, Sandeep K. Pathak, Michael B. Johnston, Annamaria Petrozza, Laura M. Herz, Henry J.Snaith, *Lead-free organic–inorganic tin halide perovskites for photovoltaic applications,* Energy Environ. Sci., **2014**, 7, 3061- 3068

[14] Martin A. Green, Keith Emery, Yoshihiro Hishikawa, Wilhelm Warta and Ewan D. Dunlop, *Solar cell efficiency tables (Version 45), Prog. Photovolt:* Res. Appl. **2015**; 23, 1–9

[15] http://www.nrel.gov/ncpv/images/efficiency_chart.jpg (12.11.2015)

[16] Böer, K. W., *Survey of Semiconductor Physics,* Vol. II. New York: John Wiley, **2002**

[17] Fahrenbruch, A. L., and Bube, R. H., *Fundamentals in Solar Cells*, New York: Academic Press, **1983**

[18] Wright, M.; Uddin, *A. Organic—inorganic Hybrid Solar Cells: A Comparative Review*, Sol. Energy Mater. Sol. Cells, **2012**, 107, 87–111

[19] A. Facchetti, materials today, **2007**, 10, 3, 28–37

[20] Mayer, A. C.; Scully, S. R.; Hardin, B. E.; Rowell, M. W.; Mcgehee, M. D. *Polymer-Based Solar Cells*, materials today. **2007**, 10, 11, 28–33

[21] Koch, N. *Organic Electronic Devices and Their Functional Interfaces*, Chemphyschem **2007**, 8, 1438–1455

[22] McGehee D.G., Topinka M.A., *Solar cells: Pictures from the blended zone,* Nature Materials, **2006**, 5, 9, 675–676

[23] Nelson J., *Organic photovoltaic films,* Current Opinion in Solid State and Materials Science, **2002,** 6**,** 87–95

[24] Halls J.J.M., Friend R.H., Archer M.D., Hill R.D., *Clean electricity from photovoltaics*, London: Imperial College Press, **2001,** 377–445

[25] H. Hoppe and N. S. Sariciftci, *Organic solar cells: An overview,* J. Mater. Res. **2004**, 19, 7, 1924–1945

[26] Harald Hagendorfer, Karla Lienau ,Shiro Nishiwaki, Carolin M. Fella, Lukas Kranz, Alexander R. Uhl, Dominik Jaeger, Li Luo, Christina Gretener, Stephan Buecheler, Yaroslav E. Romanyuk , Ayodhya N. Tiwari, *Highly Transparent and Conductive ZnO: Al Thin Films from a Low Temperature Aqueous Solution Approach*, Adv. Mater., **2014**, 26, 632–636

[27] C. Waldauf, M. Morana, P. Denk, P. Schilinsky, K. Coakley, S. A. Choulis, and C. J. Brabec *,* Appl. Phys. Lett, **2006**, 89, 233517

[28] M. S. White, D. C. Olson, S. E. Shaheen, N. Kopidakis, and D. S. Ginley, *Inverted bulk-heterojunction organic photovoltaic device using a solution-derived ZnO underlayer, ,* Appl. Phys. Lett, **2006**, 89, 143517

[29] G. Li, C.-W. Chu, V. Shrotriya, J. Huang, Y. Yang, *Efficient inverted polymer solar cells,* Appl. Phys. Lett., **2006,** 88, 253503

[30] Jin-Mun Yun , Jun-Seok Yeo, Juhwan Kim, Hyung-Gu Jeong , Dong-Yu Kim, Yong-Jin Noh, Seok-Soon Kim, Bon-Cheol Ku, and Seok-In Na, *Solution-Processable Reduced Graphene Oxide as a Novel Alternative to PEDOT:PSS Hole Transport Layers for Highly Effi cient and Stable Polymer Solar Cells*, Adv. Mater. **2011**, 23, 4923–4928

[31] Daiki Wakizaka, Toshiki Fushimi, Hideo Ohkita, Shinzaburo Ito, *Hole transport in conducting ultrathin films of PEDOT/PSS prepared by layer-by-layer deposition technique,* Polymer 45, **2004**, 8561–8565

[32] Xinchen Li, Wallace C. H. Choy, Fengxian Xie, Shaoqing Zhangb, Jianhui Houb, *Room-temperature solution-processed molybdenum oxide as a hole transport layer with Ag nanoparticles for highly efficient inverted organic solar cells*, J. Mater. Chem. A, **2013**, 1, 6614

[33] Brian O'Reagan, Michael Grätzel, *A low cost, high-efficiency solar cell based on dye-sensitized colloidal TiO_2- films,* Nature 353, **1991**, 737 - 740

[34] J. Bisquert, D. Cahen, G. Hodes, S. Rühle, A. Zaban, *Physical chemical principles of photovoltaic conversion with nanoparticulate, mesoporous dye-sensitized solar cells,* Journal of Physical Chemistry B, 108, **2004,** 8106-8118

[35] Jessica Krüger*, Interface engineering in solid-state dye sensitized solar cells*, École Polytechnique Fédérale de Lausanne, **2003**

[36] Ravi Harikisun, Hans Desilvestro, *Long-term stability of dye solar cells,* Solar Energy 85, **2011**, 1179–1188

[37] Głowacki, E. D., Leonat, L., Voss, G., Bodea, M.-A., Bozkurt, Z., Ramil, A. M., Irimia-Vladu, M., Bauer, S., Sariciftci, N. S., *intermolecular hydrogen-bonded organic semiconductors-Quinacridone versus pentacene,* Appl. Phys. Lett., 101, **2012**, 023305

[38] Irimia-Vladu, M., Głowacki, E. D., Troshin, P. A, Schwabegger, G., Leonat, L., Susarova, D. K.; Krystal, O.; Ullah, M.; Kanbur, Y.; Bodea, M. A, Razumov, V. F., Sitter, H., Bauer, S., Sariciftci, N. S*., Indigo-a Natural Pigment for High Performance Ambipolar Organic Field Effect Transistors and Circuits*, Adv. Mater.**2012**, 24, 375–380.

[39] Głowacki, E. D.; Leonat, L.; Voss, G., Bodea, M.-A., Bozkurt, Z., Ramil, A. M., Irimia-Vladu, M., Bauer, S.; Sariciftci, N. S., *Ambipolar Organic Field Effect Transistors and Inverters with the Natural Material Tyrian Purple*, AIP Adv. **2011**, 1, 042132.

[40] H.Zollinger, *Color Chemistry: Synthesis, Properties and Application of Organic Dys and pigments*, 3rd ed. Wiley-VCHm Weinheim, **2003**

[41] C. Riordan and R. Hulstrom, *What is an air mass 1.5 spectrum?,* Photovoltaic Specialists Conference, **1990**, Conference Record of the Twenty First IEEE

[42] http://rredc.nrel.gov/solar/spectra/am1.5/ASTMG173/ASTMG173.html (20.10.2015)

[43] Alan J. Heeger, *Bulk Heterojunction Solar Cells: Understanding the Mechanism of Operation,* Adv. Mater. **2014**, 26, 10–28

[44] Harald Hoppe, Niyazi Serdar Sariciftci, *Morphology of polymer/fullerene bulk heterojunction solar cells,* J. Mater. Chem., **2006**, 16, 45–61

[45] W. Shockley, H.J.Queisser*, Detailed Balance Limit of Efficiency of p-n Junction Solar Cells,* J. Appl. Phys, **1961**, 32, 510-519

[46] Alexis De Vos, *Detailed balance limit of the efficiency of tandem solar cells*, J. Phys. D: Appl. Phys., **1980,** 13, 839-846

[47] M. D. Archer, J.R. Bolton, *Requirements for Ideal Performance of Photochemical and Photovoltaic Solar Energy Converters*, J. Phy. Chem., **1990**, 94, 21, 8028-8036

[48] M. A. Green, *High Efficiency Silicon Solar Cells*, Seventh E.C. Photovoltaic Solar Energy Conference, **1987**, 681-687

[49] A.S.Brown, M.A. Green, *Impurity photovoltaic effect: Fundamental energy conversion efficiency limits*, J. Appl. Phys., **2002**, 92, 1329

[50] M.C. Scharber, N.S. Sariciftci, Prog. in Polym. Sci., **2013**, 38, 1929–1940

[51] M. A. Green, *Radiative efficiency of state-of-the-art photovoltaic cells*, Prog. Photovolt: Res. Appl., **2012,** 20, 472–476

[52] Tauc, J.; Grigorovici, R.; Vancu, A. *Optical Properties and Electronic Structure of Amorphous Germanium*. phys. stat. sol., **1966**, 15, 627.

[53] Shigeru Ikeda, Ryo Kamai, Tetsuro Yagi, Michio Matsumura. *Electrochemical Synthesis of CuIn(Se, S)$_2$ Layer for Thin-Film Solar Cell with a Superstrate Configuration*. Journal of The Electrochemical Society, **2010,** 157, 99-103.

[54] Veldman, D.; Meskers, S. C. J.; Janssen, R. a. J. *The Energy of Charge-Transfer States in Electron Donor-Acceptor Blends: Insight into the Energy Losses in Organic Solar Cells*. Adv. Funct. Mater. **2009**, 19, 1939–1948.

[55] Beverina, L.; Drees, M.; Facchetti, A.; Salamone, M.; Ruffo, R.; Pagani, G. a. *Bulk [2]Heterojunction Solar Cells - Tuning of the HOMO and LUMO Energy Levels of Pyrrolic Squaraine Dyes*. European J. Org. Chem., **2011**, 5555–5563.

[56] Birgit Six, *Influence of Self-Assembling Monolayers on the Performance of Bulk Heterojunction Solar Cells,* TU Graz, **2014**

[57] Jong Soo Kim, Jong Hwan Park, Ji Hwang Lee, Jang Jo, Dong-Yu Kim, Kilwon Cho, *Control of the electrode work function and active layer morphology via surface modification of indium tin oxide for high efficiency organic photovoltaics,* Appl. Phys. Lett., **2007**, 91, 112111

[58] M. Halik, A. Hirsch, *The Potential of Molecular Self-Assembled Monolayers in Organic Electronic Devices,* Adv. Mater., **2011**, 23, 2689-2695

[59] J.D. Zimmermann, B. Song, O. Griffith, St. R. Forrest, *Exciton-blocking phosphonic acid-treated anode buffer layers for organic photovoltaics,* Appl. Phys. Lett., **2013**, 103, 24, 243905-1-5

[60] S. Khodabakhsh, B. M. Sanderson, J. Nelson, T. S. Jones, *Using Self-Assembling Dipole Molecules to Improve Charge Collection in Molecular Solar Cells,* Adv. Funct. Mater., **2006**, 16, 1, 95-100

[61] L. Macaraig, T. Sagaw, S. Yoshikawa, *Self-Assembly Monolayer Molecules for the Improvement of the Anodic Interface in Bulk Heterojunction Solar Cells,* Energy Procedia, **2011,** 9, 283-291

[62] F. Nüesch, M. Carrara, L. Zuppiroli, *Solution versus Vapor Growth of Dipolar Layers on Activated Oxide Substrates,* Langmuir **2003**, 19, 4871-4875

[63] A. Ulaman, Chem. Rev. **1996**, 96, 1533-1554

[64] F. Schreiber, *Structure and growth of self-assembling monolayers,* Progress in Surface Science, **2000**, 65, 151-256

[65] Hin-Lap Yip, Steven K. Hau, Nam Seob Baek, Hong Ma, Alex K.-Y. Jen, *Polymer Solar Cells That Use Self-Assembled-Monolayer-Modified ZnO/Metals as Cathodes,* Adv. Mater. **2008**, 20, 2376–2382

[66] Steven K. Hau, Hin-Lap Yip, Orb Acton, Nam Seob Baek, Hong Ma Alex K.-Y. Jen, *Interfacial modification to improve inverted polymer solar cells*, J. Mater. Chem., **2008**, 18, 5113–5119

[67] T. Young: *An Essay on the Cohesion of Fluids*. In: Phil. Trans. R. Soc. Lond.. 95, **1805**, 65–87

[68] Pierre-Gilles de Gennes: Capillarity and Wetting Phenomena, Springer New York, **2004**

[69] Anna Marzec. The effect of dyes, pigments and ionic liquids on the properties of elastomer composites. Polymers. Université Claude Bernard - Lyon I, **2014**. English.

[70] Y.-S. Kim, S.-H. Kim, T.-K. Kim, Y.-A Son,, *Characteristics of HOMO and LUMO Potentials by Altering Substituents: Computational and Electrochemical Determination,* J. of the Korean Soc. of Dyers and Finishers, **2008**, 20, 5, 41-46

[71] F. M. Fowkes, Attractive Forces at Interfaces, Ind. Eng. Chem., **1964**, 56, 12, 40-52

[72] H. G. O. Becker: "Einführung in die Photochemie", G. Thieme Verlag, Stuttgart **1983**

6.3 List of Figures

6.4 List of Tables